From the Research Center Borstel
Leibniz Lung Center
Priority Research Area Infections
Director: Prof. Dr. Ulrich Schaible

Junior Research Group Coinfection
Dr. Bianca Schneider

Impact of an Influenza A Virus Infection on the Control of Experimental Tuberculosis in Mice

Dissertation
for Fulfillment of
Requirements
for the Doctoral Degree
of the University of Lübeck

from the Department of Natural Sciences

Submitted by
Sarah Ring
from Potsdam

Lübeck 2019

First referee: PD Dr. rer. nat. Norbert Reiling

Second referee: Prof. Dr. rer. nat. Rudolf Manz

Date of oral examination: 30.10.2019

Approved for printing. Lübeck, 30.10.2019

Table of contents

Abbreviations

-/-	Gene-deficient
13-HDoHe	13-hydroxy docosahexaenoic acid
15-HETE	15-Hydroxyeicosatetraenoic acid
AAM	Alternatively activated macrophage
Ab	Antibody
Ag85B	Antigen 85B
AM	Alveolar macrophage
Anti-IL10R	Anti-IL-10 receptor
APC	Antigen-presenting cell
Arg1	Arginase 1
BCG	Bacillus Calmette-Guérin
BSA	Bovine serum albumin
BSL	Biosafety level
CCL2	CC-chemokine ligand 2
CCR2	CC chemokine *receptor type 2*
CD	Cluster of differentiation
cDNA	complementary DNA
CFSE	Carboxyfluorescein succinimidyl ester
CFU	Colony forming unit
CTL	Cytotoxic T cell
DC	Dendritic cell
dLN	draining lymph node
EDTA	Ethylenediaminetetraacetic acid
ESAT-6	Early secreted antigen target, 6-kDa protein
ETOH	Ethanol
FACS	Fluorescence-activated cell sorting
FCS	Fetal calf serum
Fizz1	*Found in* inflammatory zone 1
Foxp3	Forkhead box P3
FSC	Forward scatter
GAPDH	Glyceraldehyde-3-phosphate dehydrogenase
HA	Hemagglutinin
HBC	High burden country
HDT	Host-directed therapy
HIV	Human immunodeficiency virus
HRP	Horseradish peroxidase
i.n.	intranasal
i.p.	intraperitoneal
i.v.	intravenous
IAV	Influenza A virus
IBV	Influenza B virus
ICS	Intracellular cytokine staining
IFN	Interferon
IL	Interleukin
IL-1RA	IL-1 receptor antagonist
IRF	Interferon-regulatory factor
IMDM	Iscove's Modified Dulbecco's Medium
^{int}	intermediate
ISG	Interferon-stimulated gene
KO	Knockout
LAG-3	Lymphocyte activation gene 3
LC-MS2	Liquid chromatography *mass spectrometry*
LTBI	Latent tuberculosis infection
LXA4	Lipoxin A4

MACS	Magnetic-activated cell sorting
MDCK	Madin-Darby canine kidney
MDR	Multi-drug resistant
MEM	Minimum Essential Medium
MFI	Median fluorescence intensity
MHC	Major histocompatibility complex
moDC	Monocyte-derived DC
Mtb	*Mycobacterium tuberculosis*
MTBC	Mycobacterium tuberculosis complex
Mx1	Myxovirus resistance protein 1
MyD88	Myeloid differentiation primary response 88
n	number
NA	Neuraminidase
NF-κB	Nuclear factor 'kappa-light-chain-enhancer' of activated B-cells
NK cell	Natural killer cell
NLRP3	NOD-like receptor family, pyrin domain containing 3
NO	Nitric oxide
NOS2	Ntric oxide synthase 2 (inducible)
ns	not significant
OADC	Oleic albumin dextrose catalase
PAMP	Pathogen-associated molecular pattern
PBS	Phosphate-buffered saline
PD2	Prostaglandin D2
PFA	Paraformaldehyde
PFU	Plaque forming unit
PGE2	Prostaglandin E2
PMA/Iono	Phorbol myristate acetate/Ionomycin
PRR	Pattern recognition receptor
qRT-PCR	quantitative real-time polymerase chain reaction
RNI	Reactive nitrogen intermediates
ROS	Reactive oxygen species
RPMI	Roswell Park Memorial Institute
RT	Room temperature
SD	Standard deviation
SSC	Side scatter
tg	transgenic
TB	Tuberculosis
$TBXA_2$	Thromboxane A2
TCR	T cell receptor
TF	Transcription factor
T_H	T helper cell
TLR	Toll-like receptor
TNF	Tumor necrosis factor
TPCK	L-(tosylamido-2-phenyl) ethyl chloromethyl ketone
Treg	Regulatory T cell
TST	Tuberculin skin test
vRNPs	Viral ribonucleoproteins
WHO	World Health Organization
WT	Wildtype
XDR	Extensively drug-resistant

Abstract

Rising epidemiological evidence strongly links an influenza virus coinfection to an increased mortality in individuals with tuberculosis (TB). However, experimental data as to which immunological factors contribute to TB disease exacerbation by influenza are largely missing. The current study addressed *Mycobacterium tuberculosis* (*Mtb*)-influenza A virus (IAV) coinfection in C57BL/6 mice to elucidate IAV-induced modulations of antimycobacterial innate and adaptive immune responses.

IAV coinfection early after *Mtb* low-dose infection resulted in a rapid and sustained increased bacterial burden in the lung. Moreover, in an *Mtb* high-dose mouse model, coinfection with IAV dramatically decreased the survival. By contrast, the presence of an *Mtb* infection did not influence the antiviral immune response. Coinfected and IAV-alone-infected mice displayed comparable induction of type I/III IFN activity, IAV-specific $CD8^+$ T cell responses and control of the viral load. However, concurrent IAV infection substantially modulated adaptive and innate immune defenses in *Mtb*-infected mice. IAV coinfection caused a rapid influx of cells from the monocyte/macrophage lineage into the lungs and resulted in an inversed $CD4^+$ to $CD8^+$ T cell ratio shifted to $CD8^+$ T cells. Of note, IAV-coinfected mice showed significantly decreased frequencies of IFN-γ and TNF-producing *Mtb*-specific $CD4^+$ T cells in both lungs and draining lymph nodes (dLNs). Reduced numbers of *Mtb*-specific $CD4^+$ T cells could be linked to an impaired priming of *Mtb*-specific $CD4^+$ T cells in the dLNs despite a comparable transport of viable bacteria to the dLNs. The impact on the *Mtb*-specific immune response was accompanied by a compromised antimycobacterial innate immunity. The impairment of nitric oxide synthase 2 (*Nos2)* induction resulted in a decreased amount of reactive nitrogen intermediates in coinfected lungs. Together with an IAV-induced increased expression of Arginase-1 (*Arg1*), Found in inflammatory zone 1 (*Fizz1*) and IL-1 receptor antagonist (*Il1rn*) and a decreased IL-1α (*Il1a*) expression, this suggested that IAV infection polarized macrophages into an alternatively activated phenotype (AAMs). In fact, IAV coinfection promoted the accumulation of macrophages in the lungs that had a higher Arginase-1 and lower NOS2 production compared to macrophages from *Mtb*-alone-infected mice. Those AAMs were detected in a lung environment characterized by increased levels of anti-inflammatory lipid mediators and elevated levels of the immunosuppressive cytokine IL-10. IL-10 was rapidly induced upon IAV infection and produced by both innate and adaptive immune cells. The blocking of IL-10 receptor signaling reduced the *Mtb* burden in coinfected lungs to a level comparable to that of *Mtb*-alone-infected mice, strongly suggesting that IL-10 signaling contributed to IAV-provoked TB exacerbation. Interestingly, the effect of the anti-IL-10 receptor blockade was independent of the *Mtb*-specific T cell response indicating that the compromised innate immune response was responsible for the increased bacterial burden in coinfected mice.

Altogether, this study further emphasized the negative impact of both an IAV infection and enhanced levels of IL-10 on TB management and linked IAV-induced IL-10 production to an increased host's susceptibility to *Mtb* infection. The present study supports recommendations of implementing influenza vaccination in TB endemic areas and also suggests IL-10 as a potential target for host-directed therapy in TB.

Zusammenfassung

Epidemiologische Daten zeigen, dass Tuberkulose (TB) Patienten häufiger nach einer Influenza Virus Infektion sterben als Patienten ohne TB. Trotz dieser mehrfach beschriebenen negativen Assoziation adressierten bislang nur wenige experimentelle Studien die zugrundeliegenden immunologischen Mechanismen. In der vorliegenden Arbeit wurde daher der Einfluss einer Influenza A Virus (IAV) Infektion auf die frühe Phase einer *Mycobacterium tuberculosis* (*Mtb*) Infektion im C57BL/6 Mausmodell untersucht.

Die IAV Koinfektion zum Zeitpunkt der frühen *Mtb* Niedrigdosisinfektion führte zu einer schnellen und bleibenden Erhöhung der bakteriellen Keimlast in der Lunge. In einer *Mtb* Hochdosisinfektion führte die IAV Koinfektion zu einer deutlich reduzierten Überlebensrate. Andererseits konnte kein Einfluss der *Mtb* Infektion auf die antivirale Immunantwort beobachtet werden. Koinfizierte Tiere zeigten im Vergleich zu IAV-allein infizierten Tieren keine Unterschiede hinsichtlich der Induktion der antiviralen Typ I/III Interferone, der IAV-spezifischen $CD8^+$ T Zell Antwort oder der Kontrolle der Viruslast. Die IAV Infektion führte zu einer schnellen Einwanderung von myeloiden Zellen in die Lunge und bedingte zudem ein inverses $CD4^+$ zu $CD8^+$ T Zell Verhältnis zugunsten der $CD8^+$ T Zellen. In den Lungen und drainierenden Lymphknoten (LK) von koinfizierten Mäusen zeigte sich eine kompromittierte *Mtb*-spezifische $CD4^+$ T Zell Antwort in Hinblick auf Anzahl sowie IFN-γ- und TNF-Produktion. In den LK koinfizerter Mäuse konnte eine verringerte Aktivierung *Mtb*-spezifischer $CD4^+$ T Zellen nachgewiesen werden, ohne dass der Transport von *Mtb* zum LK beeinträchtigt war. Neben der reduzierten *Mtb*-spezifischen Immunantwort wiesen koinifzierte Mäuse verringerte anti-mykobakterielle Eigenschaften des angeborenen Immunsystems auf. Die verminderte Induktion von *Nitric oxide synthase 2* (*Nos2*) resultierte in einer reduzierten Produktion von reaktiven Stickstoffintermediaten in koinfizierten Lungen. Zusammen mit der erhöhten Expression von *Arginase-1* (*Arg1*), *Found in inflammatory zone 1* (*Fizz1*), IL-1 Rezeptor Antagonist (*Il1rn*), und einer geringeren Expression von IL-1α (*Il1a*), deuten diese Daten auf eine IAV-bedingte Polarisierung von Makropagen in einen alternativ aktivierten Phänotypen hin. Tatsächlich zeigten koinfizierte Lungen eine erhöhte Akkumulation von Makrophagen mit gesteigerter Arginase-1 und verringerter NOS2 Produktion verglichen zu *Mtb*-allein infizierten Lungen. Die koinfizierten Lungen konnten zudem durch erhöhte Mengen an anti-inflammatorischen Lipidmediatoren und gesteigerter Expression des immunsupprimierenden Zytokins IL-10 charakterisiert werden. IL-10 wurde früh nach IAV Infektion induziert und sowohl von Zellen des angeborenen als auch erworbenen Immunsystems produziert. Die Blockierung des IL-10 Rezeptor-Signalwegs reduzierte die pulmonale bakterielle Last in koinfizierten Mäusen auf ein Niveau vergleichbar zu *Mtb*-allein infizierten Mäusen. Dieser Effekt war unabhängig von der *Mtb*-spezifischen T Zell Antwort und deutet darauf hin, dass die Beeinträchtigung der anti-mykobakteriellen Eigenschaften des angeborenen Immunsystems für die erhöhte Keimlast in koinfizierten Mäusen verantwortlich war.

Zusammengefasst zeigt diese Studie, dass die IAV-induzierte IL-10 Produktion die Suszeptibilität gegenüber einer *Mtb*-Infektion erhöht. Damit wird IL-10 auch in dieser Studie als potentielles Ziel für eine wirtsorientierte TB Therapie präsentiert. Die vorliegenden Daten stützen die Einstufung von IAV als Risikofaktor für die Kontrolle von TB und somit auch die Empfehlungen, Influenza Vakzinierungen in TB-endemischen Gebieten durchzuführen.

1 Introduction

1.1 Tuberculosis

Tuberculosis (TB) ranks among the world's top ten causes of death and is the leading cause of death due to a single infectious agent[1]. The World Health Organization (WHO) reports that an estimate of 1.6 million people succumbed to TB in 2017, of those 0.3 million people were coinfected with human immunodeficiency virus (HIV)[1]. In 2017, the number of new TB cases was assessed to be 10 million of which 5.8 million were men, 3.2 million women and 1.0 million children. There are 30 countries classified as high burden countries (HBCs) that account for 87% of diagnosed TB cases worldwide. Eight of those HBCs already make up 66% of the TB incidents: India, China, Indonesia, the Philippines, Pakistan, Nigeria, Bangladesh and South Africa. For example, the incidence rate per 100,000 is ca. 567 cases in the HBC South Africa, whereas Germany as a low burden country presents on average only 7.5 TB cases per 100,000 inhabitants[2,3].

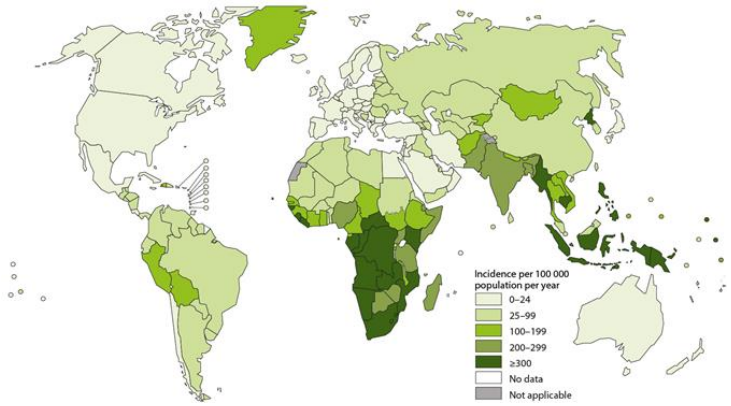

Figure 1 World map showing the estimated TB incidence rates in 2017[4]

TB is predominantly a disease of the lung (pulmonary TB) but may also manifest in extra-pulmonary organs such as the meninges, skeleton and lymphatic system[5]. The disease can present itself with symptoms such as fever, night sweats, weight loss and cough[6]. It is caused by the bacterium *Mycobacterium tuberculosis* (*Mtb*) which was first described as the causative agent by Robert Koch in 1882[7]. *Mtb* is an obligate aerobe, non-motile bacterium of the genus Mycobacteria which is characterized by a lipid-rich cell wall. This cell wall determines the specific properties of *Mtb* such as its long generation time (18-24 hours), its intracellular survival and the induced antimycobacterial immune response[8–10]. The mycolic acid is a dominant component of the cell wall and responsible for the acid-fastness of *Mtb* which is utilized for visualization of bacteria via Ziehl-Neelsen staining[9,11,12]. Other pathogenic sub-species that are closely related to *Mtb* and can cause TB are encompassed in the *Mtb* complex (MTBC)[11]. TB is not restricted to humans; for instance, *M. caprae* may cause TB in sheep and goats and *M. bovis* is the causative agent of TB in cattle[13,14]. *M. bovis* constituted the basis for the attenuated live vaccine *M. bovis* Bacille Calmette-Guérin (BCG) which was obtained after several *in vitro* passages. BCG is considered the most applied vaccine worldwide[15,16]. It shows protection against severe TB in children including miliary TB and TB meningitis, however, it largely fails to protect against pulmonary TB in adults.

Besides the lack of a protective anti-TB vaccine, there is also a demand for more effective antibiotics. The presence of multidrug-resistant (MDR) and extensively drug-resistant (XDR) TB is a major health threat and a great obstacle to WHO's END TB strategy[17]. The standard treatment of susceptible TB comprises four first-line antibiotics: isoniazid, rifampicin, pyrazinamide and ethambutol[18,19]. MDR-TB is defined as *Mtb* being resistant to at least isoniazid and rifampicin and XDR-TB describes additional resistance to any fluoroquinolone and any of the three injectable second-line aminogylcosides[20]. The rising incidence of MDR- and XDR-TB cases which require more elaborate and elongated therapy call for different treatment strategies such as host-directed therapy (HDT). HDT, unlike antibiotic treatment, does not directly target the bacterium but aims at modulating the host's antimicrobial response, thus circumventing the emergence of bacterial resistance[21].
Another challenge to the worldwide TB management poses the large reservoir of ca. 1.7 billion people, which equals 23% of the world's population, that are diagnosed with latent TB by dint of the tuberculin skin test (TST) conversion[1,22]. From those, 5-10% is expected to have a lifetime risk of experiencing reactivation and thus suffer from post-primary TB[22]. The latent stage is, opposed to the active form of TB (referred to as TB), asymptomatic and not transmissible[19]. Consequently, it is of utmost importance, besides vaccination and treatment improvement, to identify and evade risk factors that drive disease progression or reactivation in order to limit spread of the bacterium and disease outbreak(s).

1.1.1. Pathology

Mtb is an airborne pathogen that is transmitted through infectious droplets when TB patients cough or sneeze. The requirement for transmission of bacteria is active disease in contrast to latent tuberculosis infection (LTBI). In fact, only 5-10% of people who get infected with *Mtb* will develop active TB during their lifetime[22,23]. Most infected individuals remain latently infected and bacteria persist, however, the immune system is not able to reach sterile eradication of the pathogen[24].
Upon inhalation, *Mtb* is predominantly phagocytosed by alveolar macrophages (AMs)[25]. The infected AMs migrate across the alveolar epithelium into the lung parenchyma where the localized pro-inflammatory immune response induces the recruitment of mononuclear cells from neighboring blood vessels[26]. This initiates granuloma formation, the pathological hallmark of TB in humans. The aggregation of innate cells such as dendritic cells (DCs), neutrophils, monocyte-derived macrophages and natural killer (NK) cells defines the initial stages of granuloma formation[26,27]. Within the granuloma, macrophages differentiate into different types. Besides mature macrophages, multi-nucleated giant cells, foamy macrophages which accumulate lipid bodies and epithelioid macrophages can be identified[28].
After activation of the *Mtb*-specific adaptive immune response in the lung-draining lymph node (dLN), T and B cells migrate to the granuloma whereupon an organized structure forms. The maturing granuloma is characterized by new blood vessel formation and a "fibrous cuff" that consists of extracellular matrix and collagen[29]. In this stage, *Mtb*-infected macrophages form the center in which bacteria transit to a non-to-low replicating, metabolically less active status[9,30]. Late stage granulomas may show central necrosis that can develop into a liquefied core termed "caseum"[26]. The rupture of the granuloma allows the release of the bacteria into the airways and consequently the possibility of *Mtb* transmission though coughing or sneezing to a new host.

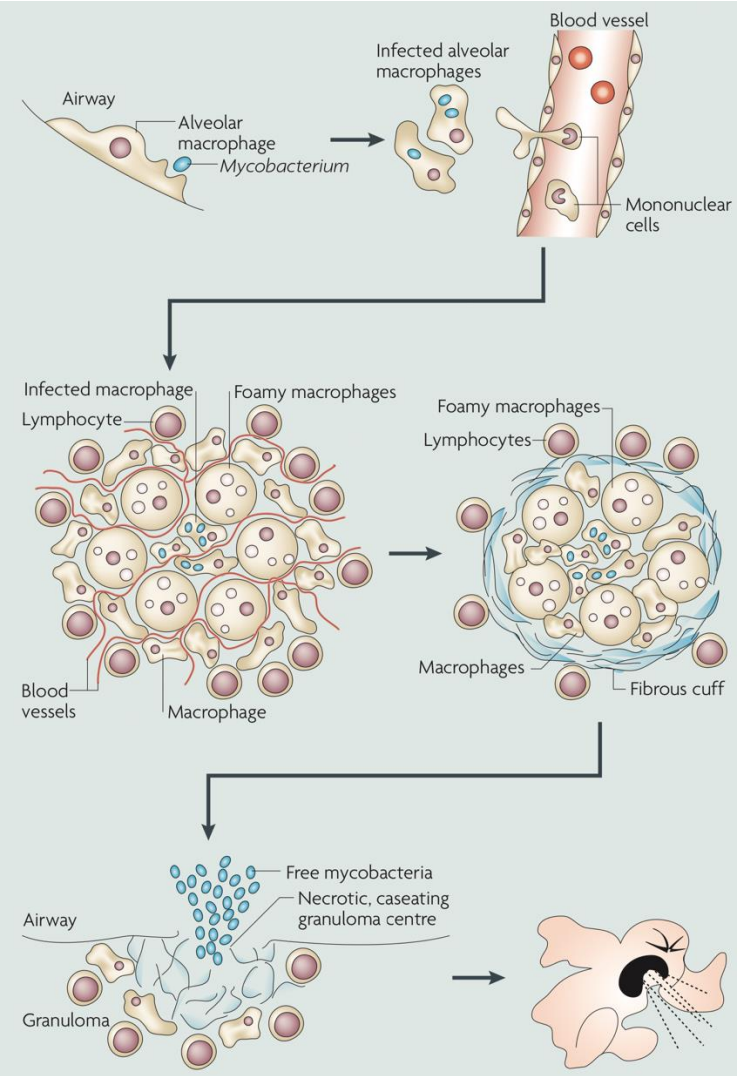

Figure 2 Granuloma formation in TB. The pathological hallmark of TB is the granuloma. Inhaled *Mtbs* infect AMs that induce a local pro-inflammatory immune response which induces the recruitment of mononuclear cells from neighbouring blood vessels to the site of infection. Macrophages within the forming granuloma can differentiate into mature macrophages, foamy macrophages, multinucleated giant macrophages (not shown) and epithelioid macrophages (not shown). In the presence of adaptive immune cells (lymphocytes), an organized granuloma structure forms. Later stage granulomas are characterized by a fibrous cuff. If the center of the granuloma necrotizes and becomes caseating, the rupture of the granuloma allows *Mtb* to enter the airways from which it may be transmitted to the next host by coughing or sneezing. (Figure from Russel *et al*.[26])

The granuloma was long perceived to play a primary protective role by walling off the infection and preventing dissemination of bacteria in the host, thus characterizing the latent TB stage. However, the granuloma is a very dynamic structure[27]. The fact that a granuloma does not aid eradication of the bacterium despite the presence of an adaptive immune response supports the notion that the dogma of the granuloma being a host-protective structure needs to be revised[31]. In fact, studies using the *M. marinum* larval zebrafish model demonstrated that a granuloma may not only be a survival niche for *Mtb* but actually support dissemination of the bacterium[32,33]. Infected macrophages from the primary granuloma were found to move rapidly within the granuloma and even be the initiators of secondary granulomas. Consequently, granuloma formation may be regarded as a double-edged sword in *Mtb* control and considered as a target for future therapeutic strategies.

1.1.2. Immune response to *Mycobacterium tuberculosis* infection

The first cells to encounter *Mtb* are AMs since they reside in the alveolar space[25]. However, it was shown that with advancing infection the newly recruited cells take over[34]. By day 14 after infection, *Mtb* were comparably distributed between AMs, DCs and neutrophils before recruited macrophages and DCs took over as main *Mtb*-infected cell populations by day 21 after infection. Phagocytosis of *Mtb* is mediated by different receptors such as scavenger, complement or mannose receptors[34]. Upon uptake, mycobacteria end up enclosed in a phagosome. The following phagosomal maturation process that results in a cellular compartment with bactericidal properties (e.g. low pH, acidic proteases, peptidases, reactive oxygen species (ROS), reactive nitrogen intermediates (RNI)) can be blocked by *Mtb*[35–38]. The recognition of conserved pathogen-associated molecular patterns (PAMPs) by Toll-like receptors (TLRs) results in myeloid differentiation factor 88 (MyD88)-mediated activation of the transcription factor nuclear factor kappa-light-chain-enhancer of activated B-cells (NF-κB)[39]. Especially TLR2, TLR4 and TLR9 were linked to the detection of *Mtb* components[40]. TLR signaling ultimately results in activation of innate immune cells which includes the secretion of cytokines such as IL-12. IL-12 is essential in activating and promoting a T helper cell (T_H) 1-polarized adaptive immune response[35]. Activation of the adaptive immune response requires DCs that transport intact mycobacteria from the lung to the lung-draining lymph nodes (dLNs: mediastinal lymph nodes)[41,42]. The migration of DCs to the dLNs occurs only 8-9 days after *Mtb* infection in mice[43]. Consequently, the activation of the adaptive immune response in *Mtb* infection is delayed compared to other infections with e.g. *Listeria monocytogenes* or influenza virus[43–45]. DCs can acquire mycobacteria and mycobacterial antigen through direct infection or via the uptake of *Mtb*-containing apoptotic cell vesicles[46]. Virulent strains of *Mtb*, like the commonly used H37Rv, were described to induce necrosis rather than apoptosis via the induction of the lipid mediator lipoxin A4 (LXA_4) which inhibits the apoptosis-promoting mediator prostaglandin E2 (PGE_2)[47,48]. This immune modulation by *Mtb* favors bacterial growth and counteracts effective T cell activation. Mycobacterial peptide antigens can be presented in a major histocompatibility complex (MHC)-I or –II context to activate *Mtb*-specific $CD8^+$ or $CD4^+$ T cells, respectively[49]. In addition to that, CD1-displayed mycobacterial lipid antigens were also highlighted to activate T cells during *Mtb* infection[50]. As mentioned before, IL-12 is required for T cell activation and T_H1 polarization. This cytokine has been shown both in mice and men to be required for successful control of *Mtb* infection[51–54]. With the onset of the adaptive immune response, *Mtb* growth is arrested and controlled[55]. Especially for this early phase of *Mtb* infection, $CD4^+$ T cells are indispensable for control of the infection[56]. This is also prominently seen in HIV-infected humans where HIV-mediated $CD4^+$ T cell depletion promotes exacerbation of TB[49,57]. Lack or loss of $CD4^+$ T cells cannot be compensated by $CD8^+$ T cells[55,56,58]. Nonetheless, $CD8^+$ T cells were found to play a pivotal role during the later stages of *Mtb* infection to guarantee long-term control in TB[59]. Both $CD4^+$ and $CD8^+$ T cells mediate their effector functions via the secretion of the cytokines IFN-γ and TNF to activate macrophages[60]. The activation of antimycobacterial effector functions within the phagocytes encompasses phagosome maturation and the production of ROS and RNI that enable the infected cell to kill *Mtb*[61–63]. The role and indispensability of nitric oxide (NO) for *Mtb* control has been shown in the mouse model but its relevance in humans is controversial[64–67]. Furthermore, activation of myeloid cells results in the secretion of the cytokines IL-1α and IL-1β which are both essential for *Mtb* control[68].

Besides cytokine-mediated activation of *Mtb*-infected phagocytes, $CD8^+$ T cells may also directly kill *Mtb*-infected cells via the induction of apoptosis by secretion of perforin, granzyme or by direct cell-cell contact via FasL-Fas[69]. Although TNF is required for *Mtb* control in terms of macrophage activation as well as granuloma formation and maintenance, it has also been linked to pathological responses resulting in tissue destruction[70,71]. In order to prevent immunopathology, anti-inflammatory regulators such as regulatory T cells (T_{reg}) and the master immunosuppressive cytokine IL-10 come into play[72,73]. Besides this host-protective effect, T_{regs} were, however, also shown to further delay the onset of the *Mtb*-specific adaptive immune response[74]. IL-10 was proposed as a risk factor for TB in humans and shown to interfere with the protective anti-*Mtb* immune response[75–81]. Additionally to T_{reg}- and IL-10-mediated impairment of *Mtb* control, type I IFNs were demonstrated to compromise TB management in both mice and men[82–87]. They were associated with decreased survival in mice and could be correlated to the extent of radiographic disease in human with active TB. Downstream signals of type I IFNs can include the induction of IL-10 or inhibition of IL-12 and IL-1[88–92].

1.1.3. Risk factors

A critical component for TB management is the identification, assessment and prevention of risk factors that drive the progression from infection to active disease.

Besides behavioral risk factors like smoking tobacco and alcohol consumption which increase the TB risk by 2-3-fold, malnutrition and indoor air pollution were also linked to an enhanced risk of developing TB[19,93]. Furthermore, type 2 diabetes mellitus is also known to increase the risk for TB by 3-fold and is moreover associated with decreased therapy success. Supporting the essential role of TNF, anti-TNF immunotherapy for treatment of autoimmune diseases such as rheumatoid arthritis was found to increase the risk for reactivating LTBI[94,95]. Accordingly, it is recommended that patients who shall be given immunosuppressive anti-TNF treatment are tested for LTBI before therapy start. However, the strongest risk factor for developing TB is by far a HIV coinfection which increases the likelihood by 17-23 times compared to people without HIV[96]. In fact, it is reported that HIV-positive patients represent 12% of all new active TB cases and 25% of TB-related deaths[19]. Moreover, HIV-infected individuals have a higher risk of experiencing reactivation of LTBI[97]. Besides the HIV infection-mediated loss of $CD4^+$ T cells, the viral infection is also associated with type I IFN production and, although controversially discussed, manipulation of macrophage activity[46]. Together, this virus-induced immunomodulation decreases the host control of *Mtb*. Other pathogens that geographically overlap with TB are parasitic helminths which are estimated to have infected over 2 billion people worldwide with the greatest prevalence in Africa, Asia and South-America[98]. The existence of different helminth subgroups with individual life cycles, organ preferences and immune responses challenges the establishment of clear clinical associations between TB and helminth infections. Nevertheless, *in vitro* and *in vivo* experiments could show that coinfection resulted in loss of *Mtb* control mainly due to the helminth-induced T_H2-based immune responses[99–102]. The greatest impact of this coinfection is suggested to be on the vaccine-induced anti-*Mtb* immune response which might be modulated by concurrent helminth infections[98]. Malaria joins the ranks of another TB co-endemic infectious disease that worsens TB outcome. Different plasmodium strains, the causative agents of distinct forms of malaria, were shown to decrease *Mtb* control in mouse models with modulating effects ranging from increased histopathology to the suggested recruitment of *Mtb*-permissive $CD11c^+$ cells[103–105].

These examples demonstrate that coinfections are worth studying since during their lifetime people become the carrier of more than one pathogen. Immunomodulation resulting from either chronic or acute coinfections can exert great impact on the host's management of the individual pathogen. A viral coinfection other than HIV has been recently discussed to impact TB control; the evidence for influenza virus-mediated impairment of *Mtb* control is pointed out in 1.3 *Mycobacterium tuberculosis*- Influenza virus coinfection.

1.1.4. Mouse models

The mouse is an indispensable tool in TB research to approach immunology-related questions. Its genetic manipulability allows the user to specifically address potentially relevant factors[106].

As for other infections and diseases that are studied, different mouse strains present different degrees of susceptibility to *Mtb* infection. Based on the survival times, C57BL/6 and BALB/c mice are resistant whereas e.g. DBA/2, C3HeB/Fej and 129Sv/J mice are *Mtb*-susceptible strains[107]. In both mice and men the lung represents the organ of primary manifestation of infection[55]. In contrast to the human situation, the bacterial burden in mice remains high although controlled on a stationary level upon the onset of the adaptive immune response[55,108]. This high bacterial burden is, however, not accompanied by disease symptoms until late after infection[109]. Eventually, all mice infected with *Mtb* show a progressive disease and succumb to infection as opposed to humans where only 5-10% of infected individuals develop disease after all[23]. Before establishment of the anti-*Mtb* adaptive immunity, bacteria grow exponentially[108]. In humans, the adaptive immune response is estimated to be active 3-8 weeks after *Mtb* infection[110,111] and in resistant mouse strains bacterial growth arrest is observed from day 20 on[55,108]. The mouse model is in many aspects a good correlate of the immunological key components observed in human TB[106,109]. For instance, the induction of type I IFNs in mice results in disease exacerbation and loss of *Mtb* control which is in line with the observed type I IFN-inducible gene signature in the blood of active TB patients[82–85]. Furthermore, the indispensability of $CD4^+$ T cells in TB is proven both in CD4-deficient mice and prominently seen in HIV-patients in which loss of $CD4^+$ T cells increases the risk to progress to disease directly or experience reactivation of LTBI[49,57,97,112]. But the mouse model has deficits in terms of TB pathology because it does not develop the stratified and well-organized granulomas that are seen in TB patients. Murine granulomatous lesions differ in cellular organization, lack the fibrous cuff and centralized necrosis[109,113]. However, this statement primarily refers to the most widely used strains C57BL/6 and BALB/c since other mouse strains such as the C3HeB/FeJ mouse develop organized, necrotizing granulomas upon *Mtb* infection[114].

Together, the mouse model with its varying degrees of susceptibility and genetic modifications displays essential features in TB control and host-pathogen interactions. Hence, it enables the elucidation of basic immunological questions but also the determination of vaccine efficacy and potential therapy success. It can further elucidate and corroborate risk factors that challenge effective host control of *Mtb* infection.

1.2. Influenza

Seasonal influenza infections put a major health threat to the human population and are responsible for an estimate of ca. 290,000-650,000 deaths annually[115]. According to the WHO, three to five million people worldwide suffer from seasonal influenza (flu) every year[116]. The flu presents itself with a sudden onset of symptoms like fever, coughing, stuffy nose, fatigue and muscle or body aches. High risk groups for severe influenza virus complications include children under 5 years old and elderly people over 65 years of age as well as pregnant women and people who suffer from immunosuppression or an underlying chronic condition[116]. In irregular unpredictable time periods, influenza virus causes pandemics which can result in up to 50% of the population being infected[117]. The most devastating pandemic dates back to 1918 and became known as the Spanish Flu, which claimed the lives of over 50 million people[118].The latest pandemic and first of the 21st century occurred in 2009, known as the Swine Flu, and was caused by an influenza A virus H1N1 strain and resulted in over 18,449 confirmed deaths in 241 countries[119]. The WHO declared the end of the pandemic in August 2010, however, the 2009 H1N1 virus still circulates within the human population[120,121].

Influenza viruses belong to the family of Orthomyxoviridae which are further divided into different genera namely influenza A, B and C viruses. Influenza A viruses (IAV) constitute the most health-threatening genus to humankind[117]. While influenza B viruses (IBV) and influenza C viruses (ICV) are causative for endemics, with C only for mild respiratory diseases, IAV is responsible for seasonal as well as pandemic influenza outbreaks. Influenza viruses are lipid bilayer-enveloped viruses with a negatively-sensed, single-stranded, segmented RNA genome[122]. IAV contains 8 segments and is further characterized by the expression of the surface glycoproteins hemagglutinin (HA), for which 16 are described, and neuraminidase (NA), for which 9 are known[122]. The viral RNA polymerase is highly error-prone and the absence of a proofreading function consequently results in high mutation rates demanding the annual renewal of vaccination to account for this so called antigenic drift[123,124].

1.2.1. Viral replication cycle

Influenza viruses replicate in epithelial cells throughout the respiratory tract[117]. While non-fatal influenza cases were described to primarily involve the trachea and the upper respiratory tract, fatal cases are characterized by signs of pneumonia reflecting that disease progression is associated with viral spread to the lower respiratory tract[117,125]. For viral infectivity, the surface glycoprotein HA is indispensable[126]. HA binds to sialic acids expressed on the host cell surface whereupon the virus is internalized by receptor-mediated endocytosis. Generally, human-adapted IAV preferentially bind to α2,6-linked sialic acid moieties which are mainly expressed in the upper respiratory tract, while α2,3-linked sialic acid moieties are dominant in the lower respiratory tract[127,128]. The receptor specificity, which differs between different IAV strains especially between human- and avian-adapted viruses, determines the course of infection and transmission. The acidic environment within the endosome enables the conformational change of the HA protein that allows the fusion of the viral with the endosomal membrane[122,129]. This fusion process allows the release of the viral ribonucleoprotein complexes (vRNPs: viral RNA segment, polymerase proteins and the nucleoprotein) into the cytosol[130,131]. Thereupon, the viral RNPs are transported to the host cell nucleus where the viral genome is transcribed and replicated. After all viral components are replicated and proteins are synthesized, the virus particle is assembled at the cytosolic

face. The virus buds from the cellular membrane utilizing the host cell lipid bilayer as its coat. The new virus is eventually released via the sialidase activity of the viral NA. In the absence of NA activity, the release of virus from the host cell is prevented and thus, the infectious cycle of the virus disrupted[122,131,132]. Consequently, the antiviral drug Oseltamivir (Tamiflu®), a neuraminidase inhibitor, acts to reduce the release of newly synthesized viruses and thereby prevents the infection of new host cells[133].

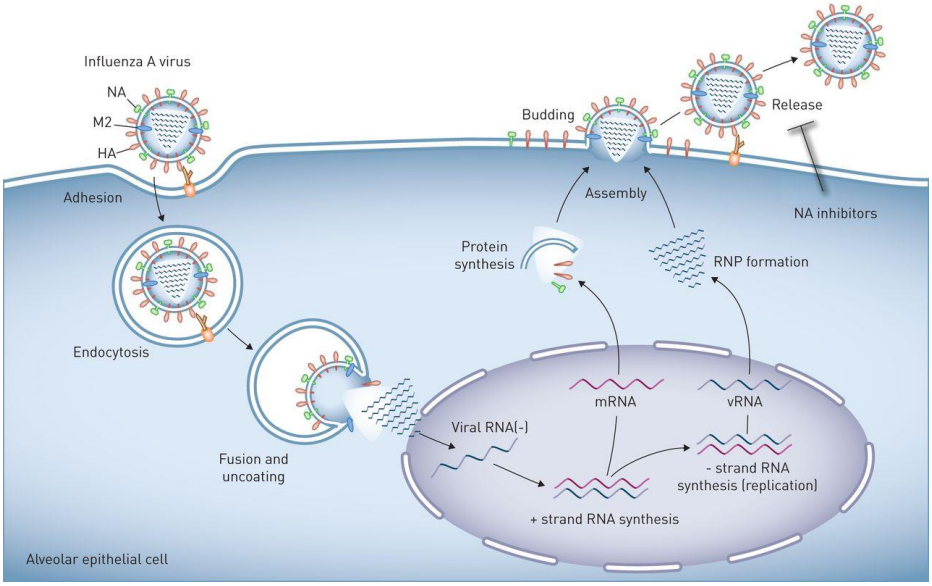

Figure 3 Replication cycle of influenza A virus (IAV). IAV is endocytosed upon binding of viral HA to the sialic acid on the epithelial cell surface. The low pH within the endosome induces conformational changes of the HA protein that allows the fusion of the viral and endosomal membrane. Next, vRNPs are released into the cytosol and transported into the nucleus where the viral RNA is replicated and transcribed. Newly synthesized viral components assemble at the host cell membrane and the virus buds from the host cell, released by the sialidase activity of the viral NA. The release and spread of new viruses can be pharmacologically inhibited by targeting the viral NA. (Figure from Herold *et al*.[134])

1.2.2. Immune response to influenza virus infection

The treatment of flu with antiviral drugs such as Tamiflu® might be helpful in severe cases, but in uncomplicated influenza cases in adults it only reduces duration of symptoms by one day[135]. Consequently, the host immune response is essential and the main determinant for the outcome of influenza infections.

Upon inhalation of infectious droplets, influenza virus productively infects type I and type II epithelial cells that represent the primary niche of viral replication[136,137]. After initial infection, both non-immune and immune cells such as macrophages and dendritic cells can be the target of viral infection[138]. Recognition of the influenza virus is ensured by diverse pattern recognition receptors (PRRs) at distinct locations within the cell[139]. The innate immune system detects the virus by at least three different types of PRRs: TLRs, retinoic acid-inducible gene I (RIG-I) and NOD-like receptor family member NOD-, LRR- and pyrin domain-containing 3 (NLRP3). The activation of either PRR ultimately results in downstream activation of NF-κB and/or interferon-regulatory factors (IRF) and subsequently, the expression of several pro-inflammatory cytokines and chemokines[139,140]. Furthermore, the NLRP3 inflammasome formation activates caspase-1 which cleaves pro-IL1β to convert it into its bioactive form[141]. Above all, the IRF-mediated expression of type I IFNs is central to antiviral immunity[142]. Type I IFNs are produced by macrophages, pneumocytes, DCs and plasmacytoid DCs (pDCs)[143,144]. Binding of type I IFNs to their cognate receptor (interferon-αβ receptor: IFNAR) initiates a signaling cascade that culminates in the expression of a

plethora of over one hundred interferon-stimulated genes (ISGs)[145,146]. Among those are genes coding for proteins that exhibit direct antiviral function e.g. myxovirus resistance 1 (Mx1) which blocks transcription of the viral genome in the nucleus[140,147]. Further downstream responses encompass the secretion of pro-inflammatory cytokines, chemokines and lipid mediators[139]. Overall, type I IFNs affect both the innate and adaptive immune response. This is essential in case antiviral proteins are insufficient to control the viral infection. Chemokines allow the recruitment of neutrophils, monocytes and NK cells to the site of infection[148]. Type I IFNs were described to activate NK cells to enable killing of virus-infected cells[149]. An effective virus can, however, establish a robust infection which demands the help of the adaptive immunity for viral clearance and control[139]. Dominant players of the anti-influenza-mediated adaptive immune response are cytotoxic $CD8^+$ T cells (CTLs) [150–152]. An interesting study in mice showed the time course of virus-specific eGFP $CD8^+$ T cells in the dLN and lung by two-photon microscopy[153]. Within the first 3 days after an H1N1 IAV infection, $CD8^+$ T cells were primed and expanded in lung-draining lymph nodes before effector T cells migrated into the lung, increased in numbers and elicited their effector functions. Antigen-specific $CD8^+$ T cells generally arrive in the lung by day 6-8 after influenza virus infection[153,154]. With the arrival of CTLs, viral titers rapidly decline due to the CTL-mediated lysis of infected cells[155]. Induction of apoptosis of infected cells is either mediated via direct cell-cell contact through FasL-Fas or by secretion of cytolytic granules that contain perforin and granzyme. Consequently, management of viral load can be seen by day 7 and viral clearance around day 10 after the viral infection[156153,155]. Beside $CD8^+$ T cells, B cells exert effector functions needed for the control of influenza virus infection[155,157]. Depending on the influenza virus strain, B cell deficiency in mice was reported to be either associated with delayed viral clearance, or in case of the highly pathogenic PR8 influenza virus with higher mortality rates[152,158]. Neutralizing antibodies produced by B cells are critical in the prevention of fatal cases of acute viral infection[155,157]. Most antibodies generated during an IAV infection are directed against the surface protein HA. $CD4^+$ T cells are mainly accredited a supporting role in terms of optimizing an orchestrated antiviral immune response[155,159]. They shape the $CD8^+$ T cell response via the secretion of T_H1-driving cytokines such as IFN-γ, IL-2 and TNF and induce proper B cell activation [159,160]. In the absence of both $CD8^+$ T cells and B cells, $CD4^+$ T cells alone were unable to mediate viral clearance and mice succumbed to infection[158]. Concurrent with the process of adaptive immunity-mediated viral clearance, the recovery phase is initiated[156,161]. This stage encompasses the release of anti-inflammatory cytokines such as TGF-β, mostly by lung epithelial cells, and IL-10 which is produced, among others, by $CD4^+$ and $CD8^+$ T cells[139,161–163]. Besides IL-10 production by T effector cells, T_{regs} are also involved in the process of dampening IAV-induced immune responses[163,164]. Counterbalancing the acute inflammatory environment is essential to prevent immunopathology and with such harm to the host. Some influenza virus strains are able to prevent TGF-β processing which can result in uncontrolled cytokine production that may eventually cause acute respiratory distress syndrome and death[165].

1.2.3. Influenza virus and bacterial coinfections

An uncontrolled inflammatory immune response may constitute one factor of influenza infection-induced disease exacerbation. However, the leading complication of influenza virus infection that is associated with high morbidity and mortality rates is the co- or secondary infection with bacteria[156,166]. In fact, it is reported that during influenza pandemics 50-95% of deaths are the result of secondary pneumonia[156]. Published autopsy case reports from the most recent influenza pandemic, the 2009 H1N1 pandemic, found that over 50% of people who died showed histological and microbiological evidence of secondary bacterial pneumonia[167]. The predominantly associated bacteria are *Streptococcus pneumoniae*, *Staphylococcus aureus*, *Haemophilus influenzae*, and *Streptococcus pyogenes*[156,166]. The time window in which both men and mice were described to be most susceptible to either co- or secondary bacterial infection is ironically the recovery phase which should actually prevent the host from harm[156,166]. With the arrival of effector T cells and the beginning of viral clearance, the host concurrently takes measures to prevent an overshooting immune response as early as day 7 after viral infection. From there on, the host is reported to be highly susceptible to bacterial infection for up to two weeks (day 7-day 14/21 after viral infection)[156,166]. On the one hand, influenza virus induces cytopathic effects[156]. On the other hand, virus infection may promote the exposure of certain receptors and further reduce the mucociliary velocity[156,168]. Altogether, influenza virus can create an environment that facilitates bacterial adherence, growth and decreases initial clearance culminating in the establishment of a bacterial infection. Nevertheless, a decreased capability to prevent or control bacterial infection can also be due to a malfunctioning immune system. In fact, viral strains that exert only minimal cytopathic effects also predisposed infected individuals to subsequent bacterial infections[156,169,170]. The impairment of efficient innate antibacterial effector functions is caused by different mechanisms that can be downstream of type I IFN signaling[91,163,171,172]. Besides the aforementioned production of the immunosuppressive cytokine IL-10, desensitized macrophages can be characteristics of the resolution phase[156]. The upregulation of the inhibitory receptor CD200R, for instance, renders macrophages less responsive to activation[173]. Although the anti-inflammatory recovery status predisposes to concurrent or subsequent bacterial infections, once the bacterial infection is established tissue damage is promoted by an excessive inflammatory response- a key feature of bacterial pneumonia that promotes the worse clinical outcome for the host[174,175].

1.2.4. Mouse models

Mice are the predominant model in IAV research for obvious reasons of prize, size, husbandry, the availability of species-specific reagents and the option for genetic manipulations. They are very much eligible to study IAV pathogenesis. However, like with other pathogens, the choice of the mouse strain can determine the outcome of viral infection. For instance, the mouse strains DBA/2J and A/J are reported to be more susceptible to IAV infection than BALB/c and C57BL/6 mice[176,177]. Further considerations need to include the virus strain and dose that shall be used in the experiments. Since α2,3-linked sialic acids are predominantly represented in the murine respiratory tract while sialic acids with α2,6 linkage are less abundant, the study of human-adapted influenza strains, that prefer α2,6 linkage, mostly requires prior adaptation in order to achieve effective infection and replication of the virus in the mouse[128,178,179]. There are, however, human-pathogenic influenza strains that are able to efficiently cause disease without the need for prior adaptation. These include the 1918 H1N1 as well as the 2009 H1N1 pandemic strain[180,181]. The pathogenesis of an

influenza virus infection in mice can be monitored by changes in body weight, the clinical score, mortality rates, viral titers and lung pathology[179]. The mouse model is also widely used in experimental studies addressing antiviral immune responses because it mirrors human kinetics of T cell responses, viral titers and the recovery phase[153,156]. This model thus represents a convenient system in which to study antiviral treatment and vaccination strategies[179]. However, there are limitations to this model system in terms of transmission studies. Controversially discussed, today's general consensus is that mice do not present an eligible model to study contact-dependent or aerosol transmission of IAV[179]. For addressing those issues, the guinea pig or the ferret, as the gold standard in IAV research, would be the model of choice[182–184].

1.3. *Mycobacterium tuberculosis*- Influenza virus coinfection

As outlined in 1.1.3 and 1.2.3, coinfection or secondary infection with another pathogen can impose an enhanced risk for individuals to experience aggravated disease resulting in higher morbidity and mortality rates. In the case of *Mtb* infection, a coinfection may challenge the fragile control mechanisms and ultimately lead to the progression to disease or TB exacerbation.

For IAV infections, it has long been known that secondary bacterial infections are among the main reasons why people succumb to the flu. Reports from the 2009 IAV pandemic did not only verify coinfections with IAV-associated pathogens such as *Streptococcus pneumonia*, but also pinpointed the significance of less common coinfections such as HIV and active TB[185]. In fact, analyses from South Africa declared that 10% of H1N1 cases who succumbed during the 2009 pandemic also had active TB[185]. This negative association was also prominently addressed by the WHO which declared that "A substantial number of deaths have occurred in patients with chronic respiratory conditions, raising concern about the possible impact of influenza on patients with active tuberculosis", an important issue that should be incorporated into TB disease management within the End TB strategy[186]. This concern is further corroborated by additional reports showing increased morbidity and mortality rates in patients with pulmonary TB from South Africa who were coinfected with influenza virus[187–189]. An interesting small case report from South Korea described the concurrency of TB and IAV in 7 patients[190]. From those, 5 were diagnosed with TB one week after IAV diagnosis and the other 2 were positively tested for TB 17 days after IAV diagnosis suggesting that IAV coinfection increases the risk to progress to active TB. In line with that, a recent report from the Gambia showed that IAV or IBV viral RNA was present in 4.3% of patients at the time of TB diagnosis[191]. Strikingly, coinfected patients had a significantly higher bacterial burden in the sputum compared to TB mono-infected patients. Intriguingly, the devastating consequences of an *Mtb*-IAV coinfection were also emphasized by retrospective analyses of the 1918-1919 Spanish influenza pandemic[192,193]. Data indicated that during this most disastrous influenza outbreak, patients with TB were more at risk to die from concurrent IAV infection compared to those without TB.

Although epidemiological data that point out an association between concurrent *Mtb* and IAV infection are increasing, experimental studies lag behind. Consequently, experimental data that addressed the underlying causes for the worse disease outcome in TB-IAV coinfection are largely missing. The earliest study dates back to 1947[194]. Mice were simultaneously infected with *Mtb* (intraperitoneally) and IAV (intranasally) and observed for 3 weeks. Coinfected mice displayed faster and more extensively developing tuberculous lesions in the lungs compared to *Mtb*-alone-infected mice. Besides applying *Mtb* via a non-physiological

route, results in terms of bacterial numbers or immune modulation were missing. A more recent study from Flórido and colleagues approached this coinfection by simultaneous intranasal application of the attenuated TB vaccine strain *M. bovis* BCG-OVA and IAV[195]. They found increased bacterial loads in the lungs of coinfected compared to BCG-alone-infected mice two weeks after infection along with reduced proliferation of transgenic OVA-specific $CD4^+$ and $CD8^+$ T cells in dLNs of coinfected mice. A third study from 2014 observed that pre-exposure of mice to IAV before infection with *Mtb* led to an increased bacterial burden in lungs of coinfected mice and greatly impacted the survival[196]. Additionally, this study elucidated the type I IFN pathway to play a major role in mediating the increased bacterial burden. Coinfected mice lacking the IFNαβ receptor (*Ifnar*$^{-/-}$ mice) were protected from an increased pulmonary bacterial burden. Nonetheless, as depicted beforehand (1.2.2 Immune response to influenza virus infection), type I IFNs exert a plethora of downstream effects. Which of those downstream mediators might play a predominant role for reducing *Mtb* control remained elusive.

1.4. Objective

The epidemiological evidence that *Mtb* and IAV coinfection results in increased mortality among coinfected patients is rising. Although *Mtb*/IAV coinfection has gained more interest during the past years, in-depth experimental studies analyzing the mechanisms for the epidemiological observations are largely missing.

The current study shall deliver insights into the immunological modulations by IAV coinfection in *Mtb*-infected C57BL/6 mice:

- Does an early IAV infection impact the initial control of *Mtb*?
- Does an underlying *Mtb* infection interfere with the antiviral immunity and viral clearance?
- Does an early IAV infection interfere with innate and adaptive immunity that are essential for *Mtb* control?

The experimental study by Redford and colleagues found that the type I IFN pathway contributed to loss of *Mtb* control[196]. Nonetheless, type I IFN signaling induces the expression of over one hundred ISGs. It was therefore of interest to elucidate:

- Which other determinant, besides type I IFNs, mediates IAV-induced loss of *Mtb* control?

2 Material and methods

2.1 Consumables

If not specified otherwise, plastic consumables were bought from Corning Life Sciences, syringes and cannulas from BD Bioscience.

2.2 Reagents

Aqua B. Braun	B.Braun
Aqua destillata (dH_2O)	Water purification system for deionized water at the Research Center Borstel
Avicel RC-581	IMCD GmbH & Co KG
Bovine serum	Biowest
Brefeldin A solution (1000x)	Biolegend
BSA	Serva
BSA solution (35%)	Sigma-Aldrich
Cell activation cocktail (w/o Brefeldin A)	Biolegend
DNase I	Roche
Dulbeccos PBS (1x)	PAN Biotech
EDTA	Roth
Ethanol (EtOH)	Merck
FCS	Biochrom AG
Glycerin	Roth
Hamster serum	Jackson Immuno Research
HEPES (1 M)	PAN Biotech
IMDM	PAN Biotech
Ketamine Ketamidor®	WDT
$KHCO_3$	Sigma-Aldrich
L-glutamine (200 mM)	PAN Biotech
Liberase TL	Sigma-Aldrich
MEM	PAN Biotech
MEM w/o phenol red (2x)	Thermo Scientific
Middlebrook 7H11 agar	Difco/BD Bioscience
Monensin solution (1000x)	Biolegend
Mouse serum	PAN Biotech
NaCl	Roth
NaN_3	Merck
NH_4Cl	Roth
Penicillin/streptomycin	PAN Biotech
peqGOLD Trifast™	peqlab
Rat serum	PAN Biotech
RPMI 1640 w/o L-glutamine	PAN Biotech
Sodium pyruvate (100 mM)	PAN Biotech
Superblock T20 (TBS) blocking buffer	ThermoScientific
TPCK-trypsin	Sigma-Aldrich
Triton X-100	Roth
TrueBlue™Peroxidase substrate	KPL Immunoassay Reagents & Kits
Trypsin 0,25 %/ EDTA 0,02 %	PAN Biotech
Tween 20	Sigma-Aldrich
Tween 80	Sigma-Aldrich
Xylazin Xylavet®	CP-Pharma
β-mercaptoethanol (50 mM)	PAN Biotech
PBS-buffer (10x Dulbeccos) powder	AppliChem

2.3 Buffers, solutions and media

0.3% Triton-X	0.3% (v/v) Triton X-100 in 1x PBS
2.5% Avicel	2.5% (w/v) Avicel in dH_2O
2x MEM	0.4% (v/v) BSA solution, 2% (v/v) L-glutamine, 2% (v/v) penicillin/streptomycin in 2x MEM w/o phenol red
4% PFA	4% (w/v) PFA in 1x PBS
7H11 agar medium	1.9% (w/v) 7H11 agar, 0.5% (v/v) glycerin, 10% (v/v) bovine serum in dH_2O
complete IMDM (cIMDM)	10% (v/v) FCS (heat-inactivated), 1% (v/v) L-glutamine, 1% (v/v) HEPES, 1% (v/v) sodium pyruvate, 0.1% (v/v) β-mercaptoethanol in IMDM w/o glutamine
complete RPMI (cRPMI)	10 % (v/v) FCS (heat-inactivated), 1% (v/v) L-glutamine, 1% (v/v) HEPES, 1% (v/v) sodium pyruvate, 0.1% (v/v) mercaptoethanol in RPMI 1640 w/o glutamine
Erythrocyte lysis buffer	155 mM NH_4Cl, 10 mM $KHCO_3$, 0.1 mM EDTA in dH_2O
FACS buffer	3% (v/v) FCS (heat-inactivated), 0.1% (w/v) NaN3, 2 mM EDTA in 1x PBS
F_c blocking buffer	1% (v/v) rat serum, 1% (v/v) mouse serum, 1% (v/v) hamster serum, 1% (v/v) anti-CD16/32 (Bioleged) in FACS-buffer
Inoculum medium	0.2% (v/v) BSA solution, 1% (v/v) L-glutamine, 1% (v/v) penicillin/streptomycin (v/v) in MEM medium
Infection medium	Inoculum medium + 1 µg/ml TPCK-trypsin
Lung digestion buffer	50 µg/ml liberase TL, 100 µg/ml DNase I in IMDM/RPMI
MACS buffer	0.5% (w/v) BSA, 2 mM EDTA in 1x PBS
MDCK medium	10% (v/v) FCS (heat-inactivated), 1% (v/v) L-glutamine, 1% (v/v) penicillin/streptomycin in MEM medium
Overlay medium	2.5% Avicel and 2x MEM (1:1), 1 µg/ml TPCK-Trypsin
Trypan blue solution	1:10 of 0.5% stock solution in 1xPBS
Wash buffer	0.05% Tween 20 in 1x PBS
WTA buffer	1% (w/v) BSA, 1% (v/v) Tween 80 in dH_2O

2.4 Cell line

The Madin-Darby canine kidney (MDCK) cell line was kindly provided by Prof. Dr. Gülsah Gabriel, Heinrich Pette Institute, Hamburg. Maintenance culture of MDCK cells was done in MDCK medium. For cell passaging, MDCK cells were washed with 1x PBS and incubated with trypsin/EDTA at 37°C, 5% CO_2 until the cell layer dispersed. The addition of FCS-containing culture medium inactivated the trypsin/EDTA and cells could be cultivated as required.

2.5 Bacteria and virus

2.5.1 *Mycobacterium tuberculosis* (*Mtb*)

Mtb H37Rv was grown in Middlebrook 7H9 broth supplemented with 10% v/v OADC to logarithmic growth phase (OD600 0.2-0.4) and aliquots were frozen at -80°C (grown by Martina Ackermann, kindly provided by the Molecular and Experimental Mycobacteriology group, Research Center Borstel).

2.5.2 Influenza A virus (IAV)

For all experiments, the 2009 pH1N1 wildtype virus A/Hamburg/05/09 (A/HH/05/09 pH1N1) isolated on 28th April from pharyngal swabs of a female patient before oseltamivir treatment as described before[197] was used. For virus stock generation, MDCK cells grown to 90% confluency in T75 flasks were washed with 1x PBS and added 1.5 ml virus-supplemented inoculum (10 µL from virus stock in 1.5 ml inoculum medium). Following, cells were incubated for 30 min at 37°C and 5% CO_2 with a 10-min interval gentle movement of the flask to ensure distribution of virus. Next, the inoculum was removed and replaced by 7 ml infection medium that contained TPCK-trypsin (Sigma-Aldrich) to enable cleavage of HA into its subunits to ensure multiple replication cycles and thus efficient production of virus. Cells were incubated until cytopathic effects reached approx. 90% (after approx. 36 hours). The virus-containing cell culture supernatant was harvested and centrifuged at 1000 xg, 4°C for 5 min to pellet cells and cell debris. The supernatant was aliquoted and stored at -80°C. To determine the virus concentration, plaque-forming units (PFUs) were determined by plaque assay (2.9.2 Determination of viral load).

2.6 Mouse strains

Mice were bred under specific-pathogen-free conditions at the Research Center Borstel or CCR2 knockout (KO) and wildtype (WT) mice (on C57BL/6 background) were bred at the Bernhard Nocht Institute for Tropical Medicine, Hamburg (CCR2 KO and CCR2 WT mice were kindly provided by Prof. Dr. Hannelore Lotter). All mice were maintained under specific barrier conditions either in the BSL-3 or BSL-2 facility at the Research Center Borstel. Male C57BL/6J mice aged between 8-12 weeks and female and male p25TCR-tg mice on a C57BL/6 background[198] aged between 12-16 weeks were used.

2.7 Animal experiments

All animal experiments were approved by the Ethics Committee for Animal Experiments of the Ministry of Energy, Agriculture, Environment, and Rural Areas of the State of Schleswig-Holstein.

2.7.1 *Mtb* infection

To mimic the natural route of infection, *Mtb* was applied via the respiratory route by employment of an aerosol chamber (Glas-Col, Terre-Haute). This system allows for lung infections by droplet-borne infectious agents. Mice were infected with an uptake of 100-200 viable bacilli per lung or ca. 2000 bacilli for high-dose infection, respectively. For all animal experiments, *Mtb* H37Rv was used.

For aerosol infection, aliquots were thawed and bacteria were separated by resuspension with a 1 ml syringe and 26G cannula. The aliquot was diluted in Braun water to a total volume of 6 ml, from which 5.5 ml were used for aerosol infection. From the residual 0.5 ml, dilutions (10^{-2} up to 10^{-5}) were plated on 7H11 agar plates to assess the bacteria count in the inoculum (input control). Mice were put in special mesh steel baskets within the aerosol chamber. After completion of the aerosol infection program (900s pre-warming, 2400s nebulizing, 2400s declouding, 900s decontamination), mice were transferred back into their IV-cages. One day after aerosol infection, the bacterial uptake dose was assessed by determination of the bacterial load from the whole lung. Weekly scoring of mice evaluated their disease status by criteria of activity, body weight, body condition and behavior (Table 1). The individual score was determined as the average of the in table 1 depicted four criteria. Mice reaching a score of 3.5 were euthanized to avoid unnecessary suffering and that time point was denoted the time of death.

Table 1 Scoring criteria for *Mtb*-infected mice

Score	Activity	Body Weight	Body Condition	Behavior
1	Very active	No change or increase	Shiny and groomed fur; clear eyes; clean body orifices	Normal
2	Active	Reduction <10%	Fur defects (less or excessive grooming)	Slight deviation
3	Less active	Reduction 10-20%	Dull/greasy and ruffled fur, decreased grooming, body orifices not well-cleaned, increased muscle tone	Unusual; impaired motor functions or hyperkinetic
4	Barely active	Reduction 20-30%	Dirty fur; sticky or damp body orifices; hunched; high muscle tone; dull eyes	Isolation from peers; lethargy; hyperkinetic; stereotypies; coordinative dysfunctions
5	Lethargic	Reduction >30%	Cramps; paralysis (trunk musculature, limbs); respiratory sounds; cold body	Vocalization of pain when grabbing; self-amputation (auto-aggressive behavior)

2.7.2 Influenza virus infection

For influenza virus infection, mice were anesthetized (12.5% ketamine, 1.25% xylazine in 1x PBS (200 µL/ 20g body weight)) and inoculated intranasally (i.n.) with 50 µL of 10^4 PFU of influenza virus (A/HH/05/09 pH1N1) diluted in 1x PBS. The inoculum was slowly and evenly applied to both nostrils.

Daily scoring of mice within the acute infection phase (14 days after IAV infection) evaluated the disease status by criteria of body weight, body condition and behavior (Table 2). The individual score was determined as the sum of the in table 2 depicted three criteria. A score of 20 over 72 hours or a score over 20 would signify the experimental end-point.

Table 2 Scoring criteria for influenza virus-infected mice

Score	Body weight	Body condition	Behavior
0	No change or increase	Shiny and groomed fur; clean body orifices	Normal (sleeping, responsive to blowing and touching, curious, social)
5		Dull and ruffled fur; dull eyes	Unusual; constrained motor function
10	Reduction >15%	Sticky or damp body orifices; abnormal body posture; high muscle tone; dehydratio	Isolation from peers; vocalization of pain; apathy; expressed hyperkinetic and/or stereotypies; coordinative dysfunction
20	Reduction >25%	Cramps; paralysis (trunk musculature, limbs); respiratory sounds; cold body	Automutilation

2.7.3 Adoptive T cell transfer

For adoptive transfer experiments, $CD4^+$ T cells from spleens of p25TCR-tg mice were magnetically isolated using the $CD4^+$ T cell isolation kit (Miltenyi Biotec) according to the manufacturer's instructions. Isolated $CD4^+$ T cells were labeled with carboxyfluorescein succinimidyl ester (CFSE, CFDA-SE, Invitrogen) and 3-5x10^6 cells in 100 µL 1x PBS were adoptively intravenously (i.v.) transferred into C57BL/6 mice 24 hours before *Mtb* infection.

2.7.4 Anti-IL-10 receptor treatment

For antibody treatment, mice were intraperitoneally (i.p.) injected with 200 µg of anti-IL-10 receptor antibody (clone 1B1.3; kindly provided by Prof. Dr. Rudolf Manz, University of Lübeck) or 200 µg of polyclonal rat serum IgG (Sigma-Aldrich) on day 5 after influenza virus infection.

2.8 Organ harvest and single cell suspensions

2.8.1 Organ harvest and homogenization

Mice were CO_2-euthanized on respective days for organ harvest. The lung, lung-draining lymph nodes (dLNs) and spleen were taken depending on the experimental set-up. Organs were homogenized in 1x PBS (mixture of 1.4 mm and 2.8 mm ceramic beads, Bertin Technologies; Minilys ®, Bertin Technologies, Program: 5000 rpm, lung: 2x 50 s; spleen: 1x 50 s, dLN 1x 20 s) and homogenates were distributed for respective analyses (bacterial load, viral load, cytokines, lipid mediators, RNA). Homogenates were stored at -80°C.

In experimental set-ups aiming at immune-phenotyping cells via flow cytometry, mice were CO_2-euthanized and intracardially perfused with pre-warmed 1x PBS (23G cannula, 20 ml syringe). Following, lung and dLN were harvested and subjected to the respective treatment to obtain single cell suspensions (2.8.2 Single cell suspension from lung and 2.8.3 Single cell suspension from dLNs). Single cell suspensions were also obtained from spleens for subsequent isolation of $CD4^+$ T cells via magnetic-activated cells sorting (2.8.4 Single cell suspension from spleen).

2.8.2 Single cell suspension from lung

Lungs harvested from PBS-perfused mice were gently cut into pieces and transferred into 50 ml tubes filled with 3 ml lung digestion buffer. Samples were incubated in a 37°C water bath, shaking for 50 minutes. Subsequent to incubation, lungs were passed through a 100 µm cell strainer with the help of a 5 ml syringe plunger into a tube filled with 10 ml cold 1x PBS. Cells were pelleted (1500 rpm, 5 min, 4°C) and subjected to erythrocyte lysis treatment (2 ml buffer, 1:45 min, RT) which was stopped with the addition of 10 ml cIMDM. After centrifugation, cells were resuspended in 1 ml cIMDM and transferred into a new 50 ml tube via a 100 µm pore size cell strainer. Following, the cell number was determined.

2.8.3 Single cell suspension from dLNs

For single cell suspension from dLNs, organs in 2 ml cIMDM were passed through a 100 µm cell strainer by dint of a 5 ml syringe plunger. Cell suspension was transferred into a 15 ml tube and centrifuged (1500 rpm, 8 min, 4°C). Remaining erythrocytes were lysed (1 ml buffer, 1:45 min, RT) and reaction was stopped by addition of 10 ml cIMDM. After centrifugation, cells were resuspended in 500 µL cIMDM and the cell number was determined.

2.8.4 Single cell suspension from spleen

Single cell suspensions from the spleen were obtained for subsequent isolation of $CD4^+$ T cells by magnetic activated cell sorting (MACS). A single cell suspension from spleen was obtained by passing organs in 2 ml cRPMI through 100 µm cell strainers with a 5 ml syringe plunger. The cell suspension was centrifuged (1500 rpm, 5 min, 4°C) and the cell pellet was treated with 2 ml erythrocyte lysis buffer (2 min, RT) before reaction was stopped by addition of 10 ml cRPMI. After centrifugation, cells were resuspended in 5 ml MACS buffer and transferred into new 50 ml tubes via a 100 µm cell strainer.

2.8.5 Determination of cell numbers

The determination of the cell numbers was either performed manually with the Neubauer hemocytometer (Marienfeld-superior) or automatized by usage of the Vi-CELL® Counter (Beckmann Coulter).

For manual cell number determination, 10 µL of the single cell suspension were mixed with 90 µL trypan blue and 10 µL from that mixture were transferred onto the Neubauer hemocytometer. Unstained, viable cells were counted.

For automatized cell number determination (flow cytometry experiments) using the Vi-CELL® counter, 25 µL of the single cell suspension were diluted with 475 µL FACS buffer and viable cells were counted in the “lung cell” program.

2.8.6 $CD4^+$ T cell isolation

Isolation of $CD4^+$ T cells was conducted from single cell suspensions obtained from spleens of p25TCR-tg mice. $CD4^+$ T cells were negatively selected with a MACS® manual separator (Miltenyi Biotec) by dint of the $CD4^+$ T cell Isolation Kit (Miltenyi Biotec) according to the manufacturer’s instructions. Obtained cells were centrifuged (1500 rpm, 5 min, 4°C) and subsequently labeled with CFSE.

2.8.6.1 CFSE staining

To assess the proliferative capacity, MACS-isolated $CD4^+$ T cells were labeled with CFSE (CFDA-SE, Invitrogen). For this, cells were labeled with a final CFSE concentration of 5 µM in warm 1x PBS for 8 min at 37°C, 5% CO_2. Afterwards, cells were washed twice with warm cRPMI and finally resuspended in the appropriate volume of cRPMI for cell counting. The cell number was determined using a Neubauer hemocytometer. Finally, the cell concentration was adjusted in 1x PBS for adoptive transfer into C57BL/6 mice.

2.9 Microbiological methods

2.9.1 Determination of the bacterial load

For determination of the bacterial load, respective organs were homogenized and tenfold serial dilutions in WTA buffer were plated onto 7H11 agar plates. Colonies were counted after an incubation period of 4 weeks at 37°C.

2.9.2 Determination of the viral load

Titers of infectious virus were determined as plaque forming units (PFU) from lung homogenates in a plaque assay on MDCK cells. For this, MDCK cells were seeded into 6-well plates and were grown to approx. 95% confluency. Subsequently, the medium was removed and cells were once washed with 1x PBS before addition of tenfold serial dilutions of lung homogenate. After a 30 min incubation (37°C, 5% CO_2, 10-min interval gentle movement), the overlay medium supplemented with 1 µg/mL TPCK-trypsin (Sigma-Aldrich) was added. Following a 72-hour incubation (37°C, 5 % CO_2), cells were washed and fixed with 4% PFA. For detection of plaques, fixed cells were permeabilized with 0.3% Triton-X 100 and subsequently incubated with primary antibody against influenza A virus nucleoprotein (9G8, abcam, ca. 1.5-2 h, RT, shaking). Afterwards, cells were washed (2x with wash buffer) before incubation with secondary HRP-conjugated rabbit anti-mouse IgG (Southern Biotech, 1 h, RT, shaking). After 2 washing steps, cells were incubated with peroxidase substrate until plaques visualized (TrueBlue™Peroxidase Substrate, KPL Immunoassay Reagents & Kits, ca. 15-20 min, RT). The substrate was washed off with tab water and plates were left to dry (RT, dark) before stained plaques were counted.

2.10 Immunological methods

2.10.1 Flow cytometry

Phenotyping of immune cells was conducted with single cell suspensions obtained from lung and dLN of *Mtb*, *Mtb*+IAV and IAV-infected mice by flow cytometry at indicated time points. Data were acquired on a BD CantoII flow cytometer and analyzed with the FCS Express software (DeNovo™ Software). The gating strategies are depicted in the supplementary figures S3-S13.

2.10.1.1 Surface staining

For staining of extracellular antigens, $5x10^5$- $1x10^6$ cells were seeded in 96 well round-bottom plates. After centrifugation (1000 rpm, 5 min, 4°C), the supernatant was decanted and 50 µL Fc-blocking buffer/well were added and incubated for 20-30 min at 4°C. Following, cells were washed with FACS buffer, plates were centrifuged and supernatants were decanted. The incubation with 50 µL of surface antibody solution/well (in FACS buffer, antibodies in table 3) was performed for 30 min at 4°C in the dark. After a washing step, cells were resuspended in 200 µL FACS buffer and analyzed.

Table 3 Antibodies for flow cytometry

If not specified otherwise, antibodies were purchased from Biolegend.

Antigen	Clone	Fluorochrome	Isotype	Dilution
CD3	17A2	APC	Rat IgG2b, κ	1:400
CD3	17A2	APC-Cy7	Rat IgG2b, κ	1:320
CD4	RM4-5	PerCP-Cy5.5	Rat IgG2a, κ	1:400
CD4	RM4-5	BV510	Rat IgG2a, κ	1:320
CD8a	53-6.7	APC-Cy7	Rat IgG2a κ	1:400
CD8a	53-6.7	BV421	Rat IgG2a κ	1:200
CD8a	53-6.7	FITC	Rat IgG2a κ	1:400
CD11b	M1-70	PerCP-Cy5.5	Rat IgG2b, κ	1:400
CD11b	M1-70	BV510	Rat IgG2b, κ	1:300
CD11c	N418	BV421	Armenian Hamster IgG	1:200
CD11c	N418	PE	Armenian Hamster IgG	1:400
CD44	IM7	PerCP-Cy5.5	Rat IgG2b, κ	1:400
CD45	30-F11	BV510	Rat IgG2b κ	1:1600
CD45	30-F11	BV421	Rat IgG2b κ	1:2000
CD62L	MEL-14	APC	Rat IgG2a κ	1:400
CD69	H1.2F3	PE-Cy7	Armenian Hamster IgG	1:400
CD90.2	53-3.1	APC e780	Rat IgG2a κ	1:1200
F4/80	BM8	PE	Rat IgG2a, κ	1:400
F4/80	BM8	BV421	Rat IgG2a, κ	1:200
LAG-3	C9B7W	BV421	Rat IgG1, κ	1:100
Ly6C	HK1.4	APC	Rat IgG2c, κ	1:400
Ly6C	HK1.4	PE-Cy7	Rat IgG2c, κ	1:600
Ly6G	1A8	APC-Cy7	Rat IgG2a, κ	1:1000
Ly6G	1A8	PerCP-Cy5.5	Rat IgG2a, κ	1:400
I-A/I-E (MHC-II)	M5/114.15.2	APC-Cy7	Rat IgG2b, κ	1:400
NK1.1	PK136	BV421	Mouse IgG2a, κ	1:100

*CD90.2 eBioscience

2.10.1.2 Tetramer staining

For detection of *Mtb*-specific $CD4^+$ T cells, staining with BV421-conjugated tetramer of I-A(b) *Mtb* ESAT6 4-17 (QQWNFAGIEAAASA; National Institute of Health Tetramer Core) was performed. Tetramers consist of four subunits of respective MHC molecules bound with a specific antigen and detect antigen-specific T cells via the corresponding T cell receptor. For tetramer staining, $1x10^6$ dLN cells or $2x10^6$ lung cells were seeded in 96 well flat-bottom plates. After centrifugation (1,000 rpm, 5', 4°C), cells were taken up in 60 µL of tetramer solution (1:200 in cIMDM) and incubated for 1:45 h at 37°C, 5% CO_2. Afterwards, 50 µL of surface antibody mix were directly added into the wells, mixed and plates were incubated for another 45 min (37°C, 5% CO_2). Subsequently, cells were transferred into a 96 well round-bottom plate, washed with FACS buffer and resuspended in 2% PFA. After a 20-min fixation, cells were washed and resuspended in 200 µL FACS buffer before data acquisition.

2.10.1.3 Dextramer staining

IAV-specific $CD8^+$ T cells were detected by staining with PE-conjugated dextramer of H1N1 peptide NP366 (ASNENVETM, Immudex). The dextramer consists of a dextran polymer backbone with multiple fluorochromes and MHC-I -peptide complexes. For dextramer staining, $1x10^6$ lung cells were seeded into 96 well round-bottom plates. After centrifugation (1,000 rpm, 5', 4°C), cells were incubated with 50 µL Fc-blocking buffer (10 min, 4°C) before addition of 10 µL of dextramer. Samples were incubated for 10 min at RT in the dark. Afterwards, cells were added 7 µL of surface antibody mix and cells were incubated for 30 min at 4°C in the dark. Next, cells were washed with FACS buffer before fixation in 2% PFA for 20 min at 4°C. After a washing step with FACS buffer, cells were resuspended in 200 µL FACS buffer before data acquisition.

2.10.1.4 Intracellular staining

The detection of intracellular cytokines and transcription factors allows the analysis of cell-specific effector functions.

For staining of intracellular proteins, $5x10^5$-$1x10^6$ cells were seeded in 96 well flat-bottom plates in 100 µL cIMDM. For *ex vivo* restimulation, 100 µL of the respective stimulating agent diluted in cIMDM and supplemented with brefeldin A and monensin (1x final concentration) were added to the cells. For polyclonal stimulation, Biolegend's cell activation cocktail (containing phorbol myristate acetate (PMA) and ionomycin (Iono)) was used in 1x final concentration. To detect cytokine production in *Mtb*-specific $CD4^+$ T cells, 30 µg/ml of C-terminal modified ESAT-6_{4-16} peptide (MTEQQWNFAGIEAAASAIQGGXKXK; Structural Biochemistry, Research Center Borstel) was used. After an incubation of 5 hours (37°C, 5% CO_2), cells were transferred into 96 well round-bottom plates, centrifuged (1,000 rpm, 5 min, 4°C) and the supernatant decanted. Following, surface antigens were stained (2.10.1.1 Surface staining). Cells were washed with FACS buffer and fixed with 100 µL fixation buffer (Biolegend) at 4°C o/n. The next day, cells were washed with intracellular staining permeablization buffer (Perm buffer, Biolegend) and stained for intracellular cytokines. For this, 50 µL of cytokine antibody cocktail (in Perm buffer, antibodies in Table 4) were added/well and incubated for 40 min at 4°C in the dark. Afterwards, cells were washed with Perm buffer before resuspension in 200 µL FACS buffer for data acquisition.

For detection of the transcription factor Foxp3, the True-Nuclear™ transcription factor buffer set (BioLegend) was used. Cells were subsequent to surface staining fixed in 2% PFA (20 min, 4°C), washed and resuspended in 200 µL FACS buffer. The next day, cells were centrifuged (1000 rpm, 5 min, 4°C), and fixed with True-Nuclear™ fixation buffer for 45 min at RT. Following fixation, cells were washed with True-Nuclear™ wash buffer and stained for Foxp3 (30 min, RT, Table 4). After that, cells were washed and finally resuspended in 200 µL FACS buffer for data acquisition.

Detection of arginase-1 and NOS2 was performed without prior ex vivo restimulation of cells. After staining of surface antigens, cells were fixed in 100 µL fixation buffer (Biolegend) for 20 min at 4°C and then washed with Perm buffer. Cells were then added 25 µL of Intra-FACS block buffer (1% anti-CD16/32, 2% rat serum in Perm buffer) and incubated for 10 min at 4°C in the dark before addition of 25 µL arginase-1 antibody (in Perm buffer). Staining of arginase-1 followed a two-step protocol applying unlabeled anti-arginase-1 prior to incubation with DyLight650 donkey F(ab')2 anti-goat IgG. After an incubation of 45 min at 4°C in the dark, cells were washed with Perm buffer and 50 µL of antibody cocktail containing DyLight650 donkey F(ab')2 anti-goat IgG and NOS2 were added. Cells were incubated for 30 min at 4°C in the dark. Subsequent to a washing step with Perm buffer and one with FACS buffer, cells were resuspended in 200 µL FACS buffer for data acquisition.

Table 4 Antibodies for flow cytometry (intracellular)

If not specified otherwise, antibodies were purchased from Biolegend.

Antigen	Clone	Fluorochrome	Isotype	Dilution
Arginase-1	polyclonal	unconjugated	Goat IgG	1:100
F(ab')2 anti-goat IgG	polyclonal	DyLight650	Donkey IgG	1:200
Foxp3	MF-14	AF647	Rat IgG2b, κ	1:100
IFN-γ	XMG1.2	APC	Rat IgG1 κ	1:160
IL-10	JES5-16E3	PE	Rat IgG2b κ	1:100
NOS2	6	FITC	Mouse IgG2a	1:200
TNF	MP6-XT22	BV421	Rat IgG1 κ	1:160

*Arginase-1	Santa Cruz Biotechnology
*F(ab')2 anti-goat IgG	abcam
*iNOS/NOS type 2	BD Bioscience

2.10.2 Quantification of chemokines by LEGENDplex™

For quantification of chemokines in lung homogenates, the bead-based immunoanalysis kit LEGENDplex™ (Biolgend) was used. Lung homogenates were centrifuged (8,000 xg, 5 min, 4°C) and the supernatant was used for the assay according to the manufacturer's instructions. Data were acquired on a BD CantoII flow cytometer and analyzed with the LEGENDplex™ software (Biolegend).

2.10.3 Quantification of reactive nitrogen intermediates

To detect reactive nitrogen intermediates (RNI), lung homogenates were deproteinated using Micron YM-30 centrifugal filters (Merck; 2x 13,000 rpm, 20 min, 4°C) and the flow-through was analyzed for NO2 after reductase-treatment according to the manufacturer's protocol (Nitrate/Nitrite Colorimetric Assay Kit, Cayman in NUNC MaxiSorp 96 well flat-bottom plates, ThermoScientific). Photometric measurement followed, reading the absorbance at 540 nm on BioTek Synergy 2 microplate reader.

2.10.4 Measurement of type I/III IFN activity

Measurement of type I and III IFN activity was performed by Martina Grasshoff (technical assistant in the group of Prof. Andrea Kröger, Otto-von-Guericke-University Magdeburg/ Helmholtz Centre for Infection Research Braunschweig). Briefly, supernatants of lung homogenates were analyzed on IFN-sensitive epithelial cells from Mx2-luciferase reporter mice. Epithelial cells express luciferase under the IFN-regulated Mx2 promoter and thus activity of type I and III IFNs could be correlated to luciferase bioluminescence. Calculated activities were obtained from an IFN-β standard curve.

2.10.5 Quantification of lipid mediators

For the analysis of lipid mediators by liquid chromatography-tandem mass spectrometry (LC-MS^2), lungs were homogenized in 1x PBS and 200 µL of lung homogenate were transferred into tubes (tubes and pipette tips from Eppendorf) filled with 800 µL methanol supplemented with 0.3% butyl hydroxyl-toluene (BHT, provided by Dr. Adam Wutkowski, Research Center Borstel) and immediately vortexed. BHT was added to prevent lipid oxidization. After a two-hour incubation (RT, 800 rpm), samples were snap-frozen in liquid nitrogen and stored at -80°C until further processing.

The following steps were performed by Dr. Adam Wutkowski (Bioanalytical Chemistry, Research Center Borstel) according to a modified acidified Bligh&Dyer protocol[199]. Briefly, samples were added an internal standard (IS) mix containing PGE2-d9, RvD2-d5, LTB4-d4, 5-HETE-d8, AA-d11 at a concentration of 500 fmol/ml before lipid extraction from chloroform and MeOH/HAc (97+3; v/v)/ water-based phase separation. Combined organic phases were dried under a slight stream of nitrogen. Lipid extracts were dissolved in 40 µL of solvent A (H_2O, ACN and 1 M ammonium acetate (59:40:1, v/v/v) and the pH was set to 5.6 using acetic acid (HAc)) and 2 µL were injected for LC-MS^2 analysis. Analysis of eicosanoids was performed with a micro-LC 1100 system (Agilent Technologies) coupled to a Q Exactive Plus mass spectrometer[200] (Thermo Fisher Scientific). The interpretation of MS data (peak detection and integration) was performed with Xcalibur software (Thermo fisher Scientific). Lipid mediators (LM) were quantified according to the IS and considering the slope of a calibration curve of 10, 25, 100, 250, 500 fmol on column using the parallel reaction monitoring (PRM)-mode. Transitions for each LM for the PRM method are summarized in Table 5. LM identification was verified by a scoring algorithm[199].

Table 5 Selected parameters for the characterization of LM during an LC-MS^2 run

Eicosanoids/ Docosanoids	IS	Lipid species	RT (min)	Precursor ion (m/z)	Product ion (m/z)	(N) CE
PUFA-O3	RvD2-d5		2.73	380.2480	175.0762	23
PG	PGE2-d9		2.43	360.2731	189.1274	33
		6-keto-PGE1α	1.56	367.2126	143.0704	23
		RvE1	1.83	349.2020	195.1027	22
		TBX2	1.88	369.2283	195.1028	22
		20-OH-LTB4	1.89	351.2177	195.1016	22
		LxA5	2.03	349.2020	115.0401	22
		PGE3	2.25	349.2020	269.1909	22
		PGF2alpha	2.30	353.2333	247.2062	35
		PGE2	2.47	351.2177	175.1121	22
		LxB4	2.72	351.2177	221.1183	22
		PGI2	2.90	351.2177	215.1070	22
		PGD2	2.81	351.2177	233.1177	22
		RvD2	3.03	375.2177	175.0761	22
		LxA4	3.14	351.2177	115.0401	22
		15-keto-PGE2	3.15	349.2020	113.0957	22
		RvD1	3.32	375.2177	233.1548	22
		PGB2	3.38	333.2071	175.1028	22
		13,14-DiH-15k-PGE2	3.77	351.2177	209.1175	22
		13,14-DiH-15k-PGD2	4.55	351.2177	207.1017	22
PUFA-O2	LTB4-d4		7.39	339.2468	197.1142	25
		5,15-DiHETE	7.01	335.2228	115.0385	25
		17,18-DiHETE	7.10	335.2228	247.1698	25
		trans-LTB4	7.20	335.2228	195.1016	25
		7-Mar1	7.35	359.2228	250.1387	22
		12-epi-LTB4	7.50	335.2228	195.1016	25
		LTB4	7.53	335.2218	195.1016	25
		epi-LTB4	7.75	335.2228	195.1016	25
		PD1	7.82	359.2228	153.0908	22
		14,15-DiHETE	8.5	335.2228	207.1387	25
		5,6-DIHETE	10.48	335.2228	145.0501	25
		12-oxo-LTB4	10.90	333.2071	179.0702	22

PUFA-O1	5-HETE-d8		33.40	327.2770	116.0448	21
		18-HEPE	22.30	317.2122	259.1700	22
		15-HEPE	27.94	317.2122	219.1383	22
		12-HEPE	31.18	317.2122	179.1065	22
		13-HODE	32.26	295.2279	195.1401	30
		9-HODE	32.45	295.2279	171.1015	30
		15-HETE	32.90	319.2279	219.1394	22
		17,18-EpETE	32.97	317.2122	215.1706	22
		17-HDoHE	33.10	343.2279	245.1542	22
		13-HDoHE	33.20	343.2279	193.1233	22
		10-HDoHE	33.29	343.2279	153.0908	22
		14-HDoHE	33.32	343.2279	205.1226	22
		8-HETE	33.33	319.2279	155.0715	22
		12-HETE	33.37	319.2279	179.1067	22
		7-HDoHE	33.41	343.2279	141.0544	22
		5-HETE	33.49	319.2279	115.0401	22
		4-HDoHE	33.67	343.2279	101.0228	22
		12-oxo-ETE	33.96	317.2122	237.1318	22
		5-oxo-ETE	33.96	317.2122	203.1806	22
		14,15-EET	33.97	319.2279	175.1480	22
		11,12-EET	34.20	319.2279	167.1078	22
		5,6-EET	34.25	319.2279	191.1803	22
		8,9-EET	34.29	319.2279	123.0801	22
PUFA	AA-d11		35.65	314.3009	270.3120	21
		EPA	35.10	301.2173	257.2273	22
		DHA	35.45	327.2329	283.2430	21
		AA	35.70	303.2329	259.2430	22
		LA	36.08	279.2326	127.0750	40

2.11. Molecular methods

2.11.1 RNA isolation

Total RNA from lung tissue was extracted from peqGOLD Trifast™ using the Direct-zol™ RNA MiniPrep Kit (Zymo Research) according to the manufacturer's protocol including a DNA digestion step. RNA was stored at -80°C until further usage.

2.11.2 cDNA synthesis

Isolated RNA was reverse transcribed using the Maxima First Strand cDNA Synthesis Kit for RT-qPCR (Life Technologies) according to the manufacturer's instruction. For cDNA synthesis, 1 µg of RNA was reverse transcribed (10 min at 25°C, 30 min at 50°C, 5 min at 85°C).

2.11.3 Quantitative real-time PCR

Quantitative realt-time-PCR (qRT-PCR) was performed to determine the relative amount of specific mRNA transcripts of interest by using LightCycler® 480 SYBR Green I Master (Roche). Per sample, 1 µL of template cDNA was mixed with 0.2 µL pre-diluted primer mix (forward and reverse, 10 µM each, Table 6), 5 µL 2x SYBR Green Master and 3.8 µL dH_2O. Measurement was performed on the Roche® LightCycler® 480 instrument (Table 7). Analysis of the relative changes was performed using LightCycler480 Software 1.5.0 SP4 (Version 1.5.0.39, Roche). For calculation, primer-dependent amplification efficiency was integrated into the software's calculations. The amplification efficiency was determined by primer-individual standard curves performed with serial dilutions of pooled cDNA. All quantifications were normalized to the level of *Gapdh* gene expression.

Table 6 Primer for qRT-PCR

Gene	Forward (5'→3')	Reverse (5'→3')
Arg1	ACAAGACAGGGCTCCTTTCAG	CTGTGATGCCCCAGATGGTT
Fizz1	ATGAACAGATGGGCCTCCTG	TCTTAGGACAGTTGGCAGCA
Gapdh	ATTGTCAGCAATGCATCCTG	ATGGACTGTGGTCATGAGCC
Il10	GGTTGCCAAGCCTTATCGGA	ACACCTTGGTCTTGGAGCTTATT
Il1a	CGCTTGAGTCGGCAAAGAAATC	ACCTGCTCCACTGCCTTGCT
Il1b	ATCAACCAACAAGTGATATTCTCCAT	GGGTGTGCCGTCTTTCATTAC
Il1rn	TGTGCCAAGTCTGGAGATGA	TTCTTTGTTCTTGCTCAGATCAGT
Mx1	ATGGGTGAACTCAGGCAATCTC	TTGACAGTCTCCTGCTTAGTGAC
Nos2	CTGCAGCACTTGGATCAGGA	TCCTTTGAGCCCTTTGTGCT

Table 7 qRT-PCR protocol

Step	Temperature	Time	Cycles
Pre-incubation/ Denaturation	95°C	10 min	1
Amplification	95°C	10 s	45
	63°C	10 s	45
	72°C	8 s	45
	72°C	1 s	45
Dissociation	95°C	10 s	1
	65°C	10 s	1
Melting curve analysis	Stepwise rising from 65°C to 95°C		

2.12 Statistics

First, data were tested for normal distribution using the Shapiro-Wilk test. Normally distributed data were analyzed with an unpaired Student's t-test (for comparison of two groups) or one-way ANOVA (comparison of three groups) followed by Tukey's multiple-comparison test. All tests were 2-tailed at the significance level $p < 0.05$. To examine the influence of two different independent variables a two-way ANOVA followed by Tukey's multiple-comparison test or Sidak's multiple comparison test was performed. A log-rank test (Mantel-Cox) was used for survival analysis. All data were analyzed using GraphPad Prism 8 (GraphPad Software, Inc.).

3 Results

In 2017, approximately 10 million people were diagnosed with active TB[1]. However, not everyone who is infected with *Mtb* develops active disease. In fact, only an estimate of 5% of infected individuals directly progress to disease[23]. Most people are latently infected, characterized as asymptomatic and non-contagious but are at lifetime risk to experience reactivation of *Mtb*-infection[19,22]. For the global TB management, it is thus of utmost importance to characterize the potential risk factors that impair host antimycobacterial control and promote direct progression or reactivation of *Mtb* infection.

Recently, there is increasing epidemiological evidence that a concurrent influenza virus infection was associated with increased mortality among TB patients[185,187–191,193,201]. Nonetheless, only a few experimental studies addressed the host's immune response during *Mtb*-IAV coinfection so far[195,196].

3.1 IAV coinfection impacts control of TB in C57BL/6 mice

This present study thus aimed to broaden the knowledge of an *Mtb*-IAV coinfection seeking to answer the question whether an IAV coinfection would interfere with the initial control of *Mtb*.

To address this question, I used C57BL/6 mice which are regarded to be resistant to TB since they are able to control bacterial growth, present limited lung pathology and show a long survival in an *Mtb* low-dose experimental setting[55]. Mice were infected via the aerosol route with the *Mtb* strain H37Rv and 12 days thereafter coinfected intranasally (i.n.) with the IAV strain A/HH/05/09 pH1N1 (Figure 4A). This time point of coinfection challenged the establishment of the *Mtb*-specific adaptive immune response and with that the initiation of *Mtb* control.

IAV infection of *Mtb* pre-infected mice (*Mtb*+IAV, in the text referred to as IAV-coinfected mice) rapidly resulted in a significantly increased pulmonary bacterial burden already on day 6 after IAV coinfection (day 18 *Mtb* infection, Figure 4B). The elevated bacterial level in the lungs of coinfected mice was more pronounced by day 9 after IAV coinfection (day 21 *Mtb* infection) and was still sustained 63 days after the viral infection (day 75 *Mtb* infection). The bacterial burden in the spleen of IAV-coinfected mice was not affected on day 9 after IAV coinfection (day 21 *Mtb* infection, Figure 4C). However, on day 36 and 63 after IAV coinfection (day 48 and day 75 *Mtb* infection), the splenic bacterial burden of coinfected mice was also elevated compared to *Mtb*-alone-infected mice. Although the bacterial burden was significantly increased in coinfected animals, coinfection did not impact the survival in the low-dose experimental setting (Figure 4D). Both *Mtb*-alone and IAV-coinfected mice survived until day 300 after *Mtb* infection.

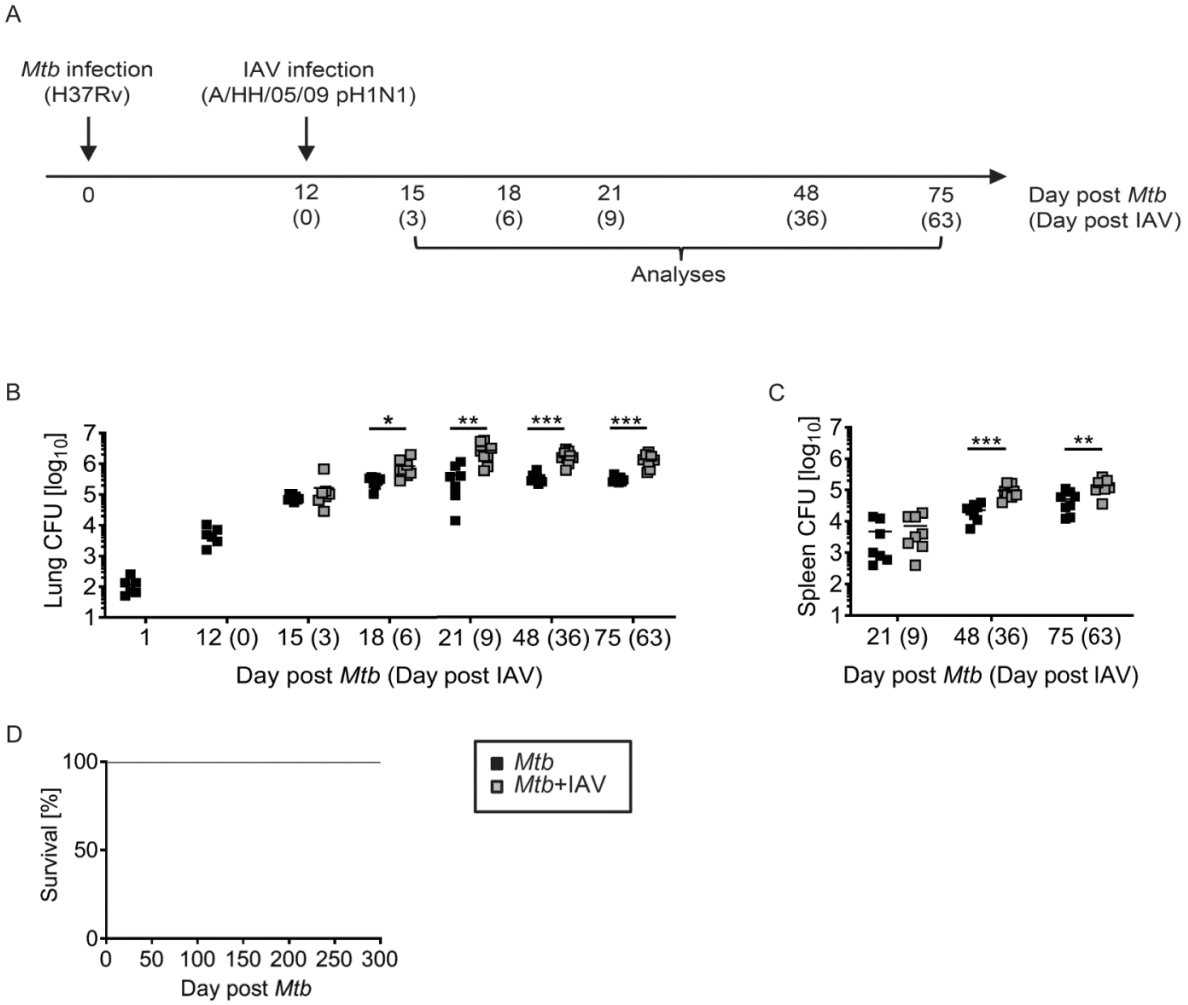

Figure 4 IAV coinfection impairs bacterial control in *Mtb*-infected mice. (A) Schematic time-line of experimental set-up. C57BL/6 mice were infected via aerosol with a low-dose of *Mtb* H37Rv and 12 days later coinfected i.n. with 10^4 PFU IAV (A/HH/05/09 pH1N1). At indicated time points, bacterial burden in (B) lung and (C) spleen were determined (n= 6 (d1, d12 *Mtb*), n= 7-9 per group, data pooled from two independent experiments). (D) *Mtb* and *Mtb*/IAV-infected mice were monitored for survival. All mice survived until day 300 after *Mtb* infection (n=8 per group, data pooled from two independent experiments). (B, C) Each data point represents one mouse. *p ≤0.05; **p ≤ 0.01, ***p ≤0.001 determined by (B,C) unpaired t-test. (Parts of data are published in Ring *et al.*,2019[202].)

Next, the impact of the same IAV infection dose was evaluated in an *Mtb* high-dose infection in C57BL/6 mice. As seen for the low-dose *Mtb* infection, IAV coinfection resulted in significantly increased pulmonary bacterial loads compared to *Mtb*-alone-infected mice on day 9 and 36 after IAV coinfection (day 21 and day 48 *Mtb* infection, Figure 5A). Strikingly, IAV challenge of *Mtb* high-dose-infected mice had significant impact on the survival (Figure 4B). While high-dose *Mtb* infection alone affected the survival only marginally and very late during infection (day 233 *Mtb* infection), some of the coinfected mice succumbed already early after IAV coinfection (day 16-29 after IAV= day 28-41 *Mtb* infection). Moreover, IAV coinfection still affected the survival at later time points (from day 92 onwards after IAV infection = from day 104 *Mtb* infection) implying long-term effects on the host's TB control.

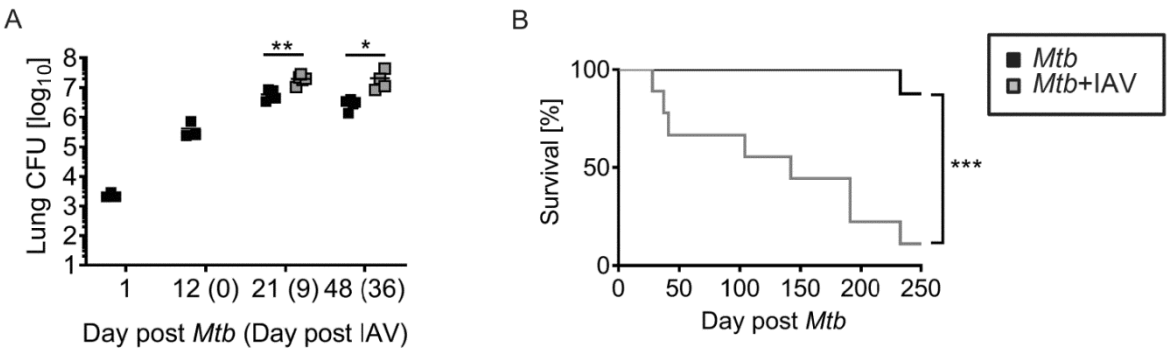

Figure 5 IAV coinfection impairs *Mtb* control and decreases survival in an *Mtb* high-dose model. C57BL/6 mice received a high-dose *Mtb* H37Rv aerosol infection and were coinfected i.n. with 10^4 PFU IAV (A/HH/05/09 pH1N1) 12 days later. (A) At indicated time points, pulmonary bacterial burden (n= 3 (d1, d12 *Mtb*), n=4-5 per group, data from one experiment) was determined. (B) Mice were monitored for survival (n=8-9 per group, data from one experiment) until day 250 after *Mtb* infection. (A-B) Each data point represents one mouse. *p ≤0.05; **p ≤ 0.01, ***p ≤0.001 determined by (A) unpaired *t* test and (B) log rank (Mantel-Cox) test. (Data are published in Ring *et al*.,2019.)

The data demonstrate that IAV coinfection in C57BL/6 mice impaired host control of *Mtb* growth in both lung and spleen and decreased the survival in an *Mtb* high-dose experimental setting. Next, I addressed whether the underlying *Mtb* infection might have also affected the control of the IAV infection.

Results 3.1: Summary

IAV infection on day 12 after *Mtb* infection resulted in loss of bacterial control and TB exacerbation in C57BL/6 mice as seen by

- a rapid and sustained increased pulmonary bacterial burden
- elevated bacterial levels in the spleen
- and a decreased survival in an *Mtb* high-dose model.

3.2 *Mtb* infection does not interfere with the antiviral immune response and viral clearance in *Mtb*-IAV coinfected mice

The loss of *Mtb* growth control during IAV coinfection could be due to an exacerbated viral infection. Consequently, I analyzed whether the coinfected host was able to control IAV infection despite the presence of an *Mtb* infection.

One way to evaluate an IAV infection in mice is based on the weight of experimental animals. Thus, the body weights of *Mtb*-alone, IAV-coinfected and IAV-alone-infected mice were recorded over time. Mice that were infected with IAV lost up to 20% of their initial body weight (Figure 6). On day 7 after IAV infection, both IAV-alone and IAV-coinfected mice showed maximal weight loss. After that time point, IAV-(co)infected mice regained weight, and reached their approximate starting weight about 2 weeks after viral infection (ca. 97% of starting weight). In contrast, the body weight of *Mtb*-alone-infected animals did not change during this observation time. The body weight course of *Mtb*-alone mice significantly differed from IAV-(co)infected animals. However, the underlying *Mtb* infection did neither increase the body weight loss nor delayed the regain of the starting weight in IAV-coinfected compared to IAV-alone-infected mice.

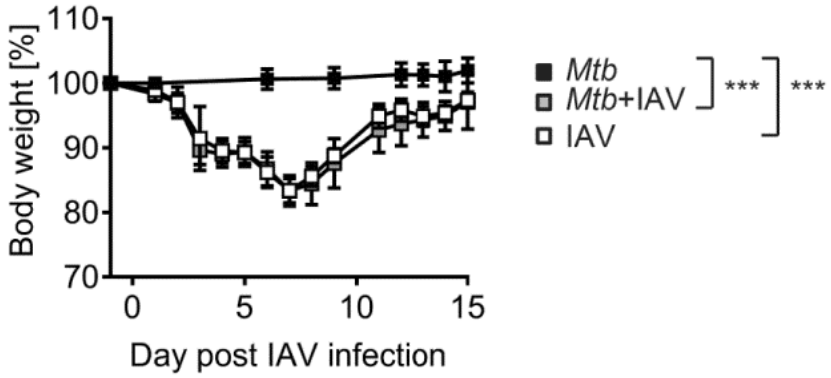

Figure 6 IAV infection results in transient body weight loss. C57BL/6 mice were infected via aerosol with a low-dose of *Mtb* H37Rv and 12 days later infected i.n. with 10^4 PFU IAV (A/HH/05/09 pH1N1). (A) Weight of IAV-(co)infected mice was monitored daily until day 15 after IAV infection (n=15-28 (on day-1 IAV); n=4-12 (on day 15 IAV) per group, representative of two independent experiments). Data are represented as mean ± SD.*p ≤0.05; **p ≤ 0.01, ***p ≤0.001 determined by One-way ANOVA followed by Tukey's multiple-comparison test.

The predominant players of the antiviral immunity are the type I IFNs which are expressed upon recognition of viral particles e.g. via the detection of viral RNA by TLR3 or RIG-I[139,142]. Thus, in order to assess whether coinfected animals were able to equally respond to the IAV infection like IAV-alone-infected mice, the activity of type I and type III IFNs in lung homogenates was analyzed (in cooperation with Prof. Andrea Kröger, Otto-von-Guericke University Magdeburg, Helmholtz Centre for Infection Research, Braunschweig). I could observe a significantly increased activity of type I/III IFNs in both IAV-alone and IAV-coinfected compared to *Mtb*-alone-infected animals already on day 3 after IAV infection (day 15 *Mtb* infection, Figure 7A).There was no difference in IFN I/III activity between IAV-alone and IAV-coinfected animals suggesting that the presence of an *Mtb* infection did not interfere with the induction of the antiviral immune response. In the course of the IAV infection, the

activity of type I/III IFNs decreased in IAV-(co)infected animals and was markedly lower by day 9 compared to day 3 after IAV infection. Type I IFNs exert their antiviral effects by activating the expression of multiple IFN-stimulated genes (ISGs)[146]. The ISG Mx1 was shown to be exclusively expressed in response to type I/III IFNs and not to the type II IFN IFN-γ[203]. To determine whether the type I/III IFNs would exert similar downstream effects in coinfected compared to IAV-alone-infected mice, Mx1 expression in the lung was analyzed by qRT-PCR. On day 3 after IAV (co)infection (day 15 *Mtb* infection) *Mx1* transcripts in both co-and IAV-alone-infected animals were significantly increased compared to *Mtb*-infected mice (Figure 7B). There was no difference in relative expression levels between coinfected and IAV-infected animals for the observed time points. With the reduction in type I/III IFN activity (Figure 7A), *Mx1* expression also decreased over time.

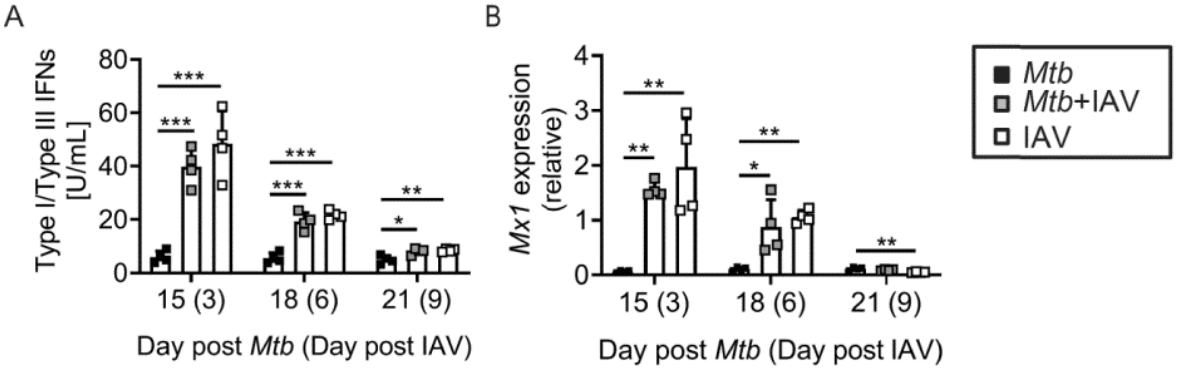

Figure 7 IAV infection induces a type I/III IFN response. C57BL/6 mice were infected via aerosol with a low-dose of *Mtb* H37Rv and 12 days later coinfected i.n. with 10^4 PFU IAV (A/HH/05/09 pH1N1). Lungs collected at indicated time points were analyzed for (A) the activity of type I/III IFNs and (B) *Mx1* expression by qRT-PCR relative to *Gapdh* expression (n= 4 per group, representative of two independent experiments). Data are represented as mean + SD. *p ≤0.05; **p ≤ 0.01, ***p ≤0.001 determined by One-way ANOVA followed by Tukey's multiple-comparison test. (Data are published in Ring *et al*.,2019.)

Among the exerted downstream effects, the initiation of the adaptive immune response is of utmost importance to efficiently clear IAV from the host. Especially cytotoxic $CD8^+$ T cells are responsible for killing virus-infected cells and thus prevent further viral replication and spread[153,155,158]. Hence, I investigated the $CD8^+$ T cell response by flow cytometry in the lung of *Mtb* and IAV-(co)infected mice. The total numbers of $CD8^+$ T cells in the lungs significantly increased in IAV-(co)infected compared to *Mtb*-alone-infected mice on day 6 after IAV infection (day 18 *Mtb* infection, Figure 8A). This increase was even more pronounced on day 9 after the viral infection (day 21 *Mtb* infection) and resulted in a significantly increased frequency of $CD8^+$ T cells among $CD45^+$ cells in IAV-(co)infected compared to *Mtb*-alone-infected mice (Figure 8A). In order to evaluate the activation status of $CD8^+$ T cells, T cells were characterized by the expression of the C-type lectin CD69, the adhesion molecule CD44 and the L-selectin CD62L. Early activated T cells express CD69 and later CD44 in the absence of CD62L expression[204,205]. CD62L is rapidly shed from T cells upon activation and is thus used to define naïve T cells. Co-expression of CD62L and CD44 at distinct expression levels may allow for differentiation of memory T cell subsets which was, however, not the focus of this present study.

In the lungs of IAV-(co)infected compared to *Mtb*-alone-infected mice, significantly increased frequencies of $CD69^+$ (Figure 8B) and $CD44^+CD62L^-$ (Figure 8C) among $CD8^+$ T cells were detected on all analyzed days. By day 9 after IAV infection (day 21 *Mtb* infection), ca. 80% of $CD8^+$ T cells were activated ($CD44^+CD62L^-$) in the lungs of IAV-(co)infected mice. The underlying *Mtb* infection in coinfected animals did not compromise the activation status since proportions of activated $CD8^+$ T cells did not differ between IAV-only and coinfected mice.

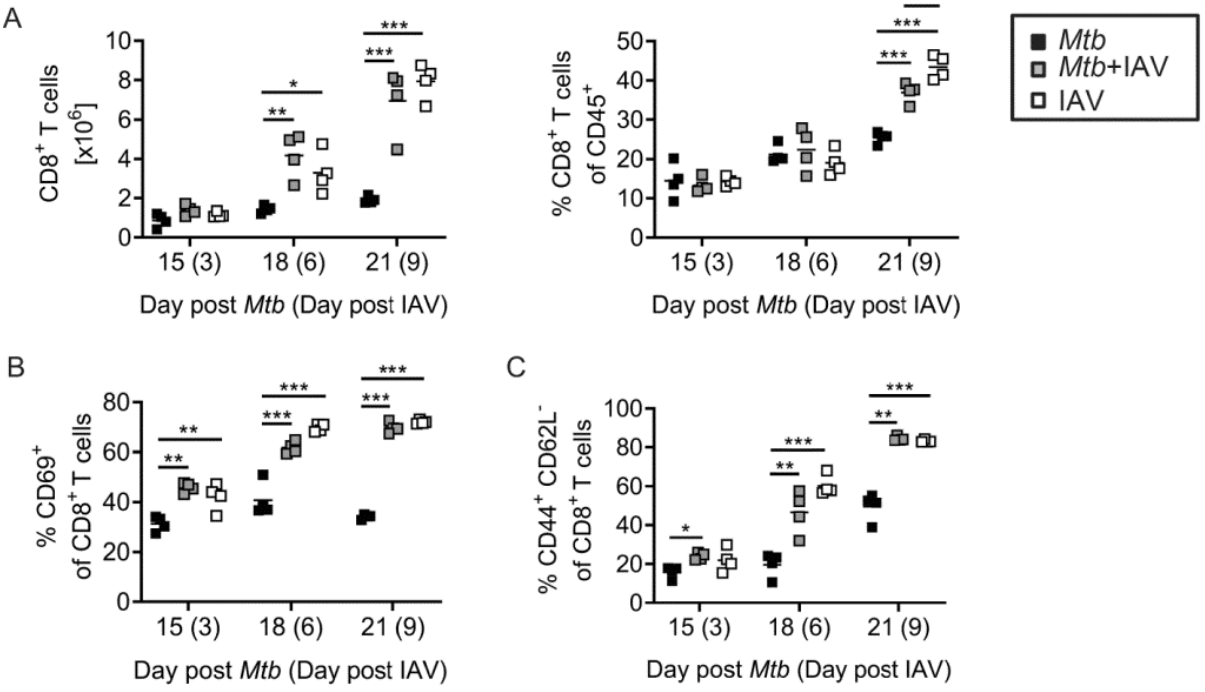

Figure 8 IAV infection induces a $CD8^+$ T cell response. C57BL/6 mice were infected via aerosol with a low-dose of *Mtb* H37Rv and 12 days later coinfected i.n. with 104 PFU IAV (A/HH/05/09 pH1N1). Lungs collected at indicated time points were analyzed by flow cytometry for (A) total lung $CD8^+$ T cell numbers and $CD8^+$ T cell frequencies among $CD45^+$ cells (n=4 per group, representative of two independent experiments). $CD8^+$ T cells were further characterized by frequencies of (B) $CD69^+$ and (C) $CD44^+CD62L^-$ cells (n=4 per group, representative of two independent experiments). Each data point represents one mouse. *p ≤0.05; **p ≤ 0.01, ***p ≤0.001 determined by One-way ANOVA followed by Tukey's multiple-comparison test.

In order to determine whether the $CD8^+$ T cells were IAV-specific, lungs were analyzed for the presence of H1N1-NP366 cells among $CD8^+$ T cells by dextramer staining and flow cytometry. The dextramer consists of a dextran polymer backbone with multiple fluorochromes and MHC-I-peptide complexes. It serves to detect $CD8^+$ T cells which harbor the specific TCR that recognizes the H1N1 peptide NP366, which is part of the influenza A virus nucleoprotein. By day 6 after IAV infection, the number and frequency of H1N1-NP366-specific $CD8^+$ T cells in IAV-(co)infected lungs was only slightly increased compared to *Mtb*-alone-infected mice (Figure 9A). However, 3 days later, H1N1-NP366-specific $CD8^+$ T cells in lungs of coinfected mice were significantly increased in both frequency and number compared to *Mtb*-only-infected animals. This is in line with the markedly increased proportion and number of total $CD8^+$ T cells on day 9 after IAV infection (Figure 8A), showing that with the general rise in $CD8^+$ T cells, the number of IAV-specific $CD8^+$ T cells also increased. The

data again demonstrate that animals that were *Mtb*-infected prior to IAV infection did not show a compromised antiviral immune response. In fact, coinfected mice tended to present even more H1N1-NP366-specific cells among $CD8^+$ T cells compared to IAV-alone-infected mice. Ultimately, the determination of the viral load in lungs of IAV and coinfected mice supported the notion of an unimpaired antiviral immunity because the *Mtb* infection did also not interfere with viral clearance. This was seen by similar viral loads in lungs of coinfected and IAV-alone-infected mice both at the initial time point 3 days after IAV infection, but also on day 9 after IAV infection on which no infectious viral particles could be detected (Figure 9B).

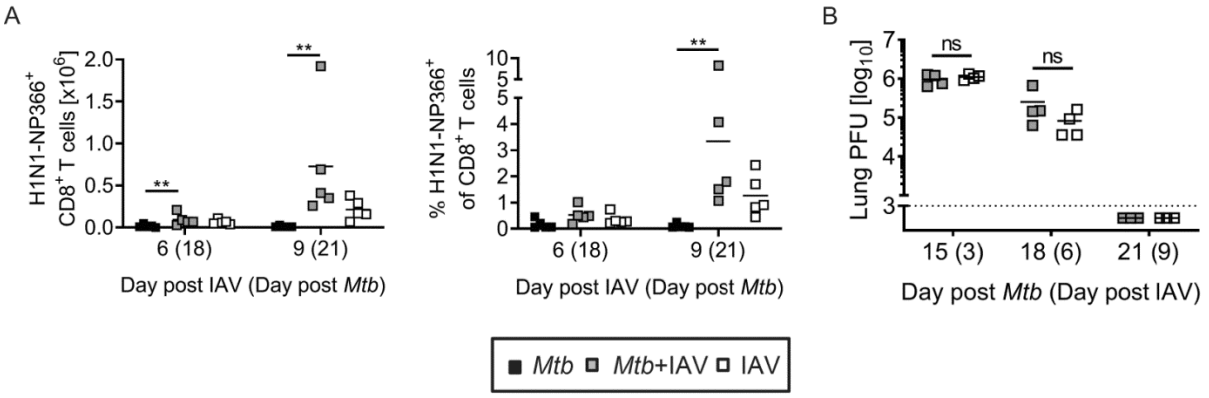

Figure 9 Presence of *Mtb* does not impair IAV-specific $CD8^+$ T cell response and viral clearance. C57BL/6 mice were infected via aerosol with a low-dose of *Mtb* H37Rv and 12 days later coinfected i.n. with 10^4 PFU IAV (A/HH/05/09 pH1N1). Lungs collected at indicated time points were analyzed by (A) flow cytometry for H1N1-NP366 dextramer-specific $CD8^+$ T cells (n=5 per group, one experiment) and (B) shows viral titers determined by MDCK plaque assay (n=3-4 per group, representative of 4 (d3 and d6) and 2 (d9) independent experiments). Each point represents one mouse. *p ≤0.05; **p ≤ 0.01, ***p ≤0.001 determined by (A) One-way ANOVA followed by Tukey's multiple-comparison test and (B) unpaired *t* test. (Data are published in Ring *et al*., 2019.)

The data indicate that an uncontrolled, exacerbated viral infection was not the cause for the loss of *Mtb* control in IAV-coinfected mice. Consequently, I analyzed whether the IAV infection altered the immune response in *Mtb*-infected animals.

Results 3.2: Summary

- The presence of an *Mtb* infection did not impact the clinical presentation of an IAV infection (similar body weight course as IAV-alone-infected mice).

- Coinfected mice showed significant inductions of antiviral immune defense mediators that did not differ from IAV-alone-infected mice with regard to
  - type I/III IFN activity
  - induction of the IRG Mx1
  - $CD8^+$ T cell response
    - numbers and frequencies among $CD45^+$ cells
    - activation
    - IAV-specific $CD8^+$ T cells
  - and viral clearance (PFU).

.

3.3 IAV coinfection results in increased cellular infiltration into the lung

The downstream effects of influenza-induced type I IFN signaling also encompass the production of different chemokines which results in the increased infiltration of immune cells to the site of infection[146].

I measured significantly increased lung per body weight ratios in IAV-(co)infected compared to *Mtb*-alone-infected mice (Figure 10A). Due to the fact that IAV-infected mice suffered from marked weight loss (Figure 6), the decrease in body weight could have entailed this ratio. However, the lung weight itself showed to be significantly higher in IAV-(co)infected compared to *Mtb*-alone-infected mice on all measured days (Figure 10B). In line with this observation, IAV-(co)infected lungs showed significantly enhanced numbers of viable cells compared to the lungs of *Mtb*-alone-infected mice on day 6 and 9 after IAV infection (day 18 and 21 *Mtb* infection, Figure 10C). While cell numbers were relatively similar in lungs of *Mtb*-alone-infected mice throughout the time points observed, the cell numbers approximately doubled in IAV-(co)infected lungs from day 3 to day 6 after IAV infection and stayed at this increased level until day 9 after IAV (co)infection (day 21 *Mtb* infection). Altogether, these data indicate an IAV-mediated influx of cells into the lungs.

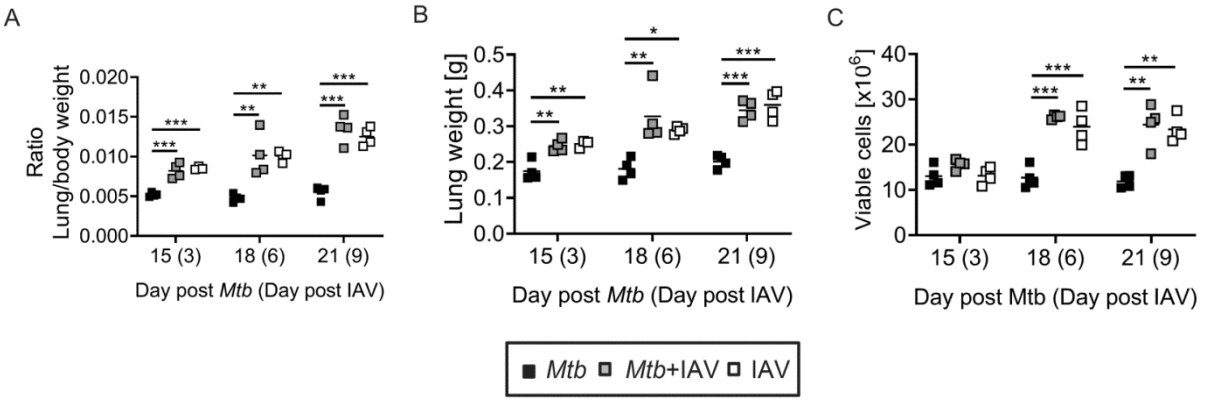

Figure 10 IAV coinfection results in increased cellular infiltration into the lung. C57BL/6 mice were infected via aerosol with a low-dose of *Mtb* H37Rv and 12 days later coinfected i.n. with 10^4 PFU IAV (A/HH/05/09 pH1N1). Mice were sacrificed and lungs were collected at indicated time points and analyzed for (A) lung/body weight ratio (n=4 mice per group, representative of two independent experiments) (B) lung weight (n=4 mice per group, representative of two independent experiments) and (C) the number of viable cells as determined by Vi-CELL® Counter (n=4 mice per group, representative of two independent experiments). Each data point represents one mouse. *p ≤0.05; **p ≤ 0.01, ***p ≤0.001 determined by One-way ANOVA followed by Tukey's multiple-comparison test.

In order to characterize the cellular infiltrates in the infected lungs, flow cytometric analyses were performed and T cells, myeloid cells and alveolar macrophages (AMs) were distinguished. The cell populations were calculated as fraction among $CD45^+$ cells to get an impression how an IAV (co)infection might shift the proportions in the lung.

The pie charts in Figure 11 display that the IAV (co)infection increases the proportion of $CD11b^+CD11c^+$ cells among $CD45^+$ cells while decreasing the frequency of AMs compared to *Mtb*-alone-infected animals. This viral-mediated impact was seen as early as 3 days after IAV coinfection (day 15 *Mtb* infection). In the *Mtb*-alone-infected lung, there was only very marginal change in the cellular composition from day 15 to day 18 after *Mtb* infection. However, on day 21 after *Mtb* infection, the proportion of both the T cell compartment as well as the myeloid cells, among which especially $CD11b^+CD11c^+$ cells, were increased compared to the earlier time points of analyses. In contrast, in the lungs of IAV-(co)infected animals, there was a gradual and rapid change in cellular composition over time. First, innate cells were predominantly represented which was especially seen on day 6 after IAV infection. They preceded the prominent influx of T cells on day 9 after IAV (co)infection. The frequencies of $CD8^+$ T cells exceeded the proportion of $CD4^+$ T cells which was not seen in the lungs of *Mtb*-alone-infected mice. The fraction of “other cells” that I did not focus on may, for example, include B cells.

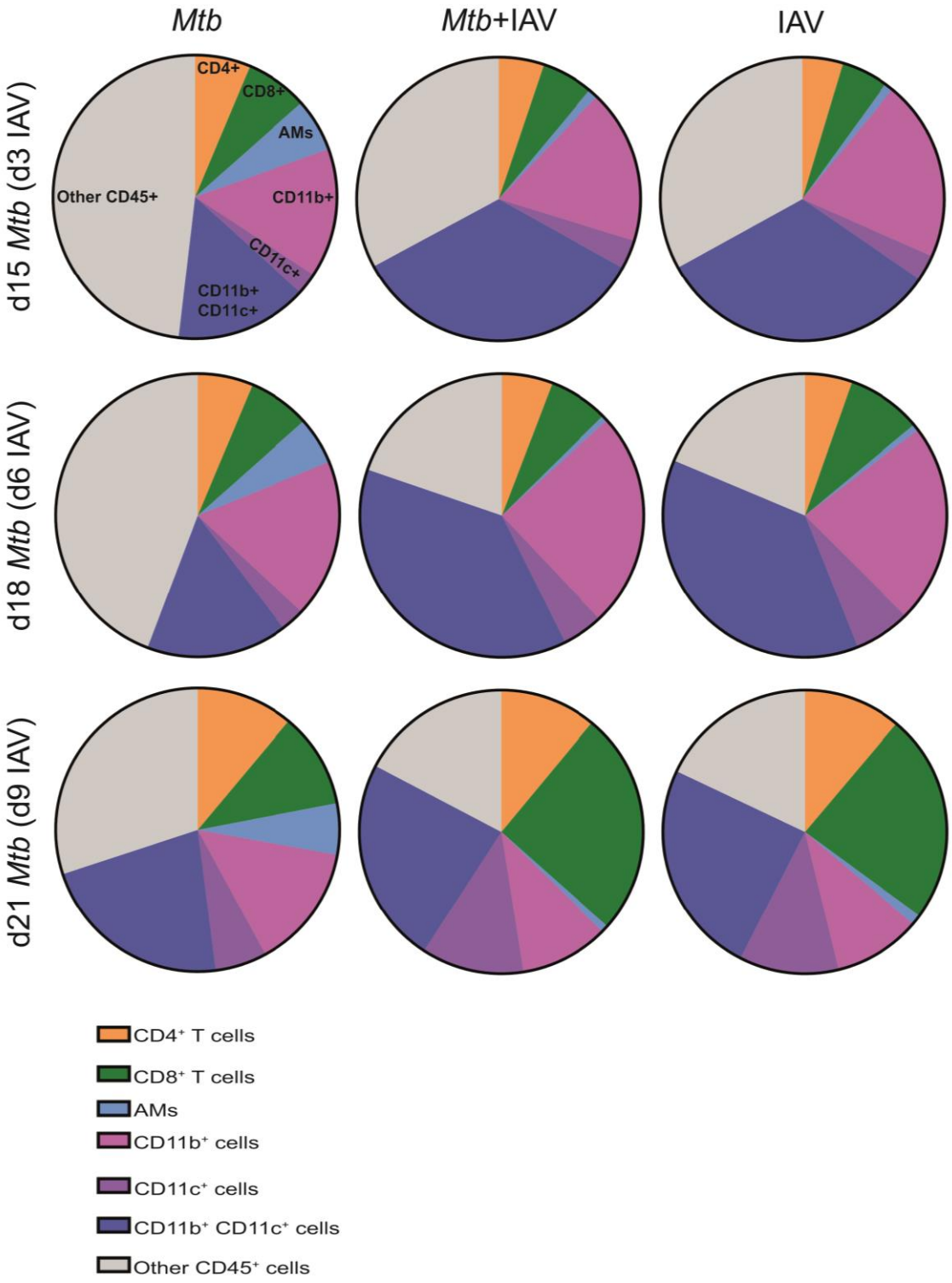

Figure 11 IAV coinfection changes the cell proportions in the lung. C57BL/6 mice were infected via aerosol with a low-dose of *Mtb* H37Rv and 12 days later coinfected i.n. with 10^4 PFU IAV (A/HH/05/09 pH1N1). Mice were sacrificed and lungs were collected at indicated time points and analyzed by flow cytometry for the frequencies of innate and adaptive immune cells among $CD45^+$ cells. Cells of interest were $CD4^+$ T cells (orange), $CD8^+$ T cells (green), Alveolar macrophages (AMs, light blue), $CD11b^+$ cells (pink), $CD11c^+$ cells (purple) and $CD11b^+CD11c^+$ cells (dark purple). The fraction 'Other $CD45^+$ cells' (grey) was calculated as the difference between 100% and the %sum of the above mentioned cell types. Data are represented as mean in parts of a whole (n=4 mice per group, data representative of two independent experiments).

AMs are the first cells to be infected upon inhalation of *Mtb*-containing droplets[25]. In the presence of an IAV infection, I detected a significant reduction in AM ($CD11b^{int}$ Auto-fluorescent $CD11c^{+}$ $MHC\text{-}II^{+}$) frequencies and could see that those cells were depleted by day 3 after IAV (co)infection (day 15 *Mtb* infection, Figure 12A, 12B) This was a rapid effect since AM frequencies were still similar between *Mtb*-alone and IAV-(co)infected mice on day 1 after IAV (co)infection (day 13 *Mtb* infection). Contrary to this observation, the frequencies of myeloid cells as identified by expression of the integrins CD11b and/or CD11c were significantly increased in IAV-(co)infected compared to *Mtb*-alone-infected mice early after IAV infection (Figure 12C-E). On day 3 and 6 after the viral infection (day 15 and 18 *Mtb* infection), especially, $CD11b^{+}CD11c^{+}$ cell frequencies were approximately three times higher in the lungs when animals were infected with IAV compared to *Mtb*-only-infected lungs (Figure 12D). The proportion of $CD11b^{+}$ and $CD11b^{+}CD11c^{+}$ cells among $CD45^{+}$ cells decreased over the time course and $CD11b^{+}$ cells even reached significantly lower frequencies compared to *Mtb*-alone-infected lungs by day 9 after IAV (co)infection (day 21 *Mtb* infection, Figure 12C and D). In contrast, $CD11c^{+}$ cells displayed a continuously rising proportion in all three infection groups, but especially increased in mice which were IAV-(co)infected (Figure 12E).

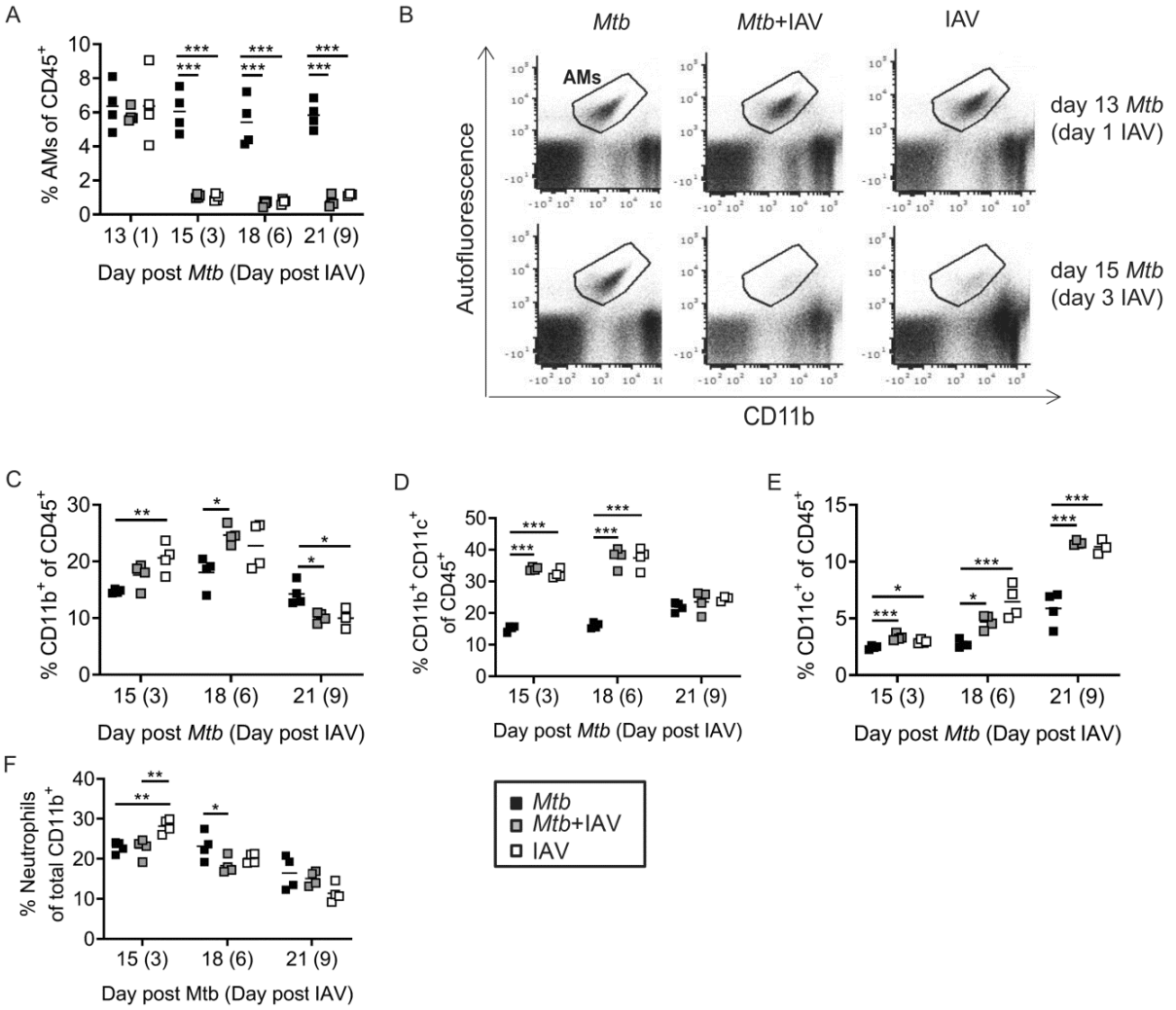

Figure 12 Impact of an IAV infection on AMs and myeloid cell populations in the lung. C57BL/6 mice were infected via aerosol with a low-dose of *Mtb* H37Rv and 12 days later coinfected i.n. with 10^4 PFU IAV (A/HH/05/09 pH1N1). Mice were sacrificed and lungs were collected at indicated time points and analyzed by flow cytometry for the frequencies of (A) Alveolar macrophages (AMs, Autofluorescent, $CD11c^+$ $MHC\text{-}II^+$). (B) depicts representative dot blots from AM gating. Lung cells were further analyzed for (C) $CD11b^+$, (D) $CD11b^+CD11c^+$ and (E) $CD11c^+$ cell frequencies among $CD45^+$ cells (n=4 mice per group, representative of two independent experiments). (F) shows neutrophil ($CD11b^+Ly6G^+$) frequencies of total $CD11b^+$ cells (n=4 mice per group, representative of two independent experiments). (A, C-F) Each data point represents one mouse. *p ≤0.05; **p ≤ 0.01, ***p ≤0.001 determined by One-way ANOVA followed by Tukey's multiple-comparison test.

The total $CD11b^+$ compartment ($CD11b^+$ and $CD11b^+CD11c^+$) comprises neutrophils, macrophages and monocytes which are recruited during an acute influenza virus infection[139]. Early after IAV infection, there was no difference in neutrophil ($CD11b^+Ly6G^+$) frequencies among $CD11b^+$ cells between *Mtb*-alone and coinfected lungs. However, in IAV-alone-infected animals, neutrophils reached significantly higher proportions among $CD11b^+$ cells compared to *Mtb*-alone and IAV-coinfected mice. Neutrophil proportions among total $CD11b^+$ cells slightly decreased over time and proportions were comparable between all three groups on day 9 after IAV (co)infection (day 21 *Mtb* infection, Figure 12F).

The total CD11b compartment was further stratified for F4/80 expression which characterizes macrophages. On day 6 and 9 after influenza virus infection, the proportion of $CD11b^{+}F4/80^{+}$ cells was significantly increased in lungs of coinfected compared to *Mtb*-alone-infected mice (Figure 13A). To account for the differentiation process and plasticity of the monocyte/macrophage lineage, $CD11b^{+}F4/80^{+}$ cells were further distinguished by the expression of Ly6C. The analyses revealed that $Ly6C^{high}$ cells among total $CD11b^{+}$ cells rapidly increased in IAV-(co)infected mice, showing significant elevation already on day 3 after viral infection (day 15 *Mtb* infection, Figure 13B). This cell fraction was still significantly higher on day 6 after IAV (co)infection, but decreased to proportions similar to that detected in *Mtb*-only-infected mice by day 9 after IAV (co)infection. On the other hand, $Ly6C^{int}$ and $Ly6C^{low/-}$ cell populations were represented in larger proportions in *Mtb*-alone-infected compared to IAV-(co)infected mice on day 3 and 6 after the viral infection (day 15 and 18 *Mtb* infection, Figure 13C and 13D) However, by day 9 after IAV (co)infection (day 21 *Mtb* infection), both subpopulations showed significantly increased proportions in IAV-(co)infected compared to *Mtb*-only infected mice.

Antonelli and colleagues observed that intranasal application of the potent type I IFN inducer poly-IC resulted in a CC chemokine receptor type 2 *(*CCR2)-dependent recruitment of *Mtb*-permissive $CD11b^{+}F4/80^{+}Gr1^{int}$ (GR1= Ly6C/Ly6G) cells into the lungs that culminated in an increased bacterial burden[82]. In lung homogenates of IAV-(co)infected mice, increased levels of the CCR2 ligand CCL2 were detected by bead assay chemokine analysis. Mice infected with IAV showed a significantly elevated CCL2 protein amount compared to *Mtb*-alone-infected mice as early as 3 days after IAV infection (day 15 *Mtb* infection, Figure 13E). This increase in CCL2 was present until day 9 after IAV infection (day 21 *Mtb* infection) although the difference to *Mtb*-alone-infected lungs was not as prominent as identified for the previous two days of analysis. As described above, lungs of coinfected mice showed increase in cell proportions that met similar characteristics as described by Antonelli and colleagues. This cell infiltration concomitant with the increase in CCL2 production raised the question whether the IAV-infection caused a CCR2-dependent recruitment of *Mtb*-permissive cells that would be responsible for the increased *Mtb* burden in coinfected lungs. In order to approach this question, CCR2 knockout (KO, $CCR2^{-/-}$) mice were used. Cells of CCR2 KO mice cannot migrate towards CCL2 since they lack the cognate receptor. I infected KO and wildtype (WT, $CCR2^{+/+}$) mice according to the *Mtb*-IAV infection protocol (Figure 4A) and analyzed the bacterial burden in lung, draining lymph nodes (dLNs) and spleen on day 21 after *Mtb* infection. Although the IAV (co)infection was associated with increased inflammation and increased CCL2 levels in lung homogenates, I could not identify a CCR2-dependent elevation of bacterial burden in the lungs because there was no difference in the bacterial load between IAV-coinfected CCR2 KO to CCR2 WT mice (Figure 13F). Consequently, the data suggest that the increased bacterial burden in our coinfection model was not CCR2-dependent.

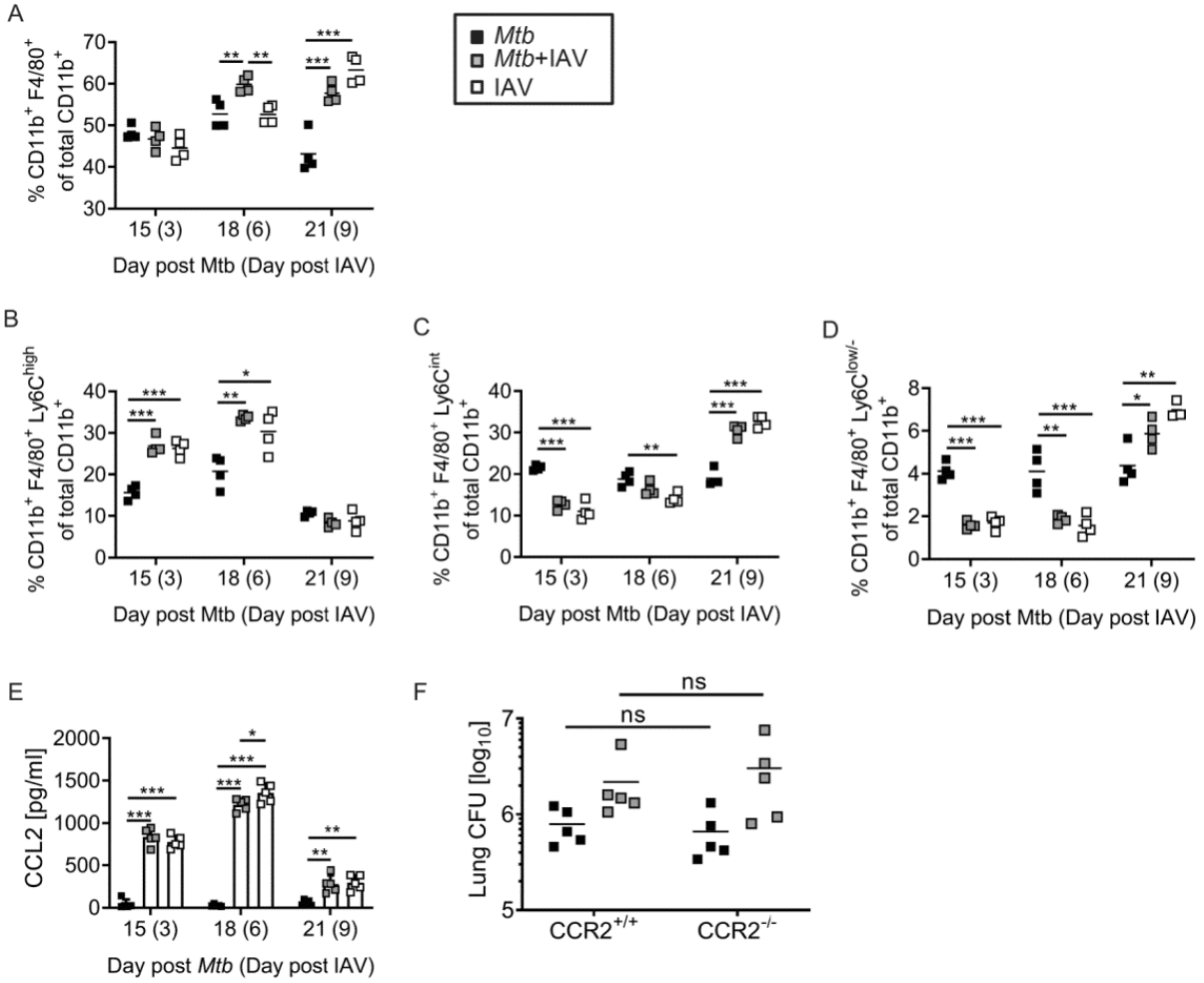

Figure 13 IAV-induced increased infiltration of CD11b$^+$F4/80$^+$Ly6C$^+$ and elevated CCL2 production are not associated with a CCR2-dependent increase of *Mtb* burden in coinfected mice. C57BL/6 mice were infected via aerosol with a low-dose of *Mtb* H37Rv and 12 days later coinfected i.n. with 10^4 PFU IAV (A/HH/05/09 pH1N1). Mice were sacrificed and lungs were collected at indicated time points and analyzed by flow cytometry for cells of the monocyte/macrophage lineage. Frequencies among total CD11b$^+$ cells were determined for (A) CD11b$^+$F4/80$^+$ (B) CD11b$^+$F4/80$^+$Ly6C^{high}, (C) CD11b$^+$F4/80$^+$ Ly6C^{int} and (D) CD11b$^+$F4/80$^+$Ly6C$^{low/neg}$ (n=4 mice per group, representative of two independent experiments). Lung homogenates were analyzed by bead assay chemokine analysis (LEGENDplex™) for (E) the amount of CCL2 (n=5 mice per group, representative of two independent experiments). (F) CCR2$^{+/+}$ and CCR2$^{-/-}$ C57BL/6 mice were infected via aerosol with a low-dose of *Mtb* H37Rv and 12 days later coinfected i.n. with 10^4 PFU IAV (A/HH/05/09 pH1N1). Mice were sacrificed on day 21 after *Mtb* infection (day 9 after IAV coinfection) and lungs were analyzed for bacterial burden (n=5 mice per group, one experiment). (A-D, F) Each data point represents one mouse and (E) data are represented as mean + SD. *p ≤0.05; **p ≤ 0.01, ***p ≤0.001 determined by (A-E) One-way ANOVA followed by Tukey's multiple-comparison test and (F) Two-way ANOVA followed by Sidak's multiple-comparison test.

In the context of an *Mtb* infection, $CD4^+$ T cells are indispensable for bacterial control[58,206]. In order to activate $CD4^+$ T cells, the presentation of the specific peptide within the MHC-II context is necessary. Hence, I characterized the proportions of MHC-II expressers among $CD11b^+$, $CD11b^+CD11c^+$ and $CD11c^+$ cells. In the lungs of IAV-(co)infected compared to *Mtb*-alone-infected mice, there were significantly increased frequencies of $MHC\text{-}II^+$ among $CD11b^+$ cells on day 6 after viral infection (day 18 *Mtb* infection, Figure 14A). However, on day 9 after viral infection (day 21 *Mtb* infection), *Mtb*-only infected lungs showed higher frequencies of $MHC\text{-}II^+$ cells among $CD11b^+$ cells. The population of $CD11b^+CD11c^+$ co-expressers presented significantly increased $MHC\text{-}II^+$ frequencies in IAV-(co)infected compared to *Mtb*-only infected lungs on all analyzed days (Figure 14B). Opposing to this observation, $CD11c^+$ cells displayed significantly reduced frequencies of $MHC\text{-}II^+$ expressing cells in IAV-(co)infected compared to *Mtb*-alone mice on all analyzed time points (Figure 14C).

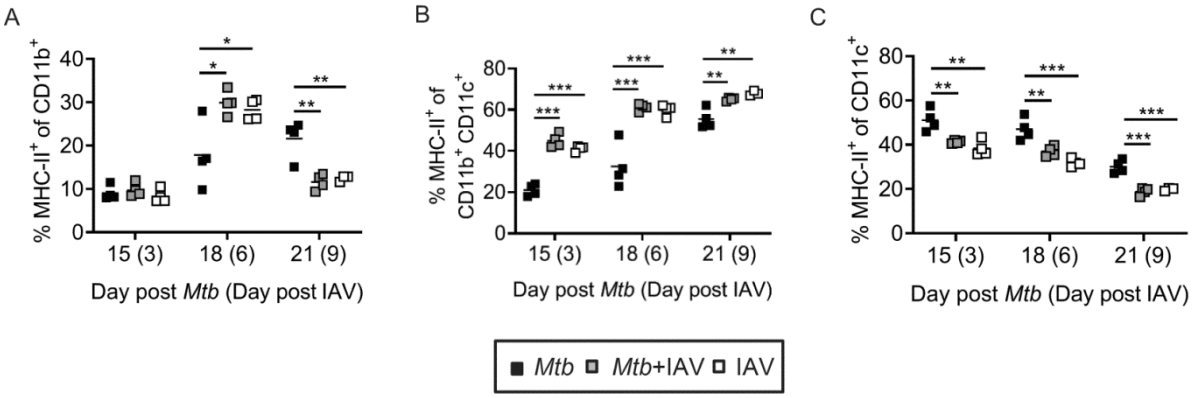

Figure 14 IAV coinfection impacts frequencies of MHC-II expressers among myeloid cells. C57BL/6 mice were infected via aerosol with a low-dose of *Mtb* H37Rv and 12 days later coinfected i.n. with 10^4 PFU IAV (A/HH/05/09 pH1N1). Mice were sacrificed and lungs were collected at indicated time points and analyzed by flow cytometry for the frequencies of MHC-II expressers among (A) $CD11b^+$ (B) $CD11b^+CD11c^+$ and (C) $CD11c^+$ cells (n=4 mice per group, representative of two independent experiments). Each data point represents one mouse. *p ≤0.05; **p ≤ 0.01, ***p ≤0.001 determined by One-way ANOVA followed by Tukey's multiple-comparison test.

The $CD11c^+$ cells encompass the dendritic cell (DC) population that is seen as the most proficient and potent antigen-presenting cell (APC) population to activate T cells. The prominent decrease in $MHC\text{-}II^+$ frequencies in IAV-coinfected compared to *Mtb*-alone-infected mice raised the question whether IAV-coinfection compromised the activation of the *Mtb*-specific $CD4^+$ T cells.

Results 3.3: Summary

IAV coinfection changed the cellular proportions in lungs of *Mtb*-infected mice.

- IAV infection promoted an early increase of myeloid cells while simultaneously depleting AMs.
- IAV coinfection resulted in an increased proportion of $CD8^+$ T cells in *Mtb*-infected lungs.
- IAV-induced increase of CCL2 concomitant with elevated frequencies of $CD11b^+F4/80^+Ly6C^+$ cells was not associated with a CCR2-dependent increase in *Mtb* burden in IAV-coinfected lungs.
- IAV infection decreased MHC-II^+ frequencies among $CD11c^+$ DCs.

3.4 IAV coinfection impairs the *Mtb*-specific immune response

Based on the observation that IAV coinfection resulted in decreased frequencies of MHC-II$^+$ cells among CD11c$^+$ DCs, I further analyzed the *Mtb*-specific CD4$^+$ T cell response. For investigating the adaptive immune response, isolated cells from lungs and dLN were characterized by flow cytometry.

The total number of CD4$^+$ T cells in the lungs was significantly higher in IAV-coinfected compared to *Mtb*-alone-infected mice on all analyzed time points (Figure 15A). However, the proportion of CD4$^+$ T cells among CD45$^+$ cells in IAV-(co)infected mice significantly dropped already by day 6 after IAV (co)infection (day 18 *Mtb* infection) below the frequency detected in *Mtb*-alone-infected lungs. This was still observed on day 9 after IAV (co)infection (day 21 *Mtb* infection) and could be accredited to the aforementioned IAV-induced enhanced infiltration of CD8$^+$ T cells (Figure 8A, Figure 11). The decrease in CD4$^+$ T cell frequencies concomitant with the increased proportion of CD8$^+$ T cells ultimately resulted in an inverse CD4$^+$ to CD8$^+$ T cell ratio in IAV-(co)infected animals, significantly shifting the balance towards CD8$^+$ T cells compared to *Mtb*-alone-infected animals (Figure 15B).

IAV (co)infection led to significantly increased frequencies of CD69 expressers among CD4$^+$ T cells already on day 3 after IAV (co)infection (day 15 *Mtb* infection, Figure 15C). In lungs of both *Mtb* and IAV-(co)infected animals, proportions of CD69$^+$ among CD4$^+$ T cells rose over time to about 50% in *Mtb*-infected and approx. 70% in IAV-(co)infected lungs by day 9 after IAV (co)infection (day 21 *Mtb* infection). A comparable picture was seen for CD44$^+$CD62L$^-$ cells among CD4$^+$ T cells; activated T cells were significantly increased in IAV-(co)infected compared to *Mtb*-alone-infected lungs from day 3 until day 9 after IAV coinfection (day 15-day 21 *Mtb* infection, Figure 15D).

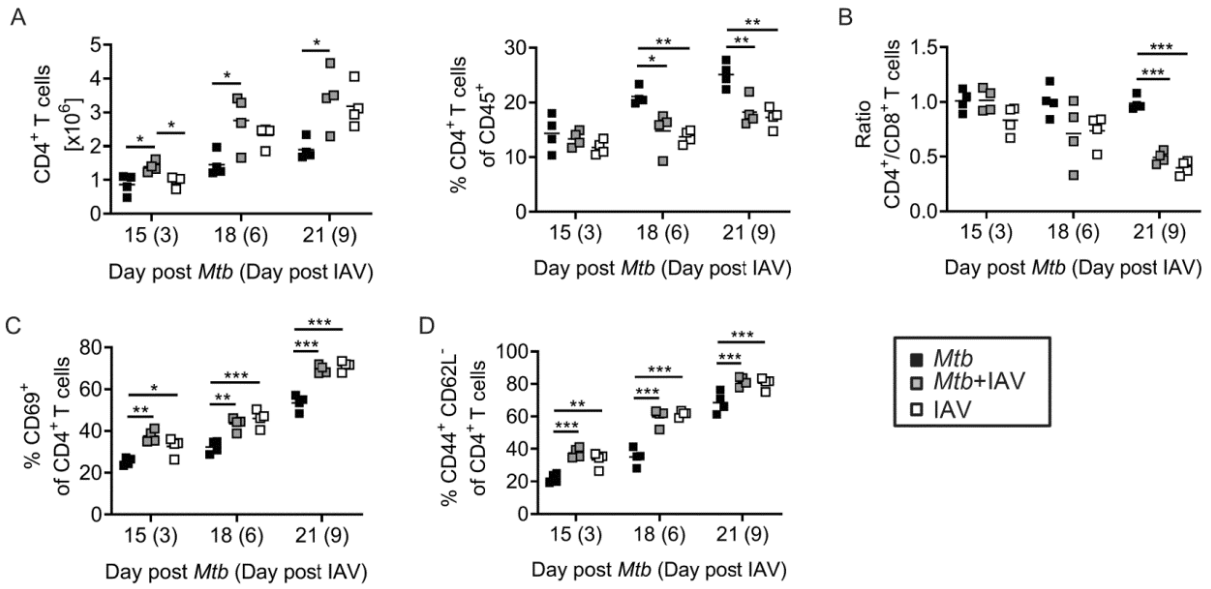

Figure 15 Impact of IAV coinfection on CD4$^+$ T cells. C57BL/6 mice were infected via aerosol with a low-dose of *Mtb* H37Rv and 12 days later coinfected i.n. with 10^4 PFU IAV (A/HH/05/09 pH1N1). Lungs were analyzed by flow cytometry at indicated time points for (A) total CD4$^+$ T cell numbers and CD4$^+$ T cell frequencies among CD45$^+$ cells and (B) ratio of CD4$^+$ to CD8$^+$ T cells. CD4$^+$ T cells were further characterized by frequencies of (C) CD69$^+$ and (D) CD44$^+$ CD62L$^-$ cells (n=4 mice per group, representative of two independent experiments). Each data point represents one mouse.*p ≤0.05; **p ≤ 0.01, ***p ≤0.001 determined by One-way ANOVA followed by Tukey's multiple-comparison test. (Part of data is published in Ring *et al*., 2019.)

The activation of CD4$^+$ T cells as seen by CD69 and CD44 expression was not compromised by IAV coinfection. I thus investigated the impact of the viral coinfection on CD4$^+$ T cell effector functions in terms of the TNF and IFN-γ response. TNF and especially IFN-γ are essential cytokines for activation of host cells like macrophages to enable them to kill *Mtb*[49]. Cytokine-producing CD4$^+$ T cells were detected upon ex vivo restimulation of lung single cell suspensions either polyclonally with phorbol myristate acetate/ionomycin (PMA/Iono) or specifically with the *Mtb* peptide ESAT-6$_{1-20}$ followed by intracellular cytokine staining (ICS) and flow cytometry.

Already on day 6 after IAV infection (day 18 *Mtb* infection), the frequency of both TNF and IFN-γ producers among CD4$^+$CD44$^+$ cells was significantly reduced in coinfected compared to *Mtb*-alone-infected animals upon polyclonal restimulation (Figure 16A). This difference in T cell cytokine producers between *Mtb*-alone to IAV-(co)infected mice was even more pronounced on day 9 after IAV (co)infection (day 21 *Mtb* infection) with significantly decreased proportions in IAV-(co)infected lungs. Next, I determined whether this compromised response to unspecific restimulation in IAV-coinfected mice would also extent to the *Mtb*-specific CD4$^+$ T cell population. On day 15 and day 18 after *Mtb* infection, no prominent response of TNF and/or IFN-γ producing T cells could be detected and there was no difference between the infection groups (Figure 16B). However, on day 21 after *Mtb* infection, *Mtb*-specific CD4$^+$ T cell responses could be detected in lungs from *Mtb*-alone-infected lungs. The restimulation with ESAT-6$_{1-20}$ peptide resulted in the induction of TNF and

IFN-γ producers among $CD4^+CD44^+$ T cells in *Mtb*-alone-infected lungs which was absent in IAV-coinfected mice.

Correspondingly, frequencies of TNF and IFN-γ producers among $CD4^+CD44^+$ T cells were significantly decreased in IAV-coinfected compared to *Mtb*-alone-infected lungs. In line with the reduced *Mtb*-specific $CD4^+$ T cell effector functions, *Mtb*-specific I-A^b ESAT-6_{4-17} $CD4^+$ T cells were also diminished in coinfected compared to *Mtb*-alone-infected mice on day 9 after IAV-(co)infection (day 21 *Mtb* infection, Figure 16C). I-A^b ESAT-6_{4-17}-specific $CD4^+$ T cells, detected by tetramer staining and flow cytometry, were reduced in both total numbers and frequencies among $CD4^+$ T cells.

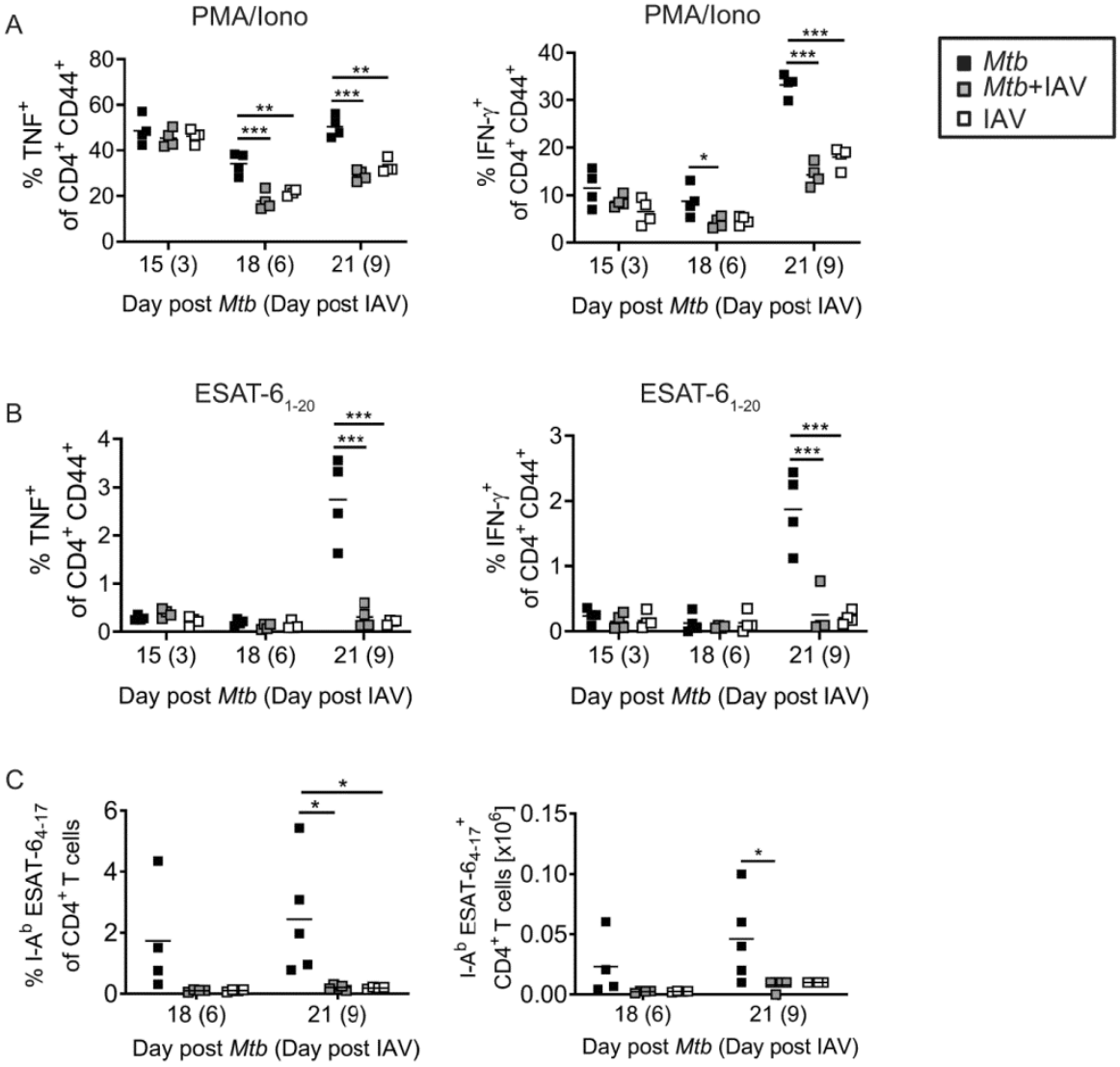

Figure 16 IAV infection impairs the *Mtb*-specific $CD4^+$ T cell response. C57BL/6 mice were infected via aerosol with a low-dose of *Mtb* H37Rv and 12 days later coinfected i.n. with 10^4 PFU IAV (A/HH/05/09 pH1N1). Lungs were analyzed by flow cytometry at indicated time points for (A, B) TNF and IFN-γ producing $CD4^+$ T cells upon ex vivo restimulation with (A) PMA/Iono and (B) ESAT-6_{1-20} peptide (n=4 per group, d15 and d18 *Mtb* representative of two independent experiments, d21 *Mtb* representative of four independent experiments) and further analyzed for (C) I-Ab ESAT-6_{4-17}-specifc $CD4^+$ T cells (d18 *Mtb* n=4 per group, one experiment; d21 *Mtb* n=4-5 per group, representative of two independent experiments), Each data point represents one mouse. *p ≤0.05; **p ≤ 0.01, ***p ≤0.001 determined by One-way ANOVA followed by Tukey's multiple-comparison test. (Data are published in Ring *et al*., 2019.)

Based on the observations that in the lungs of IAV-coinfected mice both the *Mtb*-specific $CD4^+$ T cell effector functions were impaired and the number of *Mtb*-specific $CD4^+$ T cells was reduced, it could be assumed that either the T cell recruitment and/or the T cell priming in the dLNs was impacted by the concomitant influenza virus infection. Accordingly, *Mtb*-specific $CD4^+$ T cells were investigated in the dLN because it is the place where the *Mtb*-specific immune response is initiated[42]. Upon activation, *Mtb*-specific T cells clonally expand and migrate to the site of infection, the lung, where they are reactivated to exert their effector functions. Similarly to the lung, I could observe significantly decreased numbers and frequencies of *Mtb*-specific I-A^b ESAT-6_{4-17} $CD4^+$ T cells in coinfected dLN on day 9 after IAV coinfection (day 21 *Mtb* infection, Figure 17A). Moreover, specific *ex vivo* restimulation with ESAT-6_{1-20} peptide showed that TNF^+ and IFN-γ^+ $CD4^+$ T cells were significantly reduced in coinfected compared to *Mtb*-alone-infected mice (Figure 17B). Since number and frequency of I-A^b ESAT-6_{4-17}-specific $CD4^+$ T cells were diminished in coinfected dLN, it was addressed whether the priming of *Mtb*-specific $CD4^+$ T cells was compromised in IAV-coinfected mice. For this, I isolated $CD4^+$ T cells from p25 T cell receptor (TCR)-transgenic (tg) mice. Those $CD4^+$ T cells express a TCR that recognizes mycobacterial Ag85B in a MHC-II A(b)-restricted manner[198]. Isolated p25 TCR-tg $CD4^+$ T cells were CFSE-labeled and adoptively transferred into naïve mice one day before *Mtb* infection. Mice were then subjected to the standard *Mtb*-IAV infection protocol (Figure 4A). On day 21 after *Mtb* infection (day 9 IAV infection), cells from dLNs were isolated and $CD4^+$ T cells were analyzed for proliferation by CFSE dilution. The CFSE-labeling enables the detection of cell proliferation because during every cell division fluorescent dye-cell protein conjugates are evenly distributed between mother and daughter cell. This results in a decrease of fluorescence intensity by half which is used to follow the different cell generations. On day 9 after IAV (co)infection (day 21 *Mtb* infection), the proportion of proliferated p25TCR-tg $CD4^+$ T cells was significantly reduced in the dLNs of coinfected compared to *Mtb*-alone-infected mice (Figure 17C). This suggests that priming of *Mtb*-specific $CD4^+$ T cells was defective in IAV-coinfected mice. For T cell priming, the antigen must be efficiently transported from the lung to the dLN. Comparing the resistant C57BL/6 to the susceptible C3H mouse strain, one of the features that causes the increased susceptibility of the C3H strain is the delayed transport of *Mtb* antigen to the dLN[41]. Nonetheless, there were no differences in the bacterial levels in the dLNs between *Mtb*-alone and IAV-coinfected animals (Figure 17D) suggesting that the transport of viable bacteria was not compromised by concurrent IAV infection.

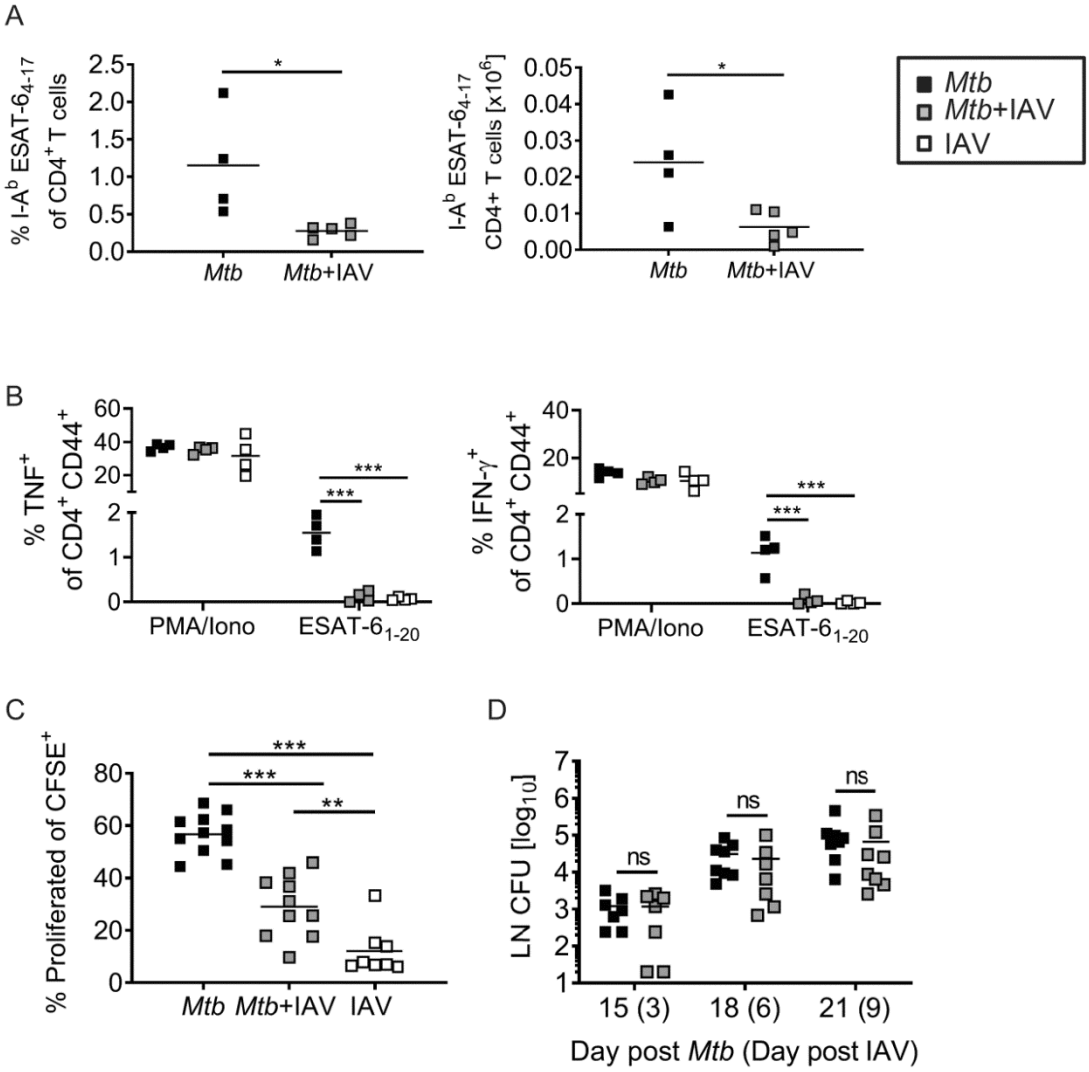

Figure 17 Impaired priming of *Mtb*-specific CD4$^+$ T cells in dLN of coinfected mice. C57BL/6 mice were infected via aerosol with a low-dose of *Mtb* H37Rv and 12 days later coinfected i.n. with 10^4 PFU IAV (A/HH/05/09 pH1N1). Lung-draining lymph nodes (dLN) were collected 9 days after IAV (co)infection (day 21 *Mtb*) and analyzed by flow cytometry for presence of (A) I-Ab ESAT-6$_{4-17}$-specific CD4$^+$ T cells (n=4-5 per group, representative of two independent experiments) and (B) TNF and IFN-γ producing CD4$^+$ T cells upon ex vivo restimulation with PMA/Iono or ESAT-6$_{1-20}$ peptide (n=4 per group, representative of two independent experiments). (C) dLN from mice that received CFSE-labeled CD4$^+$ T cells from p25TCR-tg mice were collected at day 21 *Mtb* (day 9 IAV) and analyzed for the proportion of proliferated CD4$^+$ T cells cells by flow cytometry (n=8-11 per group, representative of two independent experiments). (D) dLN were collected at indicated time points and analyzed for bacterial burden (n=7-8 per group, pooled data from two independent experiments). Each data point represents one mouse. *p ≤0.05; **p ≤ 0.01, ***p ≤0.001 determined by (A, D) unpaired *t* test and (B,C) One-way ANOVA followed by Tukey's multiple-comparison test. (Data are published in Ring *et al*., 2019.)

Results 3.4: Summary

IAV coinfection compromised the establishment and effector functions of the *Mtb*-specific immune response in coinfected mice.

- Lungs and dLN of coinfected mice had decreased IFN-γ and TNF $CD4^+$ T cell frequencies upon ESAT-6_{1-20} restimulation.
- IAV-coinfected lungs and dLN had reduced I-A^b ESAT-6_{4-17}-specific $CD4^+$ T cell numbers and frequencies.
- IAV coinfection impaired *Mtb*-specific $CD4^+$ T cell priming in dLNs despite a comparable transport of viable bacteria to the dLNs.

3.5 IAV coinfection establishes an anti-inflammatory environment and polarizes macrophages into an alternatively activated phenotype

$CD4^+$ T cells from IAV-coinfected compared to *Mtb*-alone-infected mice showed decreased TNF and IFN-γ responses. Since those cytokines are required for macrophage activation, I next investigated whether innate antimycobacterial effector functions were impacted in coinfected mice. To do so, lung homogenates were analyzed via qRT-PCR for the expression of (inducible) nitric oxide synthase 2 (NOS2). In lung homogenates from *Mtb*-alone-infected mice, an induction of *Nos2* expression over time was detected (Figure 18A). In contrast, there was no increase in relative expression levels of *Nos2* in IAV-(co)infected lungs over time. Correspondingly, lungs from IAV-(co)infected mice had significantly reduced *Nos2* in comparison to *Mtb*-alone-infected lungs on day 6 after IAV (co)infection (day 18 *Mtb* infection) and still reduced on day 9 after the viral infection (day 21 *Mtb* infection).This phenotype on the transcriptional level also translated into significantly lowered amounts of reactive nitrogen intermediates (RNI) in lung homogenates from IAV-(co)infected compared to *Mtb*-alone-infected mice on day 9 after IAV-(co)infection (day 21 *Mtb* infection, Figure 18B).

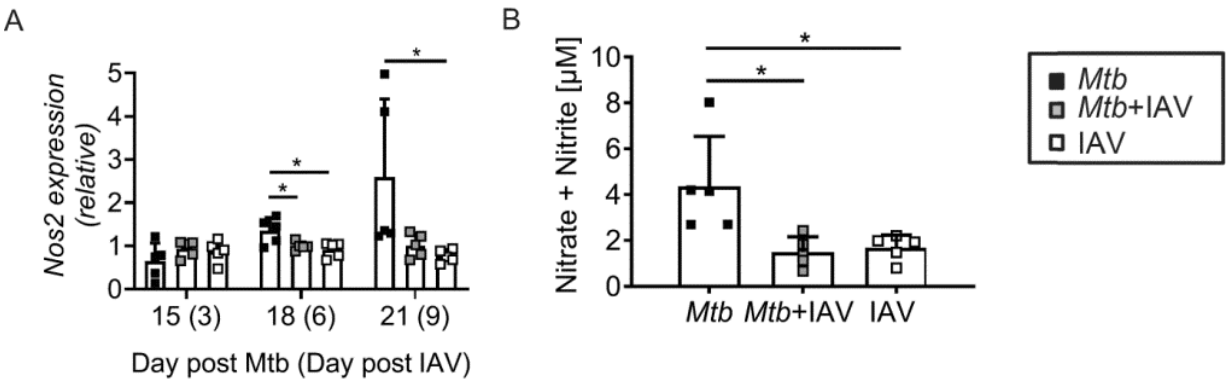

Figure 18 IAV coinfection impairs induction of *Nos2* and RNI. C57BL/6 mice were infected via aerosol with a low-dose of *Mtb* H37Rv and 12 days later coinfected i.n. with 10^4 PFU IAV (A/HH/05/09 pH1N1). Lungs were collected at indicated time points and analyzed for (A) *Nos2* expression (gene expression determined by qRT-PCR relative to *Gapdh*, n=4-5 per group, representative of two independent experiments).and (B) amount of RNI (n=5 per group, one experiment). Data are represented as mean + SD. *p ≤0.05; **p ≤ 0.01, ***p ≤0.001 determined by One-way ANOVA followed by Tukey's multiple-comparison test. (Data are published in Ring *et al*., 2019.)

The production of RNI occurs downstream of the NOS2-mediated metabolization of arginine. Arginine can be metabolized by both NOS2 and arginase-1 (Arg1) which are competing for the substrate availability. The dominating enzyme is an important determinant for the characterizing effector phenotype of macrophages[207]. Since coinfected lungs had a lower relative *Nos2* expression, the expression levels of its counterpart Arg1 were determined in lung homogenates. On day 6 and 9 after IAV infection (day 18 and 21 *Mtb* infection) *Arg1* levels were significantly increased in IAV-(co)infected compared to *Mtb*-only-infected lungs (Figure 19A). There was no induction of *Arg1* in lungs of *Mtb*-alone-infected mice over time. An increase in *Arg1* expression with concomitantly decreased *Nos2* expression suggests that macrophages polarized into an alternatively activated phenotype[207].To further circumstantiate

this notion, the expression of Fizz1 was examined[208]. Fizz1 is described as a specific marker for murine alternatively activated macrophages[209]. Indeed, *Fizz1* expression was significantly increased in IAV-(co)infected lungs on day 6 and 9 after viral infection (day 18 and 21 *Mtb* infection, Figure 19B). In order to specifically address the macrophage population in the lung with respect to NOS2 and ARG-1 production, I performed ICS and subsequent flow cytometry analyses. Among total $CD11b^+$ cells, the frequency of the macrophage population ($CD11b^+F4/80^+CD11c^+Ly6C^+Ly6G^-$) was significantly elevated in IAV-(co)infection compared to *Mtb*-alone-infected mice on day 6 and 9 after viral infection (d18 and d21 *Mtb* infection, Figure 19C). In line with the qRT-PCR data of *Arg1*, the median fluorescence intensity (MFI) of ARG-1 of the macrophage population was significantly enhanced in IAV-(co)infected compared with *Mtb*-alone-infected animals on both analyzed days (Figure 19D) suggesting a higher ARG-1 production on a single cell basis. On day 6 after IAV (co)infection, the MFI of NOS2 was significantly higher in macrophages from IAV-(co)infected animals compared to *Mtb*-alone-infected mice (Figure 19E). However, by day 9 after IAV (co)infection (day 21 *Mtb* infection) macrophages from IAV-(co)infected lungs presented a decreased MFI of NOS2. This ultimately resulted in an inverse ARG-1/NOS2 ratio (Figure 19F) significantly shifted to ARG-1 in mice infected with IAV compared to *Mtb*-only-infected mice.

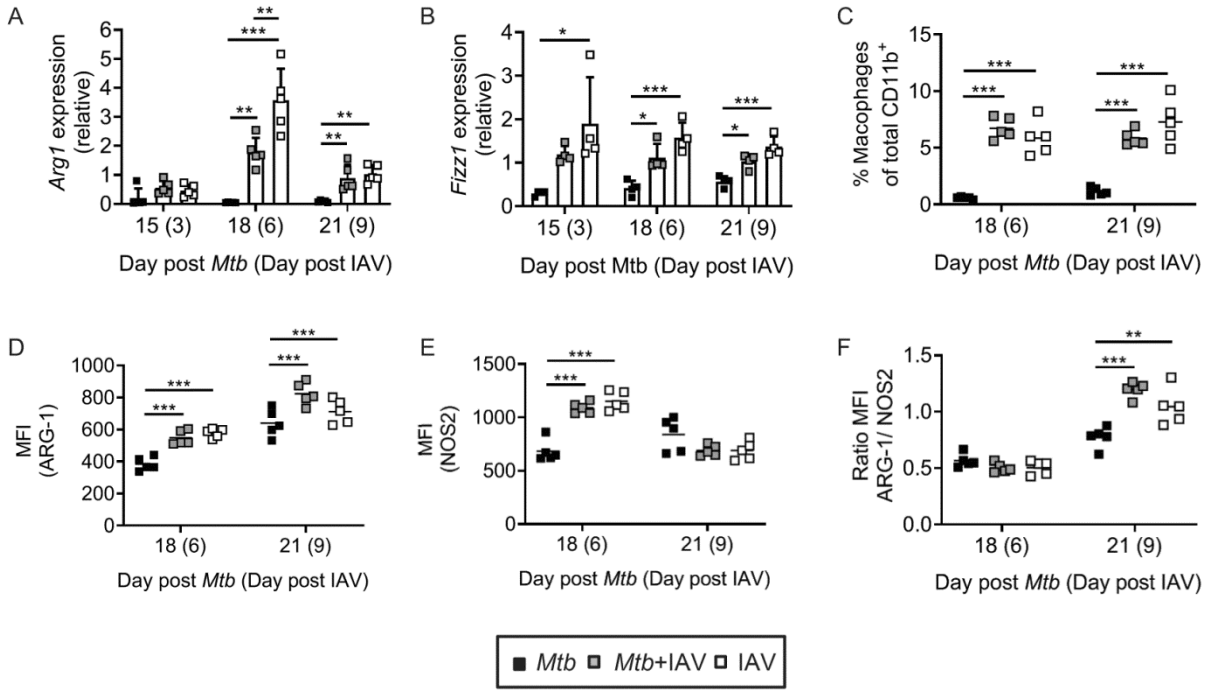

Figure 19 Alternatively activated macrophages in coinfected mice. C57BL/6 mice were infected via aerosol with a low-dose of *Mtb* H37Rv and 12 days later coinfected i.n. with 10^4 PFU IAV (A/HH/05/09 pH1N1). Lungs were collected at indicated time points and analyzed for (A) *Arg1* and (B) *Fizz1* gene expression (gene expression determined by qRT-PCR relative to *Gapdh*, n=4-5 per group, representative of two independent experiments). Lungs were collected on day 18 and day 21 *Mtb* (day 6 and day 9 IAV) and analyzed by flow cytometry for (C) macrophage ($CD11b^{high}F4/80^+CD11c^+Ly6C^+Ly6G^-$) frequencies among total $CD11b^+$ cells (n=5 per group, one experiment) and their (D,E) median fluorescence intensity (MFI) for (D) ARG-1 and (E) NOS2 (n=5 per group, one experiment). (F) shows the ratio of the MFI of ARG-1 to the MFI of NOS2 in the defined macrophages. (A-B) Data are represented as mean + SD and (C-F) each point representing one mouse. *p ≤0.05; **p ≤ 0.01, ***p ≤0.001 determined by One-way ANOVA followed by Tukey's multiple-comparison test. (Parts of data are published in Ring *et al*., 2019.)

Besides production of RNI, IL-1 was found to be indispensable for *Mtb* control in the mouse model. Different studies showed a higher TB susceptibility in Il1a−/−, Il1b−/− and Il1r1−/− mice[68]. In experimental TB, IL-1α and IL-1β production was detected in $CD11b^+$ myeloid subsets[68]. Accordingly, I examined the expression of IL-1α and IL-1β in lung homogenates and found both transcripts to be significantly increased in IAV-(co)infected lungs compared to *Mtb*-alone-infected mice on day 3 after viral infection (day 15 *Mtb* infection, Figure 20A and 20B). In *Mtb*-alone-infected lungs, *Il1a* was induced over time. In contrast, *Il1a* transcripts rapidly decreased in IAV-(co)infected mice to significantly reduced levels compared to *Mtb*-alone-infected lungs on day 6 and 9 after IAV (co)infection (day 18 and 21 *Mtb* infection). On the other hand, *Il1b* expression was not induced in *Mtb*-alone-infected lungs until day 21 after *Mtb* infection (Figure 20B). Nonetheless, the reduction in relative expression levels over the time, as seen for *Il1a,* was also prominent for *Il1b* in IAV-(co)infected lungs. Both IL-1α and IL-1β signal via the IL-1 receptor 1 (IL-1R1) and can promote their expression via a positive-feedback loop[210]. The prevention of IL-1 signaling can thus result in a decrease of IL-1 expression. With the induction of the IL-1 receptor antagonist (IL-1RA, *Il1rn*) that binds IL-1R1 but does not induce downstream signaling, the positive feedback signaling of IL-1 can be disrupted[211,212]. Indeed, *Il1rn* expression was significantly upregulated in IAV-(co)infected compared to *Mtb*-alone-infected lungs on day 3 and 6 after viral infection (day 15 and 18 *Mtb* infection, Figure 20C) suggesting that induction of *Il1rn* contributed to the reduction of *Il1a* and *Il1b* expression in IAV-(co)infected mice.

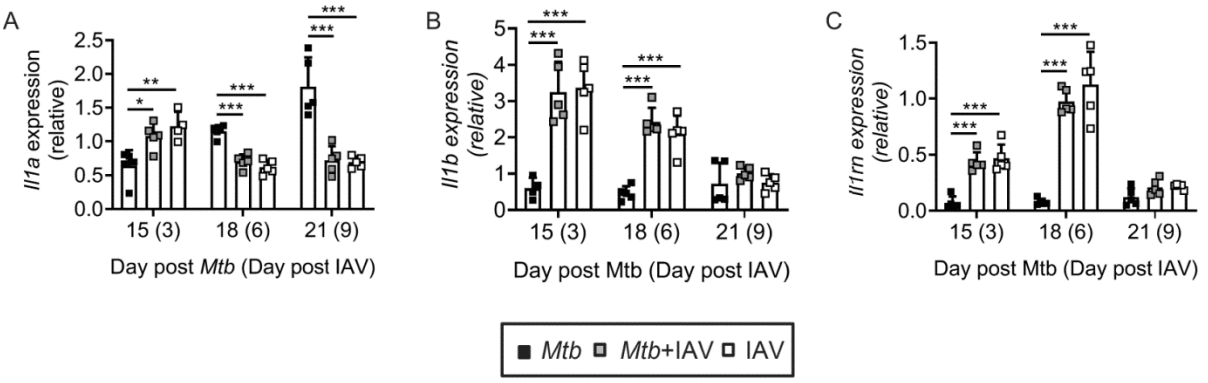

Figure 20 IAV coinfection reduces IL-1 expression. C57BL/6 mice were infected via aerosol with a low-dose of *Mtb* H37Rv and 12 days later coinfected i.n. with 10^4 PFU IAV (A/HH/05/09 pH1N1). Lungs were collected at indicated time points and analyzed for relative gene expression of (A) *Il1a*, (B) *Ilb* and (C) *Il1rn*. Gene expression determined by qRT-PCR relative to *Gapdh* (n=4-5 per group, representative of two independent experiments). Data are represented as mean + SD *p ≤0.05; **p ≤ 0.01, ***p ≤0.001 determined by One-way ANOVA followed by Tukey's multiple-comparison test. (Parts of data are published in Ring *et al*., 2019.)

The induction of IL-1RA can be a downstream event of type I IFN signaling to limit IL-1 signaling[90]. Type I IFNs and IL-1 were described to counter-regulate each other. IL-1 can reduce type I IFN production via the induction of the lipid mediator PGE2. With regard to an *Mtb* infection, PGE2 is attributed beneficial effects[47] while blocking PGE2 signaling during an IAV infection ameliorated infection outcome[213]. Thus, it was of interest how PGE2 levels were regulated during this *Mtb*-IAV coinfection.

The analysis of lung homogenates for PGE2 and other lipid mediators by chromatography-tandem mass spectrometry, LC-MS^2, (in cooperation with PD Dr. Dominik Schwudke and Dr. Adam Wutkowski, Research Center Borstel) showed an early increase in PGE2 production 3 days after IAV infection in lungs of IAV-only infected mice (Figure 21A). PGE2 levels steadily increased in lungs of IAV-(co)infected mice over the observed time course and were significantly increased compared to PGE2 levels from *Mtb*-alone-infected lungs on day 6 and 9 after IAV (co)infection (day 18 and day 21 *Mtb* infection). There was no induction in PGE2 production in lungs of *Mtb*-alone-infected lungs until day 21 after *Mtb* infection.

The data on NOS2, Arg1 and IL-1 indicate compromised antimycobacterial effector functions and an anti-inflammatory environment in the lungs of IAV-coinfected mice from day 6 to day 9 after IAV infection. In fact, PGE2 is also accredited to mediate anti-inflammatory effects[214–216]. Besides PGE2 upregulation, analyses of other lipid mediators revealed that PDE2, TXA_2, 13-HDoHE and 15-HETE were also significantly elevated in lungs of IAV-(co)infected compared to *Mtb*-alone-infected mice (Figure 21B-E). This increased production was especially prominent on day 9 after viral infection (day 21 *Mtb* infection). Together with PGE2, those lipid mediators were associated with the induction of resolution and to exert anti-inflammatory activities[214,217–219].

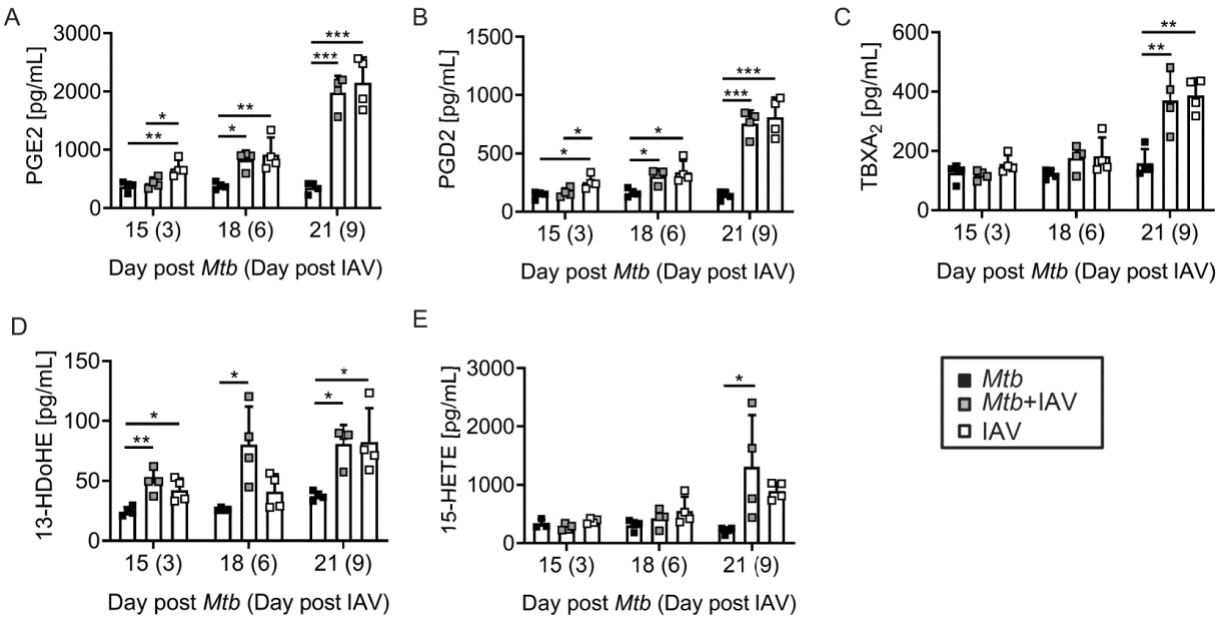

Figure 21 IAV infection induces anti-inflammatory lipid mediators. C57BL/6 mice were infected via aerosol with a low-dose of *Mtb* H37Rv and 12 days later coinfected i.n. with 10^4 PFU IAV (A/HH/05/09 pH1N1). At indicated time points, lung homogenates were analyzed by LC-MS^2 for lipid mediators (A) PGE2, (B) PGD2, (C) $TBXA_2$ (D) 13-HDoHE (E) 15-HETE (n=4 mice per group, representative of two independent experiments). Data are represented as mean + SD *p ≤0.05; **p ≤ 0.01, ***p ≤0.001 determined by One-way ANOVA followed by Tukey's multiple-comparison test. (Part of data is published in Ring *et al*., 2019.)

These data, together with the aforementioned reduced $CD4^+$ T cell effector functions, strongly indicate a down-regulation of the pro-inflammatory immune response at the later stages of IAV coinfection. Due to the fact that IL-10 is the most prominent immunosuppressive cytokine and known to be induced in IAV infections[156,161], I next addressed its role in this *Mtb*-IAV coinfection model.

Results 3.5: Summary

IAV coinfection downregulated innate antimycobacterial effector responses and upregulated mediators of an anti-inflammatory immune response in coinfected mice.

- IAV-coinfected lungs showed decreased *Nos2* expression and reduced RNI production.

- IAV coinfection polarized macrophages towards an alternatively activated phenotype as indicated by the expression profile of total lung homogenates:
    - reduced *Nos2* expression
    - increased *Arg1* and *Fizz1* expression
    - reduced *Il1a* and increased *Il1rn* expression
- and corroborated by flow cytometry:
    - ARG-1/NOS2 ratio shifted to ARG-1 in macrophages.

- IAV coinfection increased the production of anti-inflammatory lipid mediators in the lung.

3.6 IAV-induced IL-10 impairs *Mtb* growth control in coinfected mice

In IAV infection, IL-10 is linked to both beneficial and detrimental outcomes depending on the experimental study. The presence of IL-10 in *Mtb* infection is associated with an increased susceptibility of the host[75,76,79–81,220,221]. Accordingly, I investigated whether concomitant IAV infection would interfere with bacterial control in an IL-10-dependent manner.

The analysis of *Il10* transcripts from lung homogenates showed a significantly elevated relative expression in IAV-coinfected compared to *Mtb*-alone-infected animals already on day 3 after IAV infection (day 15 *Mtb* infection, Figure 22A). By day 6 and day 9 after IAV-(co)infection (day 18 and day 21 *Mtb* infection), *Il10* expression levels were further increased resulting in an even more pronounced difference between IAV-(co)infected and *Mtb*-only-infected mice. In contrast, there was no induction of *Il10* expression in *Mtb*-alone-infected lungs over time.

Next, I sought to identify the cellular sources of IL-10 by flow cytometry. Single cells isolated from lungs were subjected to *ex vivo* restimulation either polyclonally with PMA/Iono or specifically with *Mtb*-peptide ESAT-6_{1-20} followed by ICS and flow cytometric analyses. I could detect IL-10 producers among cells of both innate and adaptive immunity (Figure 22B-G, J). The IL-10 response of innate cells to only polyclonal, but not *Mtb*-specific, restimulation preceded the response of the $CD4^+$ and $CD8^+$ T cells (Figure 22B-E, J). IL-10 producing $CD4^+$ and $CD8^+$ T cell frequencies among $CD45^+$ cells reached significantly increased frequencies in IAV-(co)infected compared to *Mtb*-alone-infected lungs by day 6 and/or day 9 after IAV (co)infection (day 18 and/or day 21 *Mtb* infection, Figure 22F and 22G). Among the innate cell types analyzed, monocyte-derived DCs (moDCs, $CD11c^+CD11b^+Ly6C^+$, Figure 22B), $CD11b^+$ DCs ($CD11c^+CD11b^+$, Figure 22C), neutrophils ($CD11b^+Ly6G^+$, Figure 22D) and natural killer (NK) cells ($CD3^-NK1.1^+$, Figure 22E) were found to be prominent IL-10 producers that showed significantly increased IL-10 frequencies throughout the days of interest. Both neutrophils and $CD4^+$ T cells also showed significantly enhanced MFIs for IL-10 on either day 3 and 6 (neutrophils, Figure 22H) or day 6 and 9 ($CD4^+$ T cells, Figure 22I) after IAV (co)infection indicating a higher IL-10 production on a single cell basis. However, none of the analyzed cell types responded to *ex vivo* restimulation with ESAT-6_{1-20} (myeloid cells tested day 15-day 21 *Mtb* infection; adaptive cells and NK cells tested day 18 and day 21 *Mtb* infection; data not shown). IL-10-producing cells were only detected upon polyclonal restimulation which indicates IAV and not *Mtb*-induced IL-10 stimulation.

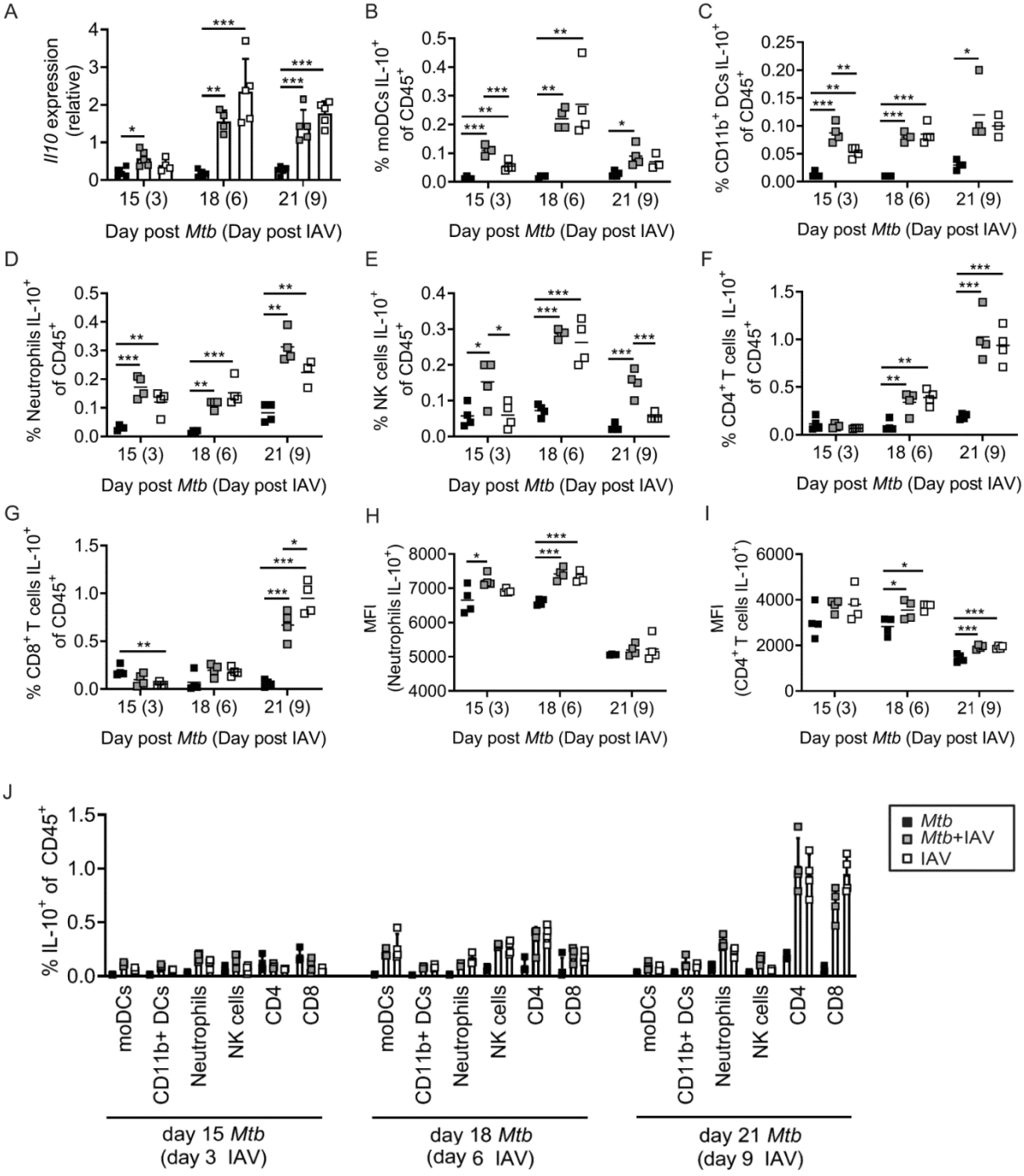

Figure 22 IAV infection stimulates the production of IL-10 by innate and adaptive immune cells. C57BL/6 mice were infected via aerosol with a low-dose of *Mtb* H37Rv and 12 days later coinfected i.n. with 10^4 PFU IAV (A/HH/05/09 pH1N1). Lungs were collected at indicated time points and analzed for (A) *Il10* expression by qRT-PCR relative to *Gapdh* expression (n=4-5 per group, representative of two independent experiments) and (B-I) IL-10 producing cells of the innate and adaptive immunity among $CD45^+$ cells by flow cytometry with (B) moDCs (monocyte-derived dendritic cells), (C) $CD11b^+$ DCs, (D) neutrophils, (E) natural killer (NK) cells (F) $CD4^+$ and (G) $CD8^+$ T cells (n=3-4 per group, data representative of two independent experiments). (H-I) show MFIs of IL-10-producers among (H) neutrophils and (I) $CD4^+$ T cells (n=3-4 per group, data representative of two independent experiments). (J) depicts a summary of the frequencies of $IL\text{-}10^+$ cell types of $CD45^+$ per day (n=3-4 per group, data representative of two independent experiments). (A, J) Data are represented as mean + SD or (B-I) each point representing one mouse. *p ≤0.05; **p ≤ 0.01, ***p ≤0.001 determined by (A-I) One-way ANOVA followed by Tukey's multiple-comparison test. (Data are published in Ring *et al*., 2019.)

$CD4^+$ T cells were the major IL-10–producing cells among $CD45^+$ cells on day 9 after IAV (co)infection (day 21 *Mtb* infection, Figure 22J). A prominent inhibitory $CD4^+$ T cell subset are regulatory T cells (T_{reg}). T_{regs} are immunosuppressive cells, identified by the transcription factor Forkhead box P3 (Foxp3)[222], that are essential to maintain peripheral immune-tolerance and that cease an excessive immune response to prevent immunopathology[72]. However, they may also be deleterious when dampening a required effector immune response. In order to mediate their suppressive effects, T_{regs} can act via cell-cell contact or via the secretion of e.g. IL-10[223].

Correspondingly, I further delineated the $CD4^+$ T cell population for the presence of T_{regs}. Indeed, IAV (co)infection resulted in a significant increase in $Foxp3^+CD4^+$ T cells compared to *Mtb*-alone-infected mice on day 6 after IAV (co)infection (day 18 *Mtb* infection, Figure 23A). At this time point, T_{reg} frequencies peaked, however, they were still significantly elevated on day 9 after viral infection (day 21 *Mtb* infection). IL-10 producing T_{regs} were identified upon polyclonal but not upon *Mtb*-peptide specific (data not shown) *ex vivo* restimulation. Significantly increased IL-10 producing T_{reg} frequencies were detected on day 6 and 9 after viral infection (day 18 and day 21 *Mtb* infection, Figure 23B). Moreover, on day 6 after IAV (co)infection, T_{regs} from IAV-infected mice showed a significantly higher MFI for IL-10 indicating a higher production of IL-10 on a single cell basis, which was reversed on day 9 after IAV (co)infection (day 21 after *Mtb* infection, Figure 23C).

T_{reg}-mediated suppression can be a reason for the reduced effector T cell functions in IAV-(co)infected compared to *Mtb*-alone-infected mice. The down-modulation of T cell effector functions can also be conferred via the upregulation of co-inhibitory receptors on T cells. One of such surface proteins can be lymphocyte-activation gene 3 (LAG-3). LAG-3 is a CD4 homologue that binds to MHC-II with higher affinity than CD4 and can be expressed on activated $CD4^+$ T cells. LAG-3 was, amongst others, described to mediate inhibitory intrinsic signaling in effector T cells that inhibit T cell expansion and can diminish TNF and IFN-γ production[224,225]. IAV (co)infection increased the frequency of $LAG\text{-}3^+$ cells among $CD4^+$ T cells in comparison with *Mtb*-alone-infected mice. Significantly enhanced proportions of LAG-3 expressers were already detected on day 3 after IAV-coinfection (day 15 *Mtb* infection, Figure 23D) with more pronounced elevation compared to *Mtb*-infected mice on day 6 and day 9 after viral infection (day 18 and day 21 *Mtb* infection). $CD4^+$ T cells characterized by LAG-3 also responded to polyclonal restimulation with significantly enhanced IL-10 producers in IAV-(co)infected compared to *Mtb*-alone-infected mice on day 6 and 9 after the viral infection (day 18 and day 21 *Mtb* infection, Figure 23E, F).

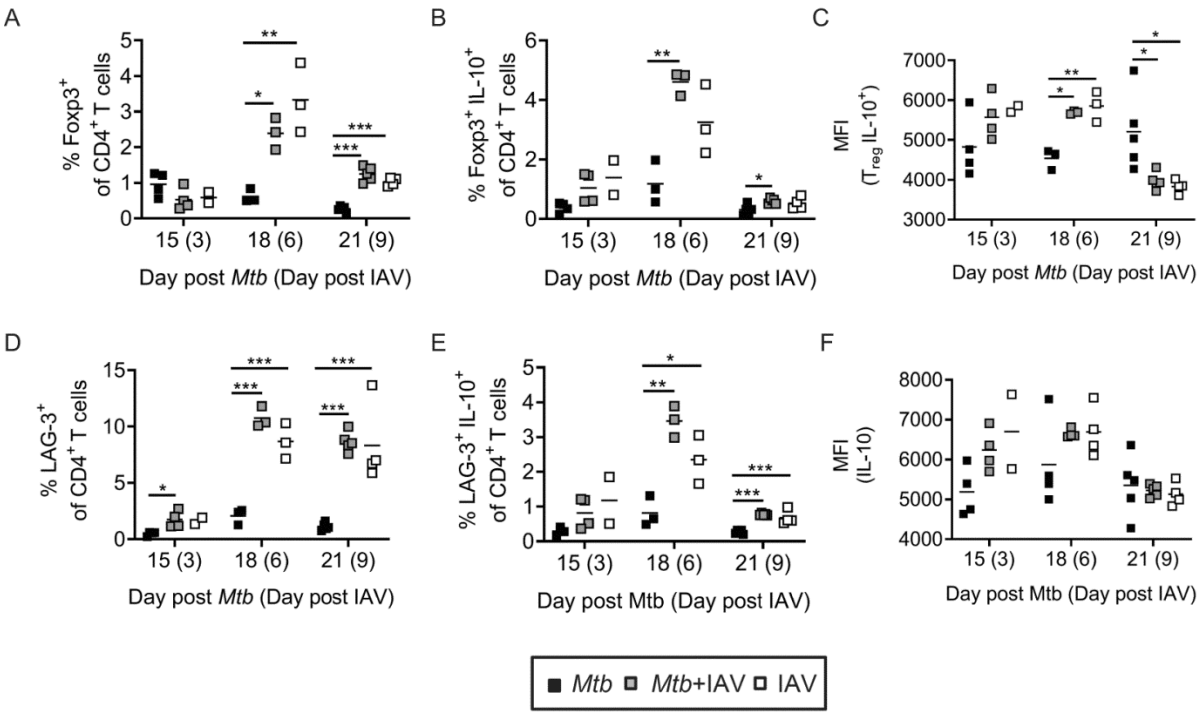

Figure 23 IAV infection induces regulatory T cells and increases frequency of co-inhibitory LAG-3 expressers. C57BL/6 mice were infected via aerosol with a low-dose of *Mtb* H37Rv and 12 days later coinfected i.n. with 10^4 PFU IAV (A/HH/05/09 pH1N1). Lungs were collected at indicated time points and analyzed by flow cytometry for (A) presence of Foxp3$^+$ CD4$^+$ T cells, (B) IL-10 producing Foxp3$^+$ CD4$^+$ T cells and (C) the median fluorescence intensity (MFI) of IL-10 produced by Foxp3$^+$ CD4$^+$ T cells. Further frequencies among CD4$^+$ T cells are shown for (G) LAG-3$^+$ frequencies, (H) IL-10 producing LAG-3$^+$ expressers among CD4$^+$ T cells and (I) MFI for IL-10 produced by LAG$^+$ CD4$^+$ T cells (n=3-5 per group (d15 IAV n=2), representative of two independent experiments). Each data point represents one mouse. *p ≤0.05; **p ≤ 0.01, ***p ≤0.001 determined by (A-C) One-way ANOVA followed by Tukey's multiple-comparison test. (Parts of data are published in Ring *et al*., 2019.)

So far, the data showed that IAV coinfection resulted in a compromised *Mtb*-specific CD4$^+$ T cell response and polarization of macrophages towards an alternatively activated phenotype. The suppressed adaptive and innate effector functions were concurrent with an increased IL-10 production by both innate and adaptive immune cells. In order to ultimately determine whether the IAV-induced IL-10 immune response conferred the exacerbation of *Mtb* infection, I next blocked IL-10 receptor signaling.

Mice were subjected to the standard *Mtb*-IAV infection protocol (Figure 4A) and given a single dose of anti-IL-10 receptor antibody (anti-IL-10R Ab, clone 1B1.3) or isotype control on day 5 after IAV infection (day 17 *Mtb* infection, Figure 24A). On day 9 after IAV coinfection (day 21 *Mtb* infection), mice were sacrificed and the pulmonary bacterial burden was determined. The anti-IL-10R treatment did not affect the bacterial load in *Mtb*-alone-infected animals (Figure 23B). Blocking of IL-10 receptor signaling could, however, reduce the bacterial burden in IAV-coinfected lungs to a level comparable to *Mtb*-single-infected lungs indicating that IL-10R signaling greatly contributed to the loss of bacterial control in IAV-coinfected mice.

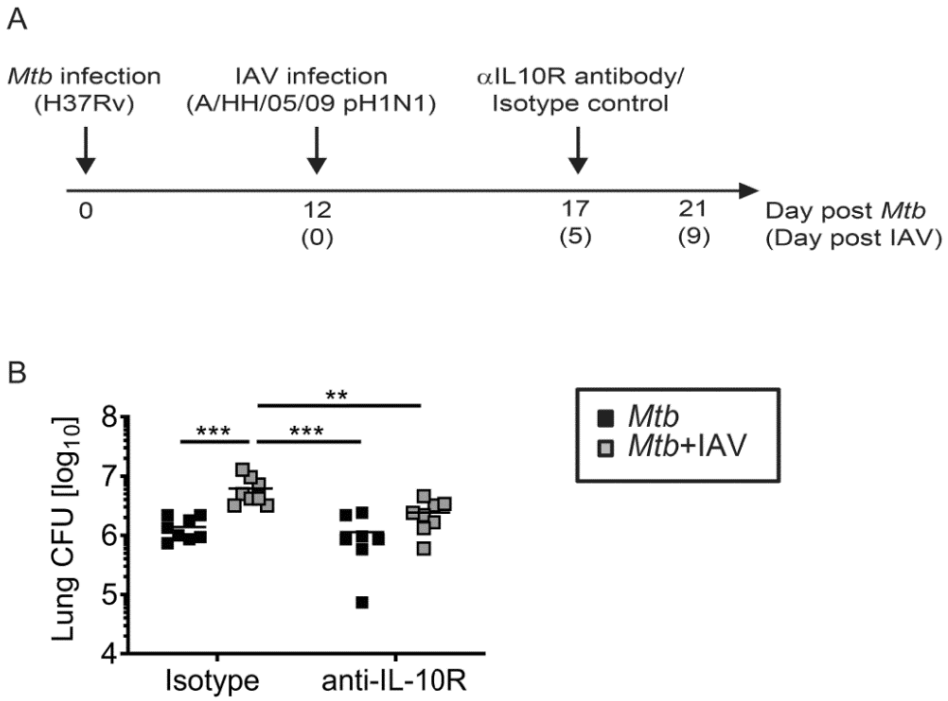

Figure 24 Anti-IL-10R treatment reduces *Mtb* load in coinfected mice. C57BL/6 mice were infected via aerosol with a low-dose of *Mtb* H37Rv and 12 days later coinfected with 10^4 PFU IAV (A/HH/05/09 pH1N1). (A) Schematic time-line of experimental set-up. 200 µg anti-IL-10R antibody (αIL10R antibody, clone 1B1.3) or isotype control (polyclonal rat serum IgG) were administered i.p. on day 5 after IAV infection (day 17 *Mtb*). (B) Lungs were collected at day 21 *Mtb* (day 9 IAV) and analyzed for bacterial burden (n=7-8 per group, pooled data from two independent experiments). Each data point represents one mouse. **p ≤ 0.01, ***p ≤0.001 determined by (B) Two-way ANOVA followed by by Tukey's multiple-comparison test. (Data are published in Ring *et al*., 2019.)

In order to address the basis of improved bacterial control after IL-10R blockade, I investigated whether anti-IL-10R treatment restored the *Mtb*-specific $CD4^+$ T cell response in IAV coinfected mice. Blocking of IL-10 signaling did not result in increased numbers and/or frequencies of $I\text{-}A^b$ ESAT-$6_{4\text{-}17}$-specific $CD4^+$ T cells in the lungs of anti-IL-10R-treated coinfected compared to untreated or isotype-treated coinfected mice (Figure 25A, B). Furthermore, anti-IL-10R treatment did not enhance the frequency of IFN-γ producers and thus could not improve *Mtb*-specific $CD4^+$ T cell effector function based on T_H1 cytokine production (Figure 25C). This suggests that the blocking of IL-10R signaling conferred its beneficial effects on *Mtb* control in a T cell-independent manner.

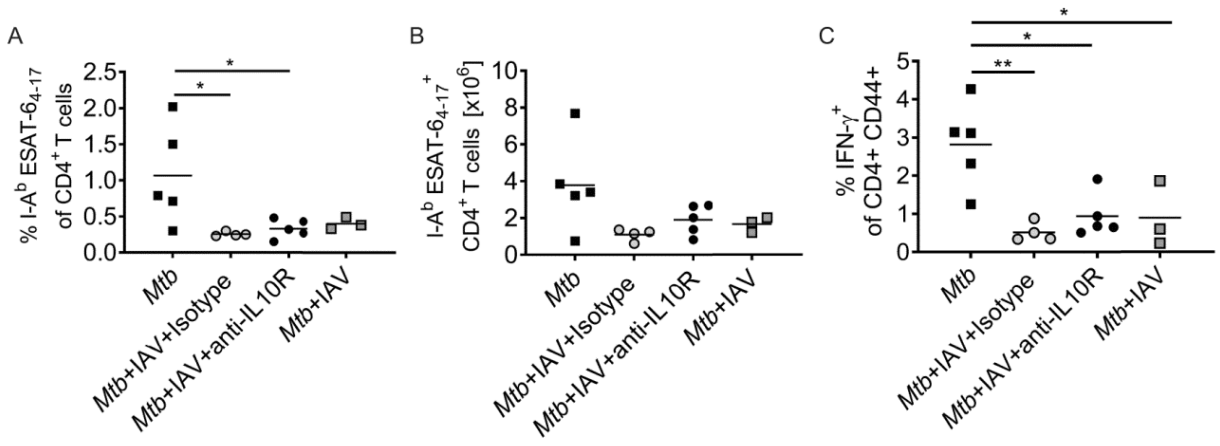

Figure 25 Anti-IL-10R treatment does not restore *Mtb*-specific T cell responses in coinfected mice. C57BL/6 mice were infected via aerosol with a low-dose of *Mtb* H37Rv and 12 days later coinfected with 10^4 PFU IAV (A/HH/05/09 pH1N1). 200 µg anti-IL10R antibody (1B1.3) or isotype control (polyclonal rat serum IgG) were administered i.p. on day 5 after IAV infection (day 17 *Mtb*). Lungs were analyzed by flow cytometry on day 21 *Mtb* (day 9 IAV) for (A, B) I-Ab ESAT-6_{4-17}-specifc CD4$^+$ T cells (n=3-5 per group, one experiment), and (C) IFN-γ producing CD4$^+$ T cells upon ex vivo restimulation with ESAT-6_{1-20} peptide (n=3-5 per group, one experiment). Each data point represents one mouse. *p ≤0.05; **p ≤ 0.01, determined by one-way ANOVA followed by Tukey's multiple-comparison test. (Data are published in Ring *et al*., 2019.)

Supporting the T cell data of the anti-IL-10R treatment, flow cytometric analyses of lung cells showed that by day 16 after IAV coinfection (day 28 *Mtb* infection), (*Mtb*-specific) CD4$^+$ T cell effector functions, in terms of IFN-γ and TNF producers, were restored in IAV-coinfected mice (Figure 26A-B,26D-E) despite the presence of still significantly increased frequencies of IL-10 producing CD4$^+$ T cells (Figure 26C). A comparable proportion of IL-10 producing CD4$^+$ T cells between *Mtb*-alone and IAV-coinfected mice was detected on day 36 after IAV coinfection (day 48 *Mtb* infection) while IAV-alone-infected lungs still presented significantly enhanced IL-10 producing CD4$^+$ T cells. There was no IL-10 response upon ex vivo restimulation with ESAT-6_{1-20} on either day (data not shown).

The restoration of CD4$^+$ T cell effector function by day 16 after IAV coinfection (day 28 *Mtb* infection) was not connected to a reduction in the bacterial load since bacterial levels were still significantly elevated (Figure 4B). This, together with the T cell-independent effect of the anti-IL-10R treatment, indicate that in our experimental coinfection set-up a compromised *Mtb*-specific CD4$^+$ T cell response was not the major determinant for the loss of *Mtb* control.

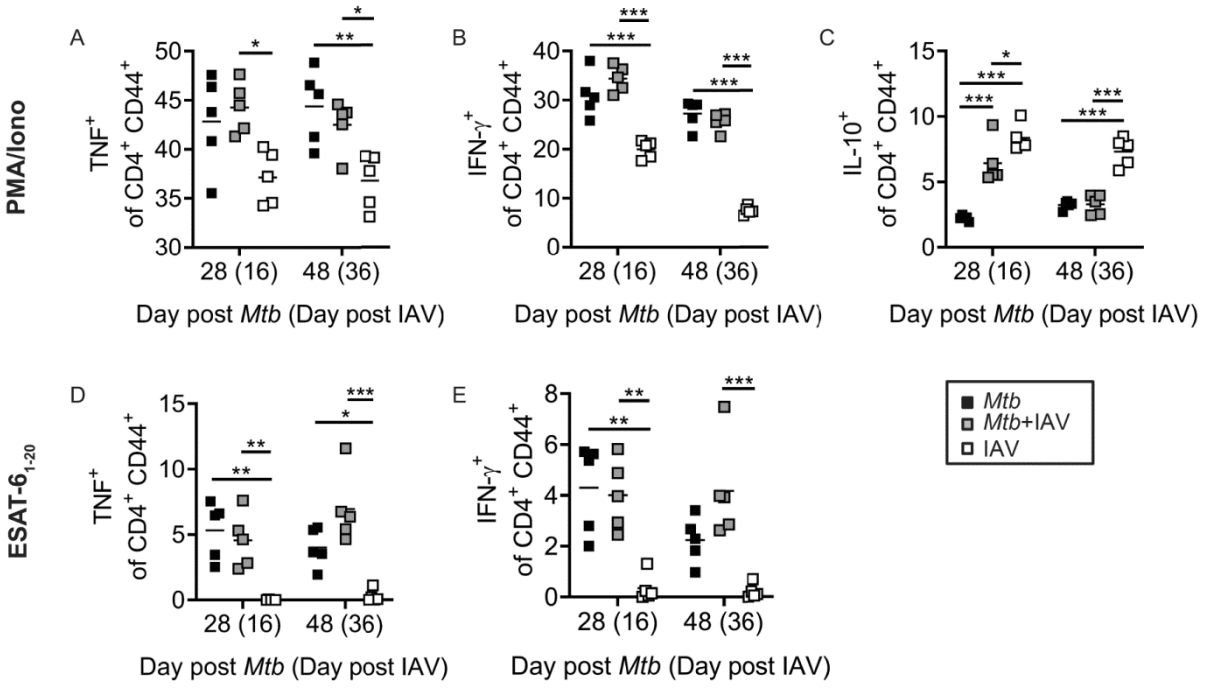

Figure 26 Restoration of *Mtb*-specific CD4$^+$ T cell response after recovery from acute IAV infection. C57BL/6 mice were infected via aerosol with a low-dose of *Mtb* H37Rv and 12 days later coinfected with 10^4 PFU IAV (A/HH/05/09 pH1N1). Lungs were analyzed by flow cytometry on indicated time points for TNF, IFN-γ and IL-10 producing CD4$^+$ T cells upon ex vivo restimulation with (A) PMA/Iono and (B) ESAT-6$_{1-20}$ peptide (no IL-10 responders), n=5 mice per group, representative of two independent experiments. Each data point represents one mouse. *p ≤0.05; **p ≤ 0.01, ***p ≤0.001 determined by One-way ANOVA followed by Tukey's multiple-comparison test.

Results 3.6: Summary

IAV-induced IL-10 contributed to the loss of *Mtb* control in IAV-coinfected animals.

- IAV infection upregulated *Il10* expression in the lungs of coinfected mice.
- IL-10 was produced by cells of both the innate and adaptive immune system.
- CD4$^+$ T cells were a major source of IL-10 among CD45$^+$ cells in IAV (co)infected mice. IAV infection increased the frequencies of T_{reg} and CD4$^+$ T cells that expressed the co-inhibitory receptor LAG-3.
- Blocking IL-10 receptor signaling prevented increased pulmonary *Mtb* burden in IAV-coinfected mice.
- Amelioration of the IAV-mediated TB exacerbation was independent of the *Mtb*-specific CD4$^+$ T cell response.

4 Discussion

Increasing epidemiological evidence strongly indicates that IAV infection impairs effective control of *Mtb* in humans. However, experimental data as to which immunological changes occur during this coinfection and contribute to loss of *Mtb* control are largely missing. The current study addressed *Mtb*-IAV coinfection in C57BL/6 mice in order to elucidate the immune modulations of both the innate and the adaptive immune responses that are involved in controlling *Mtb* infection.

4.1 Impact of an IAV infection on *Mtb* control and vice versa

Retrospective analyses of mortality data from the 1918-1919 influenza pandemic (Spanish Flu) suggest that an IAV coinfection had a negative impact on TB patients[192,193,226]. It was concluded that people with TB were at a higher risk to die from an influenza virus infection than people without TB. This negative association was also highlighted in more recent epidemiological analyses, and also emphasized for the latest IAV pandemic in 2009[185,187–191,201]. For instance, it was declared for South Africa that 10% of H1N1 cases who succumbed during the 2009 pandemic also had active TB[185]. A very recent report from the Gambia further showed that at the time of TB diagnosis 4.3% of patients had viral RNA from influenza A or B viruses present in their sputum[191]. Strikingly, coinfected patients presented with a significantly higher bacterial burden in the sputum compared to patients infected with *Mtb* only. Taken together, the epidemiological data suggest that an IAV infection may promote primary progressive TB, exacerbation of TB or reactivation of latent TB infection.

In the current study, the impact of an IAV infection on the control of a pre-existing *Mtb* infection was analyzed in C57BL/6 mice. Mice were infected with a low-dose of *Mtb* H37Rv and 12 days thereafter coinfected with a sub-lethal dose of the IAV strain A/HH/05/09 pH1N1. On day 12 after *Mtb* infection, the *Mtb*-specific immune response is not yet present in the lung. It is expected to be established around day 20 after *Mtb* infection and halts the exponential growth of the mycobacteria[55]. IAV coinfection of *Mtb*-infected mice resulted in a rapid increase of pulmonary mycobacterial burden as early as 6 days after IAV coinfection (day 18 *Mtb* infection) that was even more pronounced on day 9 after IAV coinfection (day 21 *Mtb* infection). The enhanced bacterial levels in coinfected mice were observed until the latest time point of analyses, namely day 63 after IAV infection (day 75 *Mtb* infection). These data are in line with previous experimental studies which also found IAV coinfection associated with an increased mycobacterial lung burden[195,196]. This appears to be independent of the time point of IAV coinfection as pre-existing, simultaneous as well as subsequent IAV infections all resulted in eventual loss of bacterial growth control as seen in coinfection experiments with both *Mtb* and *M. bovis* BCG. In the current study, the IAV coinfection had persisting effects on TB which is reflected by the controlled but still significantly elevated mycobacterial burden in the lungs of coinfected compared to *Mtb*-alone-infected mice. *Mtb*-IAV-coinfected mice could control the bacterial level after day 21 of *Mtb* infection but were unable to reach a bacterial load comparable to that of *Mtb*-alone-infected mice although the virus was mostly cleared by day 9 after IAV infection (day 21 *Mtb* infection). Consequently, despite the acute nature of the IAV infection and the transient presence of replicating virus, this study demonstrates that an IAV infection can exert long-

term consequences on the *Mtb*-infected host. Interestingly, IAV infection was previously shown to induce epigenetic changes in the host cell[227,228]. Repressive histone modifications on promoters of genes important for antibacterial immunity were found as a response to IAV-induced type I IFN signaling. Since epigenetic changes can be passed on to daughter cells, this mechanism could explain the long-term consequences of IAV coinfection even after viral clearance that were identified in this study. The present study further shows that although IAV infects the lung, it also systemically affects *Mtb* control. This could be seen in an increased splenic bacterial burden in coinfected compared to *Mtb*-alone-infected mice. Of note, the enhanced bacterial load was observed later than in the lungs (day 36 after IAV infection = day 48 after *Mtb* infection). Elevated *Mtb* loads in the spleen by that time could be either due to loss of bacterial control within the organ, a consequence of increased bacterial dissemination from the lung to the spleen or both. For IAV infections, it was reported that although the lung is the primary site of infection, IAV-specific $CD8^+$ T cells are also primed in the spleen where they can subsequently give rise to memory T cells[229]. Moreover, another study showed germinal center formation in the spleen up to three weeks after IAV infection[229]. Additionally, a study by Yoo *et al.* described a late-activator antigen-presenting cell (LAPC) population in IAV-infected mice that migrated from the lungs to the dLN and spleen[229]. There, LAPCs initiated an anti-inflammatory T_H2-based immune response. As the name suggests, LAPCs had delayed migration kinetics compared to DCs and peaked in dLN and spleen around day 8 after viral infection in contrast to DCs which were highest in numbers in the dLN by day 3 after viral infection. Hence, those studies show that the spleen is an important organ in the context of an IAV-induced immune response both at the initial stages but also after viral clearance. Accordingly, the above described immune responses could perturb control of *Mtb* in the spleen even after the immediate antiviral immune response. Furthermore, cells such as DCs that traffic from the lung to the spleen might aid *Mtb* dissemination.

Especially in countries with a high prevalence of TB cases, factors such as overcrowding, multiple *Mtb* infections and a late TB diagnosis can result in patients suffering from a high *Mtb* burden[230]. This scenario can be reflected by a high-dose *Mtb* infection in mice. To investigate how an IAV coinfection impacts the control of a high-dose *Mtb* infection, C57BL/6 mice were subjected to the same experimental set-up as above, except for being infected with a tenfold dose of *Mtb* compared to the standard low-dose. Comparable to the low-dose experiment, IAV challenge of mice infected with a high-dose of *Mtb* resulted in a significant increase of bacterial loads in the lungs of coinfected compared to *Mtb*-alone-infected mice on day 9 after IAV infection (day 21 *Mtb* infection). This enhanced pulmonary *Mtb* load was still present on day 36 after IAV infection (day 48 *Mtb* infection). Further time points would need to be included to assess whether the *Mtb* burden could be controlled on that elevated level as seen for the low-dose study. In contrast to the low-dose *Mtb* infection in which IAV coinfection did not influence the survival, IAV coinfection of high-dose *Mtb*-infected mice significantly decreased the survival compared to *Mtb*-alone-infected mice. High-dose *Mtb* infection alone, however, only marginally impacted the survival at very late time points. The challenge of high-dose *Mtb*-infected mice with a sub-lethal IAV dose resulted in acute and delayed mortality; some mice already succumbed early after IAV coinfection (day 16-29 after

IAV= day 28-41 after *Mtb* infection) while another group died at later timer points (from day 92 onwards after IAV infection = day 104 after *Mtb* infection). This again suggests persisting IAV-mediated increase of the host's susceptibility to TB. High-dose *Mtb*-infected mice were also coinfected with IAV when the *Mtb*-specific immune response was not yet established. Nonetheless, exuberant replication of *Mtb* due to the coinfection might not be the main determinant for early loss of *Mtb* growth control in the high-dose model. The difference in the pulmonary bacterial load between *Mtb*-alone and coinfected mice was comparable to the difference seen in the low-dose model. Furthermore, the increased bacterial burden in coinfected mice did not rise further but was controlled on an elevated level (analyzed time points: day 9 and 36 after IAV infection = day 21 until day 48 after *Mtb* infection). A more likely explanation might be that coinfected mice suffered from an increased and uncontrollable inflammatory response. Such an excessive inflammatory immune response could correlate to a high frequency of infected epithelial cells. These are the predominant host cells of IAV and can also be infected by *Mtb*. In a study where *Mtb* was applied intra-tracheally, 10% of intracellular bacteria were detected in epithelial cells[231]. Hence, a higher bacterial input in our model may result in more total epithelial cells being infected by *Mtb*. The additional coinfection with IAV may cause loss of epithelial cell integrity due to increased apoptosis/necrosis induction by both pathogens[232,233]. This may ultimately cause an acute respiratory distress syndrome. A study by Davidson and colleagues indeed showed that morbidity and mortality in IAV-susceptible 129 mice after acute IAV infection was associated with type I IFN-mediated upregulation of the apoptosis-inducing receptor DR5 on lung epithelial cells[234]. Lack of IFNαβ signaling in 129 mice reduced lung damage and excessive inflammation by, among others, reducing DR5 expression. The 129 mice are characterized by a higher IFNαβ response compared to C57BL/6 mice. IFNα treatment of IAV-infected C57BL/6 mice increased morbidity demonstrating a type I IFN-dose-dependent pathogenic impact. Type I IFNs are reported to be also induced by *Mtb* and exert detrimental effects in TB[83,85,86]. In the present study, low-dose *Mtb* infection alone did not show an induction of type I/III IFN activity until day 21 after *Mtb* infection. The type I IFN response was only elicited in the presence of IAV. However, in the *Mtb* high-dose- IAV coinfection the type I IFN response might have been potentiated by the presence of the underlying *Mtb* infection entailing the detrimental effects on host survival. Consequently, the role of DR5 and type I IFNs for the decreased survival in the IAV-coinfected *Mtb* high-dose model should be investigated. In addition to that, the interaction of infected epithelial cells with immune cells promotes further cytokine production that lead, if not counter-regulated, to an excessive inflammatory response. Future studies should address why some mice showed delayed progression of TB (longer period of being asymptomatic after coinfection) and which factors then triggered the disease progression. A potential approach might be the cytokine/chemokine profiling of serum samples within a detailed coinfection follow-up study. Serum samples may allow for regular and longitudinal analyses of living animals and onset of symptoms might be ascribed to prior changes in the cytokine profile. That IAV-mediated exacerbation can be delayed is also reflected by a study by Redford *et al.*[196]. IAV pre-infected mice (IAV infection 28 days before *Mtb* infection) presented with an increased bacterial burden not before day 120 after *Mtb* infection. This further indicates that IAV coinfection can destabilize *Mtb* control during

the chronic plateau phase in which bacterial numbers are kept at a certain level by the host. This is supported by our own data showing that IAV coinfection on day 30 after *Mtb* infection resulted in an increased pulmonary bacterial burden by day 41/42 after IAV infection (day 71/72 *Mtb* infection) in coinfected compared to *Mtb*-alone-infected mice (Supplement, Figure S1). There was, however, no initial difference in the bacterial burden after 9 days after IAV coinfection (day 39 *Mtb* infection) which is in contrast to the rapid effect induced by IAV coinfection on day 12 after *Mtb* infection. On day 12 after *Mtb* infection, *Mtb* is still in the exponential growth phase while on day 30 after *Mtb* infection, the bacteria are controlled by the host's immune response and supposedly in a dormant state. Dormancy is characterized by reduced replication and metabolic activity of *Mtb*[9,30]. This could explain the difference of immediate opposing to the delayed increased bacterial burden seen between day 12 and day 30 of IAV coinfection. Reactivation and as such recrudescence of bacterial growth were linked to the upregulation of *Mtb* genes of the resuscitation-promoting factor (RPF) family[235]. Correspondingly, transcriptional and metabolic profiling of *Mtb* and *Mtb*-infected cells in *Mtb*-alone compared to the IAV-coinfected host could elucidate whether, when and to which extent IAV supports *Mtb* growth and especially regrowth in the chronic *Mtb* infection[236,237].
While the data clearly demonstrate that IAV coinfection exerts detrimental effects on *Mtb* control, a pre-existing *Mtb* infection neither affected the antiviral immune response nor impacted the viral clearance in *Mtb*-IAV-coinfected compared to IAV-alone-infected animals (viral load was also not affected in the *Mtb* high-dose study and IAV on day 30 after *Mtb*; Supplement, Figure S1 and S2). This underlines that the acute IAV infection provokes a very robust immune response which was not affected by concurrent infection in this study and others found in the current literature but instead sensitizes the host to bacterial infections[156].

4.2 IAV-mediated inflammation in *Mtb*-IAV coinfection

The robust anti-IAV immune response evokes the recruitment of mononuclear cells such as monocytes to the site of infection[238]. The monocyte/macrophage lineage presents a versatile phenotype with a rather continuous than clear-cut differentiation status[239]. Monocytes that transmigrate into the lung may differentiate into different cell types such as monocyte-derived DCs or monocyte-derived macrophages. Alveolar epithelial cells are the major producers of the monocyte-attracting CC-chemokine ligand 2 (CCL2) and CC-chemokine ligand 5 (CCL5) during the early antiviral response[240]. The present data show an early induction of CCL2 upon IAV (co)infection in the lungs whereas *Mtb*-alone-infected mice displayed only minor protein levels of this chemoattractant. CCL2 expression can be induced downstream of type I IFN-signaling[241,242]. This was also seen in a study in which mice received poly-IC, a potent inducer of high type I IFN levels, which resulted in increased *Ccl2* expression[82]. The study further showed that poly-IC treatment led to CCR2-dependent recruitment of an *Mtb*-permissive monocyte/macrophage population characterized as $CD11b^{+}F4/80^{+}GR1^{+}$ (Gr1 also known as Ly6C/Ly6G). This was concluded based on the observation that poly-IC treatment of CCR2 knockout (KO) mice did not result in the increased pulmonary *Mtb* burden as seen in CCR2 wildtype (WT) mice. In our study, increased type I/III IFN activity in IAV-(co)infected lungs was concomitant with augmented CCL2 and elevated frequencies of $CD11b^{+}F4/80^{+}Ly6C^{high/int/low}$ cells in the lungs of IAV-(co)infected compared to *Mtb*-alone-

infected mice. However, CCR2-deficiency could not prevent the IAV-induced increased pulmonary bacterial level in coinfected mice. A reason for the discrepancy in the relevance of CCR2 between the studies might be that poly-IC treatment was applied to induce continuously high levels of type I IFNs (treatment twice per week; analysis 4th week after *Mtb* infection). In contrast, in the present study, which used a physiological relevant type I IFN stimulus, type I/III IFN activity was already reduced by day 6 after IAV (co)infection and reached comparable levels to that of *Mtb*-alone-infected mice by day 9 after IAV (co)infection (day 21 *Mtb* infection). CCR2-deficiency also did not exert any effects on the bacterial burden in *Mtb*-alone-infected mice. This was expected because it was shown that CCR2-dependent control of *Mtb* was only relevant in a high-dose *Mtb* infection[243]. Together, these data again suggest that mice can compensate the loss of CCR2 until a certain threshold of either pathogen burden or pathogen-induced immune mediator is reached[244,245]. Obviously, in the present *Mtb*-IAV coinfection study CCR2 did not play a major role in compromising *Mtb* control.

While the IAV (co)infection resulted in an increased cell infiltration, it also depleted AMs from the lungs as early as 3 days after IAV infection (day 15 *Mtb* infection). AMs exert a protective role in IAV infection, however, induction of apoptosis was also reported as a host defense mechanism to prevent further spread of the virus[246–249]. The consequences of AM depletion for IAV control may depend on the viral strain and the time point of depletion. For instance, it was reported that the absence of AMs was only detrimental for IAV control when AMs were depleted before but not 3 or 5 days after IAV infection[249]. In contrast, IAV-induced AM depletion was linked to an enhanced susceptibility to *Streptococcus pneumoniae* in a coinfection study in which bacterial superinfection was installed 7 days after IAV infection[248]. With regard to the *Mtb* infection, AMs are the first cell type to be infected and are responsible for dissemination of the bacterium into the lung parenchyma[25]. Depletion of AMs before and continuously throughout *Mtb* infection resulted in better outcome of pulmonary TB[250]. However, when only the activated lung macrophages were depleted (depletion from day 2 after *Mtb* infection), *Mtb* control was reduced[251]. The relevance of IAV-induced AM depletion for the increased *Mtb* burden in the present coinfection model remains to be determined. A study that addressed the distribution of *Mtb* in different cell populations showed that by day 14 after *Mtb* infection AMs were not the major *Mtb*-infected cell type in the *Mtb*-infected host anymore[34]. Hence, the impact of the IAV-mediated depletion of AMs on *Mtb* dissemination in this model might be minor. However, the type of IAV-induced host cell death could modulate the subsequent immune response. In the study of IAV-*Streptococcus pneumoniae* coinfection, it was concluded that IAV induces necroptosis of AMs[248]. Necroptosis is a form of regulated necrosis often associated with virus-provoked cell death and was observed to be dependent on receptor-interacting serine/threonine-protein kinase 3 (RIPK3)[252,253]. Interestingly, in *Mtb* infection RIPK3-deficient macrophages demonstrate an improved bacterial control *in vitro* and *in vivo*[254]. Since the type of induced cell death can be IAV strain-dependent, analyzing which type is triggered *in vivo* by the 2009 pH1N1 isolate used in this study could put the AM depletion into perspective in terms of relevance for *Mtb* control[232]. That the type of cell death can play an important role in the control of an *Mtb* infection is also represented by the adverse consequences of necrosis versus apoptosis induction in *Mtb*-

infected cells[48]. Virulent *Mtb* can modulate the type of cell death via the induction of the lipid mediator LXA4 that inhibits the pro-apoptotic lipid mediator PGE2[48]. In accordance with the opposing roles of apoptosis and necrosis in *Mtb* control, PGE synthase-deficient ($PGE2^{-/-}$) mice were shown with increased pulmonary *Mtb* burden[48]. In the present study, LXA4 was not detected in the lungs of either infection group but PGE2 levels increased over time in IAV-(co)infected lungs. There was no induction of PGE2 in *Mtb*-alone-infected lungs within the observation time. Nonetheless, PGE2 cannot be attributed a protective function in coinfected mice because coinfected mice had increased bacterial levels despite higher levels of PGE2 compared to Mtb-alone-infected mice. In fact, a study by Moreno and colleagues associated high PGE2 levels with immunosuppressive effects resulting in TB disease progression in BALB/c mice[255]. Their results indicated that the high concentration of PGE2 reduced the expression of T_H1 cytokines such as IFN-γ and further the expression of NOS2, which are important mediators of protection against an *Mtb*-infection[66,67,255–257]. Accordingly, the IAV-induced enhanced levels of PGE2, which are concomitant with the increased bacterial burden in coinfected mice, suggest an anti-inflammatory role of PGE2 in the present study. Thus, PGE2 could be a mediator of the IAV infection-induced resolution phase[156]. This phase is initiated with the onset of the antiviral adaptive immune response between day 6 and 8 after the viral infection[156,166]. It is characterized by an anti-inflammatory environment, among others mediated via the immunosuppressive cytokine IL-10, that sensitizes the host to bacterial infections[258]. Indeed, qRT-PCR analyses of lung homogenates revealed increased *Il10* expression in the lungs of IAV-(co)infected compared to *Mtb*-alone-infected mice. IL-10 has a detrimental role in the control of TB[259]. It can affect both innate and adaptive antimycobacterial immune responses. The consequences of the IAV infection on innate and *Mtb*-specific immunity are discussed in the following chapter.

4.3 IAV coinfection compromises antimycobacterial innate and adaptive immunity

In the murine low-dose TB model, the antimycobacterial $CD4^+$ T cell response is established at around day 20 after *Mtb* infection and leads to control of bacterial growth[55]. $CD4^+$ T cells are indispensable for conferring protection against *Mtb* infection and have a decisive role especially during the early *Mtb* infection[56]. $CD8^+$ T cells, on the other hand, are described to be more relevant at later stages of *Mtb* infection and thus play an inferior role at the early onset of *Mtb*-specific adaptive immunity[59]. $CD8^+$ T cells cannot compensate for the lack of $CD4^+$ T cells supporting the superior role of $CD4^+$ T cells in *Mtb* control[56]. Hence, the focus of this study was laid on the *Mtb*-specific $CD4^+$ T cells.

The significantly increased pulmonary bacterial load in IAV-coinfected compared to *Mtb*-alone-infected mice indicates that an IAV coinfection interferes with the anti-*Mtb* $CD4^+$ T cell effector functions. Anti-*Mtb* effector functions of $CD4^+$ T cells comprise the secretion of the T_H1 macrophage-activating cytokines TNF and IFN-γ[49]. In fact, 9 days after IAV infection (day 21*Mtb* infection) flow cytometric analyses revealed that lungs from IAV-coinfected mice had significantly reduced frequencies of TNF and IFN-γ-producing $CD4^+$ T cells upon *Mtb*-specific ESAT-6_{1-20} *ex vivo* restimulation compared to *Mtb*-alone-infected mice. (Re)Activation of $CD4^+$ T cells requires the presentation of the T cell receptor (TCR)-cognate

peptide in a MHC-II-dependent context. In line with decreased frequencies of TNF^+ and IFN-γ^+ CD4+ T cells, frequencies of MHC-II-expressing DCs ($CD11c^+CD45^+$) were significantly lower in IAV-(co)infected compared to *Mtb*-alone-infected lungs at all analyzed time points (day 3-9 after IAV infection = day 15-21 after *Mtb* infection). Infection of DCs by influenza virus was reported to be associated with influenza protein NS1-mediated attenuation of DC maturation and consequently reduction of their T cell activation capacities[260]. Accordingly, it would be of interest at which frequency DCs are actually infected with the IAV in this study and whether infection of DCs would correlate with a decreased efficiency of T cell activation. Since NS1-induced effects can only be exerted in virus-infected cells, future experiments would need to address whether IAV-infected DCs also present *Mtb* antigens. To corroborate a decreased activation capacity of DCs in IAV-coinfected compared to *Mtb*-alone-infected lungs, expression of the T cell costimulatory surface proteins CD80, CD86 as well as the production of the T_H1-polarizing cytokine IL-12 by DCs could be analyzed[261,262]. Besides a direct infection with IAV, the suggested compromised induction of T_H1 cells by DCs might also be due to the aforementioned IAV-induced anti-inflammatory environment which will be discussed more closely in the next chapter. In contrast to the IAV-specific H1N1-NP366-specific $CD8^+$ T cells which were comparably induced in the lungs of coinfected and IAV-alone-infected mice, numbers and frequencies of *Mtb*-specific I-A^b ESAT-6_{4-17} $CD4^+$ T cells were markedly reduced in coinfected compared to *Mtb*-alone-infected mice. The decreased presence of *Mtb*-specific $CD4^+$ T cells in the lungs hints at the fact that not only the reactivation of *Mtb*-specific effector T cells at the site of infection was disturbed by a concurrent IAV infection, but that also the recruitment from and/or priming in the dLN was impacted. Indeed, diminished numbers of I-A^b ESAT-6_{4-17}-specific $CD4^+$ T cells were found in dLNs of coinfected compared to those from *Mtb*-alone-infected mice. This indicates that fewer *Mtb*-specific $CD4^+$ T cell numbers in the lungs were not only due to inefficient recruitment of T cells from the dLNs but that a compromised T cell priming in the dLNs already reduced the number of available *Mtb*-specific $CD4^+$ T cells that could be recruited. This notion was confirmed in an adoptive T cell transfer experiment. In the dLNs from coinfected mice, a decreased proportion of adoptively transferred *Mtb*-specific p25TCR-tg $CD4^+$ T cells proliferated compared to *Mtb*-alone-infected mice. This was not due to a decreased trafficking of *Mtb* to the dLN because there was no difference in the presence of viable bacteria between IAV-coinfected and *Mtb*-alone-infected dLNs. Thus, it can be speculated that either the antigen processing, presentation or costimulatory signaling were impaired or insufficient to prime *Mtb*-specific $CD4^+$ T cells in the dLNs of coinfected mice. This observation is in line with a study by Flórido and colleagues who found decreased proliferation of BCG OVA-specific T cells in the dLNs of BCG-IAV coinfected compared to BCG-alone-infected mice although the BCG burden in the dLNs was comparable[195]. The anti-IAV $CD8^+$ T cell response was described to be initiated in the dLNs with the arrival of DCs around day 1-3 after IAV infection[153]. Wolf *et al.* observed the activation of *Mtb*-specific $CD4^+$ T cells in the dLN around day 11-14 after *Mtb* infection[42]. Hence, both time windows of respective T cell priming actually coincided in the present coinfection model (day 1-3 after IAV infection = day 13-15 after *Mtb* infection). Intriguingly, the IAV-specific immune response was properly induced despite the underlying *Mtb* infection. This observation argues against a

general immunosuppressive environment in the dLNs and raises the question why the host failed to induce an antimycobacterial immune response or favored the antiviral immune response. One could hypothesize that *Mtb* utilized the concurrent IAV infection for its own benefits to further subvert the establishment of the anti-*Mtb* adaptive immune response. Srivastava and colleagues demonstrated that *Mtb* exploits the vesicular transport pathway to transport *Mtb* antigen out of the cell, thereby impairing $CD4^+$ T cell activation[263]. IAV was reported to use and alter the vesicular transport system for the generation and assembly of new virions[264,265]. The possibility that IAV-mediated manipulations of vesicular pathways might benefit *Mtb* by escaping presentation via MHC-II again emphasizes the importance of analyzing if DCs or more generally APCs are coinfected. Moreover, RNA-sequencing and/or proteome analyses of *Mtb*-infected DCs from dLNs of *Mtb*-alone compared to IAV-coinfected animals could reveal whether and which intracellular pathways required for *Mtb*-specific $CD4^+$ T cell activation were affected by IAV-coinfection. Here, one could discriminate coinfected DCs and *Mtb*-alone-infected DCs exposed to the IAV-induced environmental modulation. Additionally, the study by Srivastava *et al.* showed that *Mtb*-specific CD4+ T cell activation was more effective when DCs were directly infected compared to DCs that acquired antigen by antigen transfer. However, since the number of viable mycobacteria in the dLNs was comparable between *Mtb*-alone and IAV-coinfected mice, a deficit in directly-infected cells in the dLNs does not seem to be the case. Nonetheless, the analysis of the *Mtb* burden in the dLNs did not address whether cells from *Mtb*-alone compared to IAV-coinfected dLNs were infected with a comparable number of mycobacteria per cell or whether the coinfection promoted a higher number of *Mtb* in single cells. A higher *Mtb* infection rate would presumably compromise the T cell activation capacity of DCs more strongly compared to DCs carrying a lower *Mtb* burden.

As mentioned before, a major role of *Mtb*-specific $CD4^+$ T cells is the activation of *Mtb*-infected macrophages via the key activator IFN-γ[49]. The consecutive antimycobacterial effector functions of activated macrophages encompass phagosome maturation, the NADPH-dependent generation of ROS and predominantly the generation of NO and RNI by the NOS2-dependent pathway. The significant contribution of NO and RNI to *Mtb*-resistance was shown by *in vitro* and *in vivo* murine studies but its importance in human TB is controversial[64–67,266]. While *Mtb*-alone-infected mice showed induction of *NOS2* transcripts in the lung over time, transcriptional levels of *NOS2* from IAV-coinfected mice remained low until day 21 after *Mtb* infection (day 9 after IAV infection). As a consequence, lung homogenates from IAV-coinfected compared with *Mtb*-alone-infected mice had significantly reduced levels of RNI 9 days after IAV infection (day 21 *Mtb* infection). In accordance with the role of RNI for mycobacterial growth control, these results strengthen the inverse correlation of RNI to mycobacterial burden. The higher mycobacterial load in lungs of IAV-coinfected mice coincided with a lower amount of RNI compared to *Mtb*-alone-infected mice. The production of RNI is on the one hand dependent on NOS2 activity but on the other hand also on the availability of the substrate L-arginine[207]. L-arginine can also be utilized by the NOS2-competing enzyme Arg-1 to produce polyamines. In fact, qRT-PCR analyses of lung homogenates revealed a potent induction of *Arg1* in IAV-(co)infected mice on day 6 after viral infection (day 18 *Mtb* infection). Besides *Arg1*, *Fizz1*, which is also a marker for

alternatively activated macrophages[208,209], was also significantly increased in lungs of IAV-(co)infected compared to *Mtb*-alone-infected mice. Taken together, this strongly indicates that IAV (co)infection drives macrophage polarization towards an alternatively activated phenotype. In addition to the transcriptional data, flow cytometric analysis showed that macrophages ($CD11b^+F4/80^+CD11c^+Ly6C^+Ly6G^-$) from IAV-(co)infected lungs produced higher levels of ARG-1 and lower levels of NOS2 compared to *Mtb*-alone-infected macrophages, with an ultimately inversed NOS2/ARG-1 ratio in favor of ARG-1 on day 9 after IAV (co)infection (day 21 *Mtb* infection). Alternative activation of macrophages in general, but also specifically arginase-1 production by macrophages has been associated with decreased control of *Mtb*[267–269]*.* Comparable to the data presented in this study, a helminth/*Mtb* coinfection study also found an inverse NOS2/ARG-1 ratio shifted to ARG-1 concomitant with an elevated mycobacterial burden[269]. The described macrophage population from IAV-coinfected mice did not only have higher ARG-1 levels, but was also represented among $CD11b^+$ cells to a greater extent compared to *Mtb*-alone-infected mice. This indicates that IAV-coinfected lungs harbored an increased repertoire of *Mtb*-permissive cells that were unable to control bacterial growth. Future studies could address whether ARG-1 levels directly correlate to the mycobacterial number on a per cell basis in this *Mtb*-IAV coinfection. The presence of an alternatively activated phenotype in the lung is further confirmed by the high induction of IL-1 receptor antagonist (IL-1RA, *Il1rn*)[208] in IAV-(co)infected compared to *Mtb*-alone-infected mice as rapidly as 3 days after viral infection (day 15 *Mtb* infection). IL-1RA blocks IL-1R signaling and thus also the positive feedback loop of IL-1 on its own expression[212,270]. While *Mtb*-alone-infected lungs showed increasing *Il1a* expression over time, expression in IAV-(co)infected mice decreased and was already significantly lower compared to *Mtb*-alone-infected mice on day 6 after viral (co)infection (day 18 *Mtb* infection). *Il1b* expression was not found to be promoted in *Mtb*-alone-infected mice, but expression also diminished in IAV-(co)infected lungs over time. The reduced expression of *Il1a* and *Il1b* can be a decisive factor for the increased bacterial burden since *Mtb* resistance was clearly shown to be IL-1-dependent[68]. The enhanced relative expression of *Il1rn* and the decreased expression of *Il1a* both can be downstream effects of type I IFN signaling. Type I IFNs and IL-1 were reported to counter-regulate each other[90]. The type I IFN-mediated inhibition of IL-1 can be direct or indirect via the induction of IL-10 or IL-1RA. Type I IFN transcription can be, on the other hand, inhibited by IL-1 either direct or indirect by upregulation of PTGS2 (also known as cyclooxygenase-2, COX-2). PTGS2 catalyzes the synthesis of the lipid mediator PGE2 which then directly inhibits type I IFN protein expression. While *Il1a* and *Il1b* transcripts decreased over the course of IAV (co)infection, PGE2 levels steadily increased in IAV-(co)infected mice until day 9 after IAV infection (day 21 *Mtb* infection) indicating that PGE2 was likely induced independently of IL-1 in this coinfection model. A study by Coulombe and colleagues reported that mice lacking PGE2 ($Ptges^{-/-}$mice) or that were pharmacologically treated with PGE2 receptor inhibitors showed an improved outcome of IAV infection[213]. In contrast, a study with *Mtb*-infected Ptges-/-mice showed an increased susceptibility and higher bacterial burden[48]. These outcomes were in part linked to the PGE2-mediated inhibition of type I IFNs. This inhibition is detrimental in terms of IAV, but benefits *Mtb* control. In the present study decreasing type I IFN activity was

concomitant with increasing PGE2 levels in IAV-(co)infected mice suggesting a PGE2-mediated downregulation of type I IFNs. However, in this study PGE2 did neither render mice more susceptible to IAV, nor could it prevent loss of *Mtb* growth control in IAV-coinfected mice. Both effects may be due to the timing of PGE2 induction; by the time the PGE2 levels increased the antiviral immunity was already effectively controlling viral replication while *Mtb* control might have already been affected by the IAV-induced immune modulations. Furthermore, high-doses of PGE2 were associated with a reduced *Mtb* control due to the PGE2-mediated anti-inflammatory effects on innate and adaptive immune responses[215,216,271]. In line with that, PGE2 was linked to the resolution phase in IAV infection and further reported to provoke a prolonged immunosuppression during the inflammatory resolution after acute inflammation[156,214]. The reduced *NOS2* expression and increased expression of *Arg1* in coinfected mice, for instance, could be downstream effects of PGE2[272–275]. Elevated *Arg1* expression in IAV-(co)infected compared to *Mtb*-alone-infected mice was concurrent with the increase of PGE2 levels on day 6 after IAV (co)infection (day 18 *Mtb* infection). However, while PGE2 levels further increased, *Arg1* transcripts were downregulated by day 9 after IAV (co)infection (day 21 *Mtb* infection). Nonetheless, this does not exclude a PGE2-dependent induction of Arg1, but might yet again point to different functions of PGE2 depending on the cellular environment. The blockade of PGE2 signaling could help to stratify for PGE2-dependent and –independent effects and with that identify the role of PGE2 in this *Mtb*-IAV coinfection model.

The decreased pro-inflammatory IFN-γ and TNF response by *Mtb*-specific $CD4^+$ T cells and the increased frequency of alternatively-polarized macrophages as well as the reduced innate antimycobacterial mediators in IAV-coinfected mice strongly indicate an anti-inflammatory environment. This is supported by the detection of enhanced PGE2 levels together with an increase in other anti-inflammatory lipid mediators such as PGD2, 13-HDoHE and $TBXA_2$[217–219] in IAV-(co)infected lungs. These results culminate in the notion that IAV-mediated TB exacerbation is due to a dampened pro-inflammatory and antimycobacterial immune response. The predominant immunosuppressive player that is reported to be induced during IAV infection is the anti-inflammatory cytokine IL-10[156,161,258] and its role in the present coinfection will be discussed in the next chapter.

4.4 The role of IL-10 in IAV-mediated TB exacerbation

The production of IL-10 can be induced by type I IFNs in IAV infection, but can also be the result of PGE2 signaling or IAV-induced indoleamine 2,3-dioxygenase (IDO) induction[91,215,276]. This regulation is complex, cell-type-dependent and may involve multiple upstream signaling pathways[277]. IL-10 signaling during IAV infection is beneficial in terms of preventing IAV-induced immunopathology but can also increase the host's susceptibility to the viral infection[161,278]. The role of IL-10 during IAV infection may be dependent on the pathogenicity of the IAV strain and the time point of IL-10 induction. Besides impacting the host control of IAV infection and inflammation, IAV-induced IL-10 increases the susceptibility to secondary bacterial infections such as *Streptococcus pneumoniae*[278]. In the context of an *Mtb* infection, the consensus is that IL-10 negatively impacts bacterial control in the host[75,76,80,81]. Increased IL-10 production was linked to an enhanced susceptibility and

bacterial growth. However, the role of IL-10 in *Mtb*-IAV coinfection has not yet been established. In the present study, there was no marked induction of *Il10* in *Mtb*-alone-infected mice until day 21 after *Mtb* infection which is in line with other published studies using the *Mtb*-resistant C57BL/6 mouse strain[81,221]. In contrast, the *Mtb*-susceptible strain CBA/J has high IL-10 levels at earlier stages that promote a high bacterial burden and enhanced susceptibility[81,221]. Accordingly, the time point of IL-10 induction is one important determinant of the mouse-strain-dependent susceptibility to *Mtb*. As opposed to the *Mtb*-alone-infected lungs, *Il10* in the IAV-coinfected lungs was already increased 3 days after IAV-coinfection and even more prominently enhanced by day 6 and day 9 after IAV coinfection (day 18 *Mtb and* day 21 *Mtb* infection). The early rise in *Il10* expression suggests a type I IFN-dependent induction. However, activity of type I/III IFNs was already decreased by day 6 after IAV infection, which was also supported by downregulated *Mx1* transcripts. The sustained increased *Il10* expression could be the result of PGE2 signaling since PGE2 levels were increased after IAV infection in the coinfected lungs from day 6 on. Future experiments should investigate the effects of time-dependent blockade of type I IFN- or PGE2-signaling on IL-10 expression during *Mtb*-IAV coinfection. There might also be cell type-dependent differences due to the complex regulation of IL-10 production. For instance, IL-10 production by IAV-induced effector $CD8^+$ T cells was reported to be mediated by type I IFNs[91]. In the current study, IAV coinfection resulted in increased frequencies of IL-10-producing cells from both the innate and adaptive immune system with a main contribution of $CD4^+$ but also $CD8^+$ T cells by day 9 after IAV infection. A more detailed analysis of $CD4^+$ T cells revealed that IAV coinfection was also associated with increased frequencies of IL-10-producing T_{regs}. During *Mtb*-infection, pathogen-specific T_{regs} were reported to delay the migration of *Mtb*-effector T cells from the dLNs to the lung[74]. IAV infection resulted in increased T_{reg} frequencies on day 6 after viral infection (day 18 *Mtb* infection) with more IL-10 producers compared to *Mtb*-alone-infected mice. This could indeed affect the *Mtb*-effector T cell migration from the dLN to the lung. Nonetheless, T_{regs} from IAV-coinfected mice were not responsive to *ex vivo* restimulation with ESAT-6_{1-20} peptide which suggests that they were not *Mtb*-specific. Notwithstanding, it can be argued that T_{regs} non-specifically inhibited effector T cells by bystander suppression e.g. by secretion of inhibitory IL-10[279]. This kind of suppression was in fact demonstrated in a helminth coinfection and resulted in a decreased efficacy of BCG vaccination[279]. A proportion of $CD4^+$ T cells expressed the inhibitory co-receptor LAG-3. LAG-3 binds to the MHC-II-peptide complex on APCs and prevents activation of $CD4^+$ T cells reminiscent of the inhibitory co-receptors CTLA-4 and PD-1 on T cells[280]. Interestingly, LAG-3 expressing $CD4^+$ T cells were associated with active TB and an increased bacterial burden in the lungs of macaques[281]. Genetic silencing of LAG-3 in $CD4^+$ T cells increased macrophage killing of *Mtb* in an *in vitro* granuloma model suggesting LAG-3 as a potential target for HDT in TB[281]. Nonetheless, these checkpoint receptor blockers have to be further characterized in the context of TB first. For instance, anti-PD-1 therapy in a cancer patient led to the development of TB although expression of this inhibitory co-receptor was found to correlate with increased bacterial burden in TB patients[281,282]. Remarkably, in the current study the IL-10 response from the analyzed adaptive and innate immune cells was not stimulated by ESAT-6_{1-20} but only by polyclonal

restimulation indicating that IL-10 production is IAV-and not *Mtb*-induced. This is in line with the qRT-PCR data since *Il10* expression was only increased in IAV-coinfected mice. To ultimately elucidate the impact of IAV-induced IL-10 on *Mtb* control in IAV-coinfection, mice were treated with an anti-IL-10 receptor antibody (anti-IL-10R Ab) to block IL-10-mediated signaling. A single dose of anti-IL-10R Ab on day 5 after IAV-coinfection (day 17 *Mtb* infection) sufficed to prevent exacerbated pulmonary bacterial lung burden in coinfected mice as seen by comparable bacterial loads to *Mtb*-alone mice on day 21 after *Mtb* infection (day 9 IAV coinfection). This strongly indicates that IL-10 signaling contributed to IAV-induced loss of *Mtb* growth control in coinfected mice. The antil-IL-10R treatment had no effect on the bacterial burden in *Mtb*-alone-infected mice compared to the isotype-treated control group. This was expected because *Il10* expression and IL-10 producing cell frequencies from *Mtb*-alone-infected lungs were still low at that time point. Anti-IL-10R treatment did also not impact the viral infection in the current study. Surprisingly, control of bacterial burden in anti-IL-10R-treated mice did not correlate with restored *Mtb*-specific $CD4^+$ T cell numbers or effector functions. The blocking of IL-10 signaling neither increased I-A^b ESAT-6_{4-17}-specific $CD4^+$ T cell numbers nor enhanced ESAT-6_{1-20}-induced IFN-γ production in IAV-coinfected compared to untreated or isotype-control treated IAV-coinfected mice. Accordingly, the amelioration of the IAV-induced phenotype in coinfected mice upon IL-10 receptor blockage appears to be T cell-independent. In fact, the IAV-mediated increase of the pulmonary *Mtb* burden was already seen on day 6 after the viral infection (day 18 *Mtb* infection), at a time when the *Mtb*-specific T cell response is not yet established. Consequently, this rapid loss of *Mtb* growth control is most likely due to the IAV-compromised innate immune responses considering the data on alternatively activated macrophages in coinfected mice and the T cell-independent anti-IL-10R effects. Furthermore, the results from the anti-IL-10R blockage support that IFN-γ is not a reliable correlate of protection in *Mtb* infection although it is required to survive *Mtb* infections in humans and mice[256,257]. In fact, recent studies argue that protection against *Mtb* by $CD4^+$ T cells in the lung is mostly conferred by IFN-γ-independent mechanisms[283,284]. The reduced numbers of *Mtb*-specific $CD4^+$ T cells in the lungs were most likely due to defective T cell priming in the dLN of IAV-coinfected mice. The anti-IL-10R Ab was administered on day 5 after IAV infection which is day 17 after *Mtb* infection. It can thus be reasoned that blockade of IL-10 signaling was too late to exert positive effects on T cell activation. Future experiments could investigate the benefits of earlier anti-IL-10R Ab application and with that the overall relevance of IL-10 on T cell priming and effector functions in *Mtb*-IAV coinfection. Interestingly, the compromised *Mtb*-specific T cell response found in this study and comparably by Flórido *et al.* was not seen in poly-IC-treated *Mtb*-infected mice although type I IFNs interfere with the activation of APCs and T cells and induce IL-10 production in T cells[82,88,195]. This could argue for IAV-mediated type I IFN-independent mechanisms that impact the *Mtb*-specific immune response. In the coinfection study by Redford and colleagues mice were infected with *Mtb* 28 days after IAV infection, which means after the virus was already cleared[196]. This timing did not affect the *Mtb*-specific T cell response. In contrast, Flórido *et al.* infected mice simultaneously with IAV and BCG. Based on those results, one could deduce that interference with the establishment and function of the *Mtb*-specific T cell response happens in the presence of replicating virus.

This idea is further supported by data from the present study that show restored *Mtb*-specific T cell effector functions on day 16 after IAV coinfection (day 28 *Mtb* infection) albeit IL-10-producing $CD4^+$ T cell frequencies from IAV-coinfected mice were still significantly increased compared to *Mtb*-alone-infected mice. From those data it can further be postulated that IL-10 might not be the determining factor for the compromised *Mtb*-specific T cell effector functions. However, T cell-derived IL-10 could be responsible for the reduced *Mtb* control as reported before[285] [79]. Hence, the experimental set-up of the present study could be performed in mice harboring IL-10 deficient T cells. Another source of IL-10 that could drive the exacerbated *Mtb* burden in IAV-coinfected mice are innate immune cells. In a study in which macrophages overexpressed IL-10, they found an enhanced bacterial burden despite a functional T cell response[77]. As observed in the present study, macrophages were polarized into an alternatively activated phenotype. They attributed this phenotype to the autocrine IL-10 signaling. The role of macrophage-derived IL-10 for reducing *Mtb* control in the present coinfection model could be addressed in mice with IL-10-deficient macrophages. Importantly, future analyses should identify the target cell population of the anti-IL-10R treatment. Since the anti-IL10R treatment did not restore the *Mtb*-specific T cell response, blocking of IL-10 signaling most likely enhanced the antimycobacterial effector functions of macrophages. Thus, macrophages should be analyzed with respect to the NOS2/ARG-1 ratio, IL-1 production and possibly phagosome maturation since IL-10 was also shown to block phagosome-lysosome fusion[239]. Moreover, it would be interesting whether the decreased *Mtb* burden could be correlated with improved macrophage effector functions on a per cell basis. Ultimately, the anti-IL-10R treatment-mediated effect could be defined in mice with IL-10R-deficient macrophages to determine whether macrophages are the essential target of blocking IL-10 signaling. Recently, the transcription factor (TF) basic helix-loop-helix family member e40 (Bhle40) was identified as a potent repressor of *Il10* expression during *Mtb* infection[78]. With regard to the present coinfection, it would be interesting whether and through which factors IAV infection might have downregulated *Bhle40* expression in coinfected mice. It was shown that Bhle40 is expressed by both myeloid and lymphoid cells during *Mtb* infection. Myeloid cells such as $CD11b^+$ DCs constitutively expressed this TF while expression in $CD4^+$ T cells did not increase before day 21 after *Mtb* infection. In our study, the IL-10 response of the innate immune cells preceded the response of the T cells. Correspondingly, IAV-coinfection might interfere with the early expression of Bhle40 in myeloid cells resulting in increased IL-10 production and consecutive decrease of innate antimycobacterial immune functions.

The presented data emphasize the detrimental role of IL-10 in *Mtb* infection and show that an unrelated pathogen, here IAV, can be the trigger of TB-exacerbating IL-10 production. Future studies could elucidate whether this is a general IAV-mediated mechanism that impairs successful *Mtb* control. For instance, it could be investigated whether the application of anti-IL10R Ab improves the survival of IAV-coinfected mice in the *Mtb* high-dose infection. Further, the effect of anti-IL-10R blockade should be examined when mice were coinfected with IAV 30 days after *Mtb* infection. To deduce general concepts of IAV-mediated interferences with *Mtb* defenses, analyses should be performed with pathogens of varying

degrees of virulence and mouse strains that differ in susceptibility and granuloma formation. The C57BL/6 mouse model that was used in the present study is an *Mtb*-resistant strain that establishes a protective antibacterial immune response with limited lung pathology that lacks prominent characteristics of the human granuloma[55,114]. Consequently, *Mtb*-susceptible strains such as 129 or C3H mice could be employed[107]. Moreover, the viral influence on control of hypervirulent *Mtb* strains such as the HN878 strain or drug-resistant *Mtb* strains could be addressed. The hypervirulent *Mtb* strain HN878, for example, induces high levels of type I IFNs which might be escalated by concurrent IAV infection[86]. The IAV infection might be vice versa affected in this experimental model as it was shown in 129 mice. Here, high levels of type I IFNs increased the host susceptibility to IAV infection, among others, due to an increased inflammatory response[234]. Accordingly, treatment with anti-IL-10R, that prevents the immune-suppressive effects of IL-10, might have detrimental effects in HN878-IAV coinfection or *Mtb* H37Rv-IAV coinfection in 129 mice[84,234]. Hence, those models could elucidate other potential targets to prevent IAV infection-related increased susceptibility to *Mtb* infection. *Mtb*-IAV coinfection studies in different animal models could also help to assess the risk from coinfected individuals for the public health. In C3H mice which more closely reflect the lung granuloma of human TB, in contrast to C57BL/6 mice, the impact of an IAV infection on granuloma formation and maintenance in *Mtb* infection could be evaluated[114]. Thus, it could be investigated whether the viral infection interferes with the cellular composition and/or stability of the granuloma. Release of bacteria from the granuloma into the airways enables the bacterial transmission to the next host[26]. To study the effect of *Mtb*-IAV coinfection on pathogen transmission, the guinea pig would be a suitable animal model for evaluating both *Mtb* and IAV transmission to the next host(s)[183,286–288]. Altogether, future studies employing different animal models for investigating *Mtb*-IAV coinfections could help to develop both individualized treatment regimens and strategies to contain bacterial spread to improve TB control.

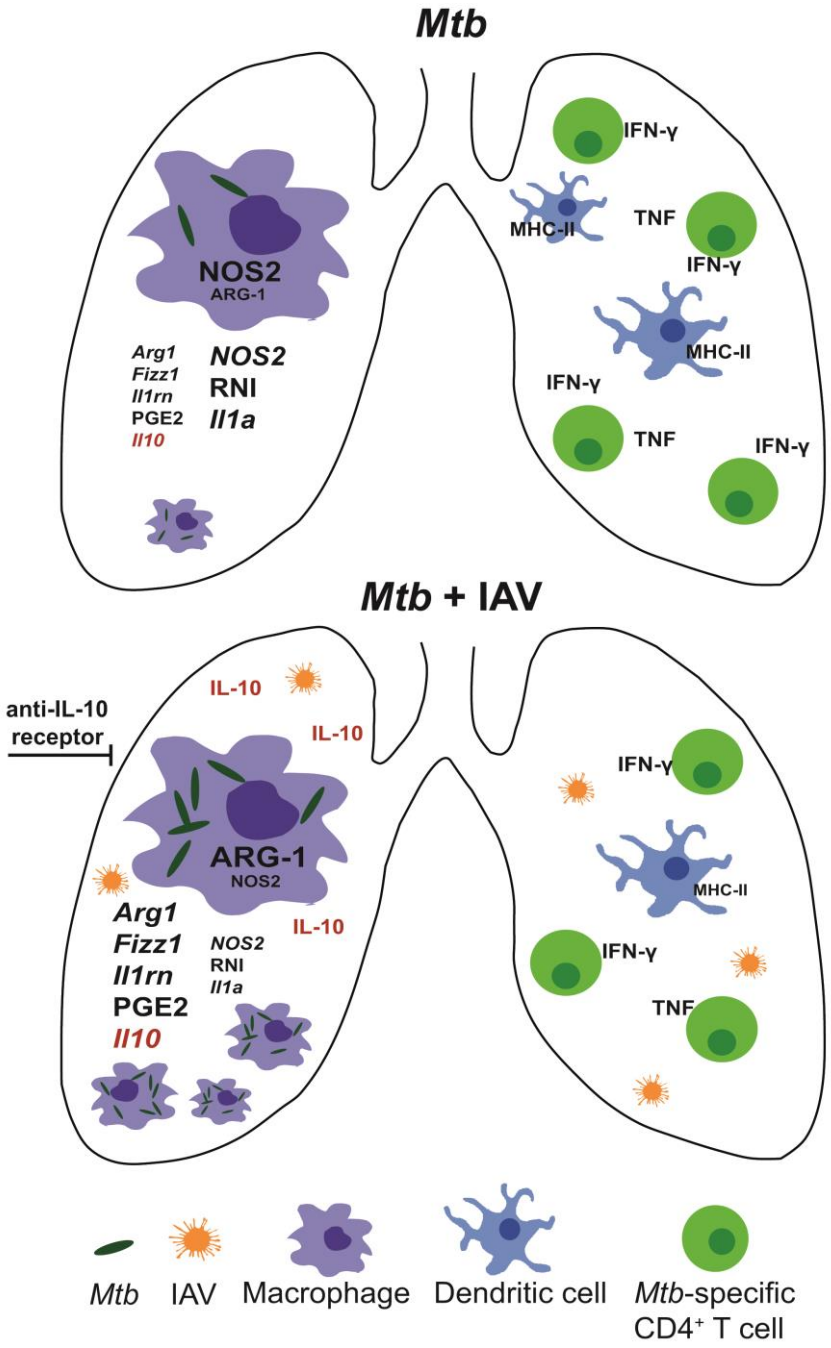

Figure 27 Graphical summary of *Mtb*-IAV coinfection in C57BL/6 mice. IAV infection of *Mtb*-infected mice resulted in an increased bacterial burden associated with the modulation of both innate and adaptive antimycobacterial immune responses. Lungs from IAV-confected mice could be characterized by an anti-inflammatory response as evident by increased expression of *Arg1*, *Fizz1*, *Il1rn* and *Il10* as well as by enhanced production of anti-inflammatory lipid mediators (not depicted). In contrast, expression of *Nos2* and production of RNI as well as the expression of *Il1a* were reduced. IAV infection resulted in increased frequencies of alternatively activated macrophages which had high ARG-1 and low NOS2 levels suggesting an increased proportion of *Mtb*-permissive macrophages in the lungs of coinfected mice. The IAV-induced production of IL-10 was found to be elicited in both innate and adaptive immune cells (cell types not depicted). Furthermore, IAV infection was associated with decreased MHC-II-expressing dendritic cells and reduced *Mtb*-specific $CD4^+$ T cells with diminished IFN-γ and TNF responses. Blockade of IL-10 signaling via IL-10 receptor antibody treatment could reduce the bacterial burden in coinfected mice to a level comparable to that of *Mtb*-alone-infected mice. Thus, IL-10 was found to be a determinant of the IAV-increased bacterial burden in coinfected mice.

4.5 Concluding remarks

The current study confirms previous data of IAV-induced TB exacerbation and accordingly supports the recommendation to implement influenza vaccination in TB-endemic areas to prevent exacerbation of disease or reactivation of LTBI[191]. Prevention of risk factors that promote active TB is indispensable to reduce *Mtb* transmission. Furthermore, the amelioration of an IAV-induced loss of *Mtb* control in coinfected mice by IL-10 blockade could be pursued as a HDT approach in TB management. A great obstacle to the WHO's END TB strategy is the increase of antimicrobial resistance; the treatment success rate of MDR-TB is only 55% compared to 82% for newly diagnosed susceptible TB[17]. Thus, improving the host's antimycobacterial defenses via adjunctive HDT instead of only targeting the pathogen directly by antibiotics could limit the occurrence of drug resistance[21]. Furthermore, given the long treatment duration for MDR-TB, combination of antimicrobial drugs with HDT might reduce the time of therapy and thus improve patient compliance and treatment success[19,21]. Increased IL-10 levels were found in active TB patient samples such as sputum and serum which demonstrates the detrimental role of IL-10 also in humans[75,220]. It would be of interest to analyze patients that are diagnosed with an *Mtb*- IAV coinfection for IL-10 levels to evaluate whether blocking IL-10 signaling might be a good intervention strategy. The potential of IL-10 as a target for HDT is also reflected in a recent study in which the application of aerosolized peptide inhibitors targeting the IL-10R alpha chain improved *Mtb* control in C57BL/6 mice[289]. However, before including HDT into the respective treatment regimen, the potential adverse effects on another pathogen or inflammatory disease need to be considered and evaluated.

Our findings renew the question whether T cell-derived IFN-γ is a good correlate for protection in *Mtb* infection and emphasize the requirement for new biomarkers especially with respect to evaluating vaccine efficacy. Ultimately, the present data underscore the importance of expanding studies beyond examining the immune responses to only an individual pathogen within the host since coinfections may be the rule rather than the exception.

References

1. World Health Organization. Global tuberculosis report. (2018).
2. World Health Organization. Tuberculosis country profiles-Germany. *https://extranet.who.int/sree/Reports?op=Replet&name=%2FWHO_HQ_Reports%2FG2%2FPROD%2FEXT%2FTBCountryProfile&ISO2=DE&LAN=EN&outtype=html* (2019).
3. World Health Organization. Tuberculosis country profiles-South Africa. *https://extranet.who.int/sree/Reports?op=Replet&name=%2FWHO_HQ_Reports%2FG2%2FPROD%2FEXT%2FTBCountryProfile&ISO2=ZA&LAN=EN&outtype=html* (2019).
4. World Health Organization. World : Estimated TB incidence rates, 2017. *http://gamapserver.who.int/mapLibrary/Files/Maps/G* (2018).
5. Harisinghani, M. G. *et al.* Tuberculosis from Head to Toe. *RadioGraphics* **20**, 449–470 (2013).
6. Lawn, S. D. & Zumla, A. Tuberculosis. *Lancet* **378**, 57–72 (2011).
7. Koch, R. Die Ätiologie der Tuberkulose. *Berliner Klin. Wochenschrift* 428–445 (1882).
8. Kaufmann, S. H. How can immunology contribute to the control of tuberculosis? *Nat. Rev. Immunol.* **1**, 20–30 (2001).
9. Gengenbacher, M. & Kaufmann, S. H. E. Mycobacterium tuberculosis: Success through dormancy. *FEMS Microbiol. Rev.* **36**, 514–532 (2012).
10. Cole, S. T. *et al.* Deciphering the biology of Mycobacterium tuberculosis from the complete genome sequence. *Nature* **393**, 537–544 (1998).
11. Wirth, T. *et al.* Acid-Fast Positive and Acid-Fast Negative Mycobacterium tuberculosis: The Koch Paradox. *PLoS Pathog.* **4**, (2008).
12. Brennan, P. J. Structure, function, and biogenesis of the cell wall of Mycobacterium tuberculosis. *Tuberculosis* **83**, 91–97 (2003).
13. Smith, N. H. *et al.* Ecotypes of the Mycobacterium tuberculosis complex. *J. Theor. Biol.* **239**, 220–225 (2006).
14. Gagneux, S. Host-pathogen coevolution in human tuberculosis. *Philos. Trans. R. Soc. B Biol. Sci.* **367**, 850–859 (2012).
15. Andersen, P. & Doherty, T. M. The success and failure of BCG- implications for a novel tuberculosis vaccine. *Nat. Rev. Microbiol.* **3**, (2005).
16. Liu, J. *et al*. BCG vaccines: their mechanisms of attenuation and impact on safety and protective efficacy. *Hum. Vaccin.* **5**, 70–78 (2009).
17. World Health Organization. The End TB Srategy. (2015). doi:10.1017/CBO9781107415324.004
18. Sotgiu, G. *et al*. Tuberculosis treatment and drug regimens. *Cold Spring Harb. Perspect. Med.* **5**, 1–12 (2015).
19. Pai, M. *et al.* Tuberculosis. *Nat. Rev. Dis. Prim.* **2**, 1–23 (2016).
20. Wallis, R. S. *et al.* Tuberculosis-advances in development of new drugs, treatment regimens, host-directed therapies, and biomarkers. *Lancet Infect. Dis.* **16**, e34–e46 (2016).
21. Kolloli, A. & Subbian, S. Host-Directed Therapeutic Strategies for Tuberculosis. *Front. Med.* **4**, (2017).
22. Flynn, J. L. & Chan, J. Tuberculosis : Latency and Reactivation. *Infect. Immun.* **69**, 4195–4201 (2001).
23. Koul, A. *et al*. K. The challenge of new drug discovery for tuberculosis. *Nature* **469**, 483–490 (2011).
24. Kaufmann, S. H. E. How can immunology contributed to TB control. *Nat. Rev. Immunol.* **1**, 20–30 (2001).
25. Cohen, S. B. *et al.* Alveolar Macrophages Provide an Early Mycobacterium tuberculosis Niche and Initiate Dissemination. *Cell Host Microbe* **24**, 439-446.e4 (2018).
26. Russell, D. G. Who puts the tubercle in tuberculosis? *Nat. Rev. Microbiol.* **5**, 39–47 (2007).

27. Ehlers, S. & Schaible, U. E. The granuloma in tuberculosis: Dynamics of a host-pathogen collusion. *Front. Immunol.* **3**, 1–9 (2012).
28. Russell, D. G. *et al*. Foamy macrophages and the progression of the human TB granuloma. *Nat. Immunol.* **10**, 943–948 (2009).
29. Silva Miranda, M. *et al*. The Tuberculous Granuloma: An Unsuccessful Host Defence Mechanism Providing a Safety Shelter for the Bacteria? *Clin. Dev. Immunol.* **2012**, 1–14 (2012).
30. Peddireddy, V. *et al*. Mycobacterial dormancy systems and host responses in tuberculosis. *Front. Immunol.* **8**, 1–19 (2017).
31. Ramakrishnan, L. Revisiting the role of the granuloma in tuberculosis. *Nat. Rev. Immunol.* **12**, 352–366 (2012).
32. Volkman, H. E. *et al.* Tuberculous granuloma formation is enhanced by a Mycobacterium virulence determinant. *PLoS Biol.* **2**, (2004).
33. Davis, J. M. & Ramakrishnan, L. The Role of the Granuloma in Expansion and Dissemination of Early Tuberculous Infection. *Cell* **136**, 37–49 (2009).
34. Wolf, A. J. *et al.* Mycobacterium tuberculosis Infects Dendritic Cells with High Frequency and Impairs Their Function In Vivo. *J. Immunol.* **179**, 2509–2519 (2007).
35. Pauwels, A. *et al*. Receptors , and Signals : Regulation of Phagosome Maturation. *Trends Immunol.* **38**, 407–422 (2017).
36. Armstrong, B. Y. J. A. & Hart, A. P. D. A. Response of cultured macrophages to Mycobacterium tuberculosis, with observations on fusion of lysosomes with phagosomes. *J. Exp. Med.* **134**, 713–740 (1971).
37. Weiss, G. & Schaible, U. E. Macrophage defense mechanisms against intracellular bacteria. *Immunol. Rev.* **264**, 182–203 (2015).
38. Kinchen, J. M. & Ravichandran, K. S. Phagosome maturation : going through the acid test. *Nat. Rev. Mol. Cell Biol.* **9**, 781–795 (2008).
39. Takeuchi, O. & Akira, S. Pattern recognition receptors and inflammation. *Cell* **140**, 805–20 (2010).
40. Kleinnijenhuis, J. *et al*. Innate Immune Recognition of Mycobacterium tuberculosis. *Clin. Dev. Immunol.* **2011**, 405310 (2011).
41. Chackerian, A. A. *et al*. Dissemination of Mycobacterium tuberculosis Is Influenced by Host Factors and Precedes the Initiation of T-Cell Immunity. *Infect. Immun.* **70**, 4501 LP – 4509 (2002).
42. Wolf, A. J. *et al.* Initiation of the adaptive immune response to Mycobacterium tuberculosis depends on antigen production in the local lymph node , not the lungs. **205**, 105–115 (2008).
43. Cooper, A. M. Cell-Mediated Immune Responses in Tuberculosis. (2008). doi:10.1146/annurev.immunol.021908.132703
44. Moskophidis, B. D. & Kioussis, D. Contribution of Virus-specific CD8+ Cytotoxic T Cells to Virus Clearance or Pathologic Manifestations of Influenza Virus Infection in a T Cell Receptor. *J. Exp. Med.* **188**, 223–232 (1998).
45. Kursar, M. *et al.* Organ-Specific CD4 + T Cell Response During Listeria monocytogenes Infection. *J. Exp. Med.* **168**, 6382–6387 (2002).
46. O'Garra, A. *et al. The immune response and tuberculosis*. *Annual review of immunology* **25**, (2013).
47. Divangahi, M. *et al*. Eicosanoid pathways regulate adaptive immunity to Mycobacterium tuberculosis. *Nat. Immunol.* **11**, 751–758 (2010).
48. Chen, M. *et al.* Lipid mediators in innate immunity against tuberculosis: opposing roles of PGE2 and LXA4 in the induction of macrophage death. *J. Exp. Med.* **205**, 2791–2801 (2008).
49. Flynn, J. L. & Chan, J. Immunology of Tuberculosis. *Annu Rev Immunol* **19**, 93–129 (2001).
50. Felio, K. *et al.* CD1-restricted adaptive immune responses to Mycobacteria in human group 1 CD1 transgenic mice. *J. Exp. Med.* **206**, 2497–2509 (2009).

51. Khader, S. A. *et al.* Interleukin 12p40 is required for dendritic cell migration and T cell priming after Mycobacterium tuberculosis infection. *J. Exp. Med.* **203**, 1805 LP – 1815 (2006).
52. Altare, F. *et al.* Impairment of Mycobacterial Immunity in Human Interleukin-12 Receptor Deficiency. *Science (80-.).* **280**, 1432 LP – 1435 (1998).
53. Tabarsi, P. *et al*. Lethal tuberculosis in a previously healthy adult with IL-12 receptor deficiency. *Eur. Respir. J.* **38**, p1813 (2011).
54. Flynn, J. L. *et al.* IL-12 increases resistance of BALB/c mice to Mycobacterium tuberculosis infection. *J. Immunol.* **155**, 2515 LP – 2524 (1995).
55. North, R. J. & Jung, Y. Immunity to Tuberculosis. *Annu. Rev. Immunol.* **22**, 599–623 (2004).
56. Mogues, B. T. *et al.* The Relative Importance of T Cell Subsets in Immunity and Immunopathology of Airborne Mycobacterium tuberculosis Infection in Mice. *J. Exp. Med.* **193**, 271–280 (2001).
57. Ellis, P. K. *et al*. CD4 count and tuberculosis risk in HIV- positive adults not on ART : a systematic review and meta-analysis. **2015**, (2017).
58. Leveton, C. *et al.* T-cell-mediated protection of mice against virulent Mycobacterium tuberculosis. *Infect. Immun.* **57**, 390 LP – 395 (1989).
59. Pinxteren, L. A. H. Van, *et al*. Control of latent Mycobacterium tuberculosis infection is dependent on CD8 T cells. *Eur. J. Immunol.* **30**, 3689–3698 (2000).
60. Flynn, J. L. *et al.* Immunology of Tuberculosis. *New York* 93–129 (2001). doi:10.1146/annurev.immunol.19.1.93
61. Flesch, I. E. A. & Kaufmann, S. H. E. Mechanisms Involved in Mycobacterial Growth Inhibition by Gamma Interferon-Activated Bone Marrow Macrophages : Role of Reactive Nitrogen Intermediates. *Infect. Immun.* **59**, 3213–3218 (1991).
62. Sarmento, A. & Appelberg, R. Involvement of reactive oxygen intermediates in tumor necrosis factor alpha-dependent bacteriostasis of Mycobacterium avium. *Infect. Immun.* **64**, 3224 LP – 3230 (1996).
63. Schaible, U. E. *et al*. Cytokine Activation Leads to Acidification and Increases Maturation of Mycobacterium avium Containing Phagosomes in Murine Macrophages. *J. Immunol.* **160**, 1290 LP – 1296 (1998).
64. Herbst, S. *et al*. Interferon Gamma Activated Macrophages Kill Mycobacteria by Nitric Oxide Induced Apoptosis. *PLoS One* **6**, e19105 (2011).
65. Nathan, C. & Shiloh, M. U. Reactive oxygen and nitrogen intermediates in the relationship between mammalian hosts and microbial pathogens. *Proc. Natl. Acad. Sci.* **97**, 8841 LP – 8848 (2000).
66. Chan, J. *et al*. Effects of Nitric Oxide Synthase Inhibitors on Murine Infection with Mycobacterium tuberculosis. *Infect. Immun.* **63**, 736–740 (1995).
67. MacMicking, J. D. *et al.* Identification of nitric oxide synthase as a protective locus against tuberculosis. *Proc. Natl. Acad. Sci.* **94**, 5243 LP – 5248 (1997).
68. Mayer-Barber, K. D. *et al.* Innate and Adaptive Interferons Suppress IL-1α and IL-1β Production by Distinct Pulmonary Myeloid Subsets during Mycobacterium tuberculosis Infection. *Immunity* **35**, 1023–1034 (2011).
69. Woodworth, J. S. M. & Behar, S. M. Mycobacterium tuberculosis-Specific CD8+ T Cells and Their Role in Immunity. *Crit. Rev. Immunol.* **26**, 317–352 (2006).
70. Lin, P. L. *et al*. Tumor necrosis factor and tuberculosis. *J. Investig. Dermatol. Symp. Proc.* **12**, 22–25 (2007).
71. Bekker, L.-G. *et al.* Immunopathologic Effects of Tumor Necrosis Factor Alpha in Murine Mycobacterial Infection Are Dose Dependent. *Infect. Immun.* **68**, 6954 LP – 6961 (2000).
72. Vignali, D. A. A. *et al*. How regulatory T cells work. *Nat. Rev. Immunol.* **8**, 523–532 (2008).
73. Couper, K. N. *et al*. IL-10: The Master Regulator of Immunity to Infection. *J. Immunol.* **180**, 5771–5777 (2008).

74. Shafiani, S. *et al*. Pathogen-specific regulatory T cells delay the arrival of effector T cells in the lung during early tuberculosis. *J. Exp. Med.* **207**, 1409–20 (2010).
75. Verbon, A. *et al.* Serum concentrations of cytokines in patients with active tuberculosis (TB) and after treatment. *Clin. Exp. Immunol.* **115**, 110–113 (1999).
76. Awomoyi, A. A. *et al.* Interleukin-10, Polymorphism in SLC11A1 (formerly NRAMP1), and Susceptibility to Tuberculosis. *J. Infect. Dis.* **186**, 1808–1814 (2002).
77. Schreiber, T. *et al.* Autocrine IL-10 Induces Hallmarks of Alternative Activation in Macrophages and Suppresses Antituberculosis Effector Mechanisms without Compromising T Cell Immunity. *J. Immunol.* **183**, 1301–1312 (2009).
78. Huynh, J. P. *et al.* Bhlhe40 is an essential repressor of IL-10 during Mycobacterium tuberculosis infection. *J. Exp. Med.* **215**, jem.20171704 (2018).
79. Moreira-Teixeira, L. *et al.* T Cell–Derived IL-10 Impairs Host Resistance to Mycobacterium tuberculosis Infection. *J. Immunol.* **199**, 613–623 (2017).
80. Redford, P. S. *et al.* Enhanced protection to Mycobacterium tuberculosis infection in IL-10-deficient mice is accompanied by early and enhanced Th1 responses in the lung. *Eur. J. Immunol.* **40**, 2200–2210 (2010).
81. Turner, J. *et al.* In vivo IL-10 production reactivates chronic pulmonary tuberculosis in C57BL/6 mice. *J. Immunol.* **169**, 6343–6351 (2002).
82. Antonelli, L. R. V *et al.* Intranasal Poly-IC treatment exacerbates tuberculosis in mice through the pulmonary recruitment of a pathogen-permissive monocyte / macrophage population. *J. Clin. Invest.* **120**, 1674–1682 (2010).
83. Berry, M. P. R. *et al.* An interferon-inducible neutrophil-driven blood transcriptional signature in human tuberculosis. *Nature* **466**, 973–977 (2010).
84. Dorhoi, A. *et al.* Type I IFN signaling triggers immunopathology in tuberculosis-susceptible mice by modulating lung phagocyte dynamics. *Eur. J. Immunol.* **44**, 2380–2393 (2014).
85. Manca, C. *et al.* Virulence of a Mycobacterium tuberculosis clinical isolate in mice is determined by failure to induce Th1 type immunity and is associated with induction of IFN-α/β. *Proc. Natl. Acad. Sci.* **98**, 5752 LP – 5757 (2001).
86. Manca, C. *et al.* Hypervirulent M. tuberculosis W/Beijing Strains Upregulate Type I IFNs and Increase Expression of Negative Regulators of the Jak-Stat Pathway. *J. Interf. Cytokine Res.* **25**, 694–701 (2005).
87. McNab, F. W. *et al.* Type I IFN Induces IL-10 Production in an IL-27-Independent Manner and Blocks Responsiveness to IFN- for Production of IL-12 and Bacterial Killing in Mycobacterium tuberculosis-Infected Macrophages. *J. Immunol.* **193**, 3600–3612 (2014).
88. McRae, B. L. *et al*. Type I IFNs Inhibit Human Dendritic Cell IL-12 Production and Th1 Cell Development. *J. Immunol.* **160**, 4298 LP – 4304 (1998).
89. Cousens, L. P. *et al*. Interferon-α/β inhibition of interleukin 12 and interferon-γ production in vitro and endogenously during viral infection. *Proc. Natl. Acad. Sci.* **94**, 634 LP – 639 (1997).
90. Mayer-Barber, K. D. & Yan, B. Clash of the Cytokine Titans : counter-regulation of interleukin-1 and type I interferon-mediated inflammatory responses. *Cell. Mol. Immunol.* **13**, 1–14 (2016).
91. Jiang, L. *et al.* Type I IFN signaling facilitates the development of IL-10-producing effector CD8+ T cells during murine influenza virus infection. *Eur. J. Immunol.* **46**, 2778–2788 (2016).
92. McNab, F. W. *et al.* Type I IFN Induces IL-10 Production in an IL-27–Independent Manner and Blocks Responsiveness to IFN-γ for Production of IL-12 and Bacterial Killing in *Mycobacterium tuberculosis* –Infected Macrophages. *J. Immunol.* **193**, 3600–3612 (2014).
93. Narasimhan, P. *et al*. Risk factors for tuberculosis. *Pulm. Med.* **2013**, (2013).
94. Miller, E. A. & Ernst, J. D. Anti-TNF immunotherapy and tuberculosis reactivation: another mechanism revealed. *J. Clin. Invest.* **119**, 1079–1082 (2009).

95. Maini, R. *et al.* Infliximab (chimeric anti-tumour necrosis factor a monoclonal antibody) versus placebo in rheumatoid arthritis patients receiving concomitant methotrexate : a randomised phase III trial. *Lancet* **354**, 1932–1939 (1999).
96. World Health Organization. HIV-Associated Tuberculosis. TB/HIV factsheet. 1–2 (2018).
97. Selwyn, P. A. *et al.* A Prospective Study of the Risk of Tuberculosis among Intravenous Drug Users with Human Immunodeficiency Virus Infection. *N. Engl. J. Med.* **320**, 545–550 (1989).
98. Babu, S. & Nutman, T. B. Helminth-Tuberculosis Co-infection: An Immunologic Perspective. *Trends Immunol.* **37**, 597–607 (2016).
99. Talaat, K. R. *et al*. Preexposure to Live Brugia malayi Microfilariae Alters the Innate Response of Human Dendritic Cells to Mycobacterium tuberculosis. *J. Infect. Dis.* **193**, 196–204 (2006).
100. Pearlman, E. *et al*. Modulation of murine cytokine responses to mycobacterial antigens by helminth-induced T helper 2 cell responses. *J. Immunol.* **151**, 4857 LP – 4864 (1993).
101. Potian, J. A. *et al.* Preexisting helminth infection induces inhibition of innate pulmonary anti-tuberculosis defense by engaging the IL-4 receptor pathway. *J. Exp. Med.* **208**, 1863 LP – 1874 (2011).
102. Lang, R. & Schick, J. Impact of helminth infection on antimycobacterial immunity-A focus on the macrophage. *Front. Immunol.* **8**, 1–11 (2017).
103. Blank, J. *et al*. One Episode of Self-Resolving Plasmodium yoelii Infection Transiently Exacerbates Chronic Mycobacterium tuberculosis Infection. *Front. Microbiol.* **7**, 152 (2016).
104. Scott, C. P. *et al*. Short Report: Modulation of Mycobacterium Tuberculosis Infection By Plasmodium in the Murine Model. *Am. J. Trop. Med. Hyg.* **70**, 144–148 (2018).
105. Mueller, A. K. *et al.* Natural Transmission of Plasmodium berghei Exacerbates Chronic Tuberculosis in an Experimental Co-Infection Model. *PLoS One* **7**, 1–9 (2012).
106. Cooper, A. M. Mouse model of tuberculosis. *Cold Spring Harb. Perspect. Med.* **5**, a018556 (2015).
107. Medina, E. & North, R. J. Resistance ranking of some common inbred mouse strains to Mycobacterium tuberculosis and relationship to major histocompatibility complex haplotype and Nramp1 genotype. *Immunology* **93**, 270–274 (1998).
108. Dunn, P. L. & North, R. J. Persistent infection with virulent but not avirulent Mycobacterium tuberculosis in the lungs of mice causes progressive pathology. *J. Med. Microbiol.* **45**, 103–109 (2019).
109. Dharmadhikari, A. S. & Nardell, E. A. What Animal Models Teach Humans about Tuberculosis. *Am. J. Respir. Cell Mol. Biol.* **39**, 503–508 (2008).
110. Wallgreen, A. The time-table of tuberculosis. *Tubercle* **29**, 245–251 (1948).
111. Poulsen, A. Some clinical features of tuberculosis I. Incubation period. *Acta Tuberc. Pneumol. Scand.* **24**, 311–346 (1950).
112. Caruso, A. M. *et al.* Mice Deficient in CD4 T Cells Have Only Transiently Diminished Levels of IFN-γ, Yet Succumb to Tuberculosis. *J. Immunol.* **162**, 5407 LP – 5416 (1999).
113. Flynn, J. A. L. Lessons from experimental Mycobacterium tuberculosis infections. *Microbes Infect.* **8**, 1179–1188 (2006).
114. Kramnik, I. & Beamer, G. Mouse models of human TB pathology: roles in the analysis of necrosis and the development of host-directed therapies. *Semin. Immunopathol.* **38**, 221–237 (2016).
115. Iuliano, A. D. *et al.* Estimates of global seasonal influenza-associated respiratory mortality: a modelling study. *Lancet* **391**, 1285–1300 (2018).
116. World Health Organization. Influenza (Seasonal). https://www.who.int/news-room/fact-sheets/detail/i (2008).
117. Taubenberger, J. K. & Morens, D. M. The Pathology of Influenza Virus Infections. *Annu Rev Pathol Mech Dis* **3**, 499–522 (2008).

118. Taubenberger, J. K. & Morens, D. M. 1918 Influenza: the Mother of All Pandemics. *Emerg. Infect. Dis. J.* **12**, 15 (2006).
119. World Health Organization. Pandemic (H1N1) 2009 - update 112. *https://www.who.int/csr/don/2010_08_06/en/* (2010).
120. World Health Organisation. H1N1 in post-pandemic period. *https://www.who.int/mediacentre/news/statements/20* (2010).
121. Su, Y. C. F. *et al.* Phylodynamics of H1N1/2009 influenza reveals the transition from host adaptation to immune-driven selection. *Nat. Commun.* **6**, 7952 (2015).
122. Bouvier, N. M. & Palese, P. The biology of influenza viruses. *Vaccine* **26**, 49–53 (2008).
123. Boni, M. F. Vaccination and antigenic drift in influenza. *Vaccine* **26**, 8–14 (2008).
124. Drake, J. W. & Holland, J. J. Mutation rates among RNA viruses. *Proc. Natl. Acad. Sci.* **96**, 13910 LP – 13913 (1999).
125. Reddy, K. P. *et al*. Relationship between upper respiratory tract influenza test result and clinical outcomes among critically ill influenza patients. *Open Forum Infect. Dis.* **3**, 1–3 (2016).
126. Bertram, S. *et al*. S. Novel insights into proteolytic cleavage of influenza virus hemagglutinin. *Rev. Med. Virol.* **20**, 298–310 (2010).
127. Couceiro, J. N. *et al*. Influenza virus strains selectively recognize sialyloligosaccharides on human respiratory epithelium; the role of the host cell in selection of hemagglutinin receptor specificity. *Virus Res.* **29**, 155–165 (1993).
128. Ibricevic, A. *et al.* Influenza virus receptor specificity and cell tropism in mouse and human airway epithelial cells. *J. Virol.* **80**, 7469–7480 (2006).
129. Stegmann, T. Membrane Fusion Mechanisms: The Influenza Hemagglutinin Paradigm and its Implications for Intracellular Fusion. *Traffic* **1**, 598–604 (2000).
130. Martin, K. & Helenius, A. Transport of incoming influenza virus nucleocapsids into the nucleus. *J. Virol.* **65**, 232 LP – 244 (1991).
131. Palese, P. *et al*. Characterization of temperature sensitive influenza virus mutants defective in neuraminidase. *Virology* **61**, 397–410 (1974).
132. Dou, D. *et al*. Influenza A virus cell entry, replication, virion assembly and movement. *Front. Immunol.* **9**, 1–17 (2018).
133. Gubareva, L. V. *et al*. Influenza virus neuraminidase inhibitors. *Lancet* **355**, 827–835 (2000).
134. Herold, S. *et al*. Influenza virus-induced lung injury: pathogenesis and implications for treatment. *Eur. Respir. J.* **45**, 1463 LP – 1478 (2015).
135. Fry, A. M. *et al.* Efficacy of oseltamivir treatment started within 5 days of symptom onset to reduce influenza illness duration and virus shedding in an urban setting in Bangladesh: a randomised placebo-controlled trial. *Lancet Infect. Dis.* **14**, 109–118 (2014).
136. Rosenberger, C. M. *et al.* Characterization of innate responses to influenza virus infection in a novel lung type I epithelial cell model. *J. Gen. Virol.* **95**, 350–362 (2014).
137. Shieh, W.-J. *et al.* 2009 Pandemic Influenza A (H1N1): Pathology and Pathogenesis of 100 Fatal Cases in the United States. *Am. J. Pathol.* **177**, 166–175 (2010).
138. Manicassamy, B. *et al.* Analysis of in vivo dynamics of influenza virus infection in mice using a GFP reporter virus. *Proc. Natl. Acad. Sci.* **107**, 11531–11536 (2010).
139. Iwasaki, A. & Pillai, P. S. Innate immunity to influenza virus infection. *Nat. Rev. Immunol.* **14**, 315–28 (2014).
140. Matzinger, S. R. *et al*. Myxovirus Resistance Gene A (MxA) Expression Suppresses Influenza A Virus Replication in Alpha Interferon-Treated Primate Cells. *J. Virol.* **87**, 1150 LP – 1158 (2013).
141. Tate, M. D. & Mansell, A. An update on the NLRP3 inflammasome and influenza: the road to redemption or perdition? *Curr. Opin. Immunol.* **54**, 80–85 (2018).
142. Takeuchi, O. & Akira, S. Recognition of viruses by innate immunity. *Immunol. Rev.* **220**, 214–224 (2007).

143. Kallfass, C. *et al*. Visualizing the Beta Interferon Response in Mice during Infection with Influenza A Viruses Expressing or Lacking Nonstructural Protein 1. *J. Virol.* **87**, 6925 LP – 6930 (2013).
144. Jewell, N. A. *et al.* Differential Type I Interferon Induction by Respiratory Syncytial Virus and Influenza A Virus In Vivo. *J. Virol.* **81**, 9790 LP – 9800 (2007).
145. Ivashkiv, L. B. & Donlin, L. T. Regulation of type i interferon responses. *Nat. Rev. Immunol.* **14**, 36–49 (2014).
146. Schneider, W. M. *et al*. Interferon-Stimulated Genes: A Complex Web of Host Defenses. *Annu. Rev. Immunol.* **32**, 513–545 (2014).
147. Zürcher, T. *et al*. Nuclear localization of mouse Mx1 protein is necessary for inhibition of influenza virus. *J. Virol.* **66**, 5059 LP – 5066 (1992).
148. Piqueras, B. *et al*. Upon viral exposure, myeloid and plasmacytoid dendritic cells produce 3 waves of distinct chemokines to recruit immune effectors. *Blood* **107**, 2613–2618 (2006).
149. Hwang, I. *et al.* Activation Mechanisms of Natural Killer Cells during Influenza Virus Infection. *PLoS One* **7**, e51858 (2013).
150. Hufford M.M. *et al*. The Effector T Cell Response to Influenza Infection. in *Oldstone M., Compans R. (eds) Influenza Pathogenesis and Control - Volume II. Current Topics in Microbiology and Immunology* (2014). doi:10.1007/82
151. Wang, Z. *et al.* Recovery from severe H7N9 disease is associated with diverse response mechanisms dominated by CD8+ T cells. *Nat. Commun.* **6**, 6833 (2015).
152. Bender, B. S. *et al*. A. Transgenic mice lacking class I major histocompatibility complex-restricted T cells have delayed viral clearance and increased mortality after influenza virus challenge. *J. Exp. Med.* **175**, 1143 LP – 1145 (1992).
153. Matheu, M. P. *et al.* Three Phases of CD8 T Cell Response in the Lung Following H1N1 Influenza Infection and Sphingosine 1 Phosphate Agonist Therapy. *PLoS One* **8**, e58033 (2013).
154. Flynn, K. J. *et al.* Virus-specific CD8+ T cells in primary and secondary influenza pneumonia. *Immunity* **8**, 683–691 (1998).
155. Kohlmeier, J. E. & Woodland, D. L. Immunity to respiratory viruses. *Annu. Rev. Immunol.* **27**, 61–82 (2009).
156. Metzger, D. W. *et al*. Immune Dysfunction and Bacterial Coinfections following Influenza. *J. Immunol.* **191**, 2047–2052 (2013).
157. Waffarn, E. E. & Baumgarth, N. Protective B Cell Responses to Flu—No Fluke! *J. Immunol.* **186**, 3823–3829 (2011).
158. Mozdzanowska, K. *et al*. CD4+T Cells Are Ineffective in Clearing a Pulmonary Infection with Influenza Type A Virus in the Absence of B Cells. *Virology* **239**, 217–225 (1997).
159. Brown, D. M. *et al*. CD4 T cell responses to influenza infection. *Semin. Immunol.* **16**, 171–177 (2004).
160. Mozdzanowska, K. *et al*. Roles of CD4+ T-Cell-Independent and -Dependent Antibody Responses in the Control of Influenza Virus Infection: Evidence for Noncognate $CD4^+$ T-Cell Activities That Enhance the Therapeutic Activity of Antiviral Antibodies. *J. Virol.* **79**, 5943 LP – 5951 (2005).
161. Sun, J. *et al*. Effector T cells control lung inflammation during acute influenza virus infection by producing IL-10. *Nat. Med.* **15**, 277–284 (2009).
162. Carding, S. R. *et al*. Activation of Cytokine Genes in T Cells during Primary and Secondary Murine Influenza Pneumonia. *J. Exp. Med.* **177**, 475–482 (1993).
163. Tavares, L. P. *et al*. The inflammatory response triggered by Influenza virus : a two edged sword. *Inflamm. Res.* (2016). doi:10.1007/s00011-016-0996-0
164. Betts, R. J. *et al.* Influenza A Virus Infection Results in a Robust , Antigen-Responsive , and Widely Disseminated Foxp3+ Regulatory T Cell Response. *J. Virol.* **5**, 2817–2825 (2012).
165. Carlson, C. M. *et al.* Transforming Growth Factor-β: Activation by Neuraminidase and Role in Highly Pathogenic H5N1 Influenza Pathogenesis. *PLOS Pathog.* **6**, 1–12 (2010).

166. Joseph, C. *et al*. Bacterial and viral infections associated with influenza. *Influenza Other Respi. Viruses* **7**, 105–113 (2013).
167. Gill, J. R. *et al.* Pulmonary Pathologic Findings of Fatal 2009 Pandemic Influenza A/H1N1 Viral Infections. *Arch. Pathol. Lab. Med.* **134**, 235–243 (2010).
168. McCullers, J. A. The co-pathogenesis of influenza viruses with bacteria in the lung. *Nat. Rev. Microbiol.* **12**, 252–62 (2014).
169. Chockalingam, A. K. *et al.* Deletions in the Neuraminidase Stalk Region of H2N2 and H9N2 Avian Influenza Virus Subtypes Do Not Affect Postinfluenza Secondary Bacterial Pneumonia. *J. Virol.* **86**, 3564 LP – 3573 (2012).
170. Mccullers, J. A. *et al*. The platelet activating factor receptor is not required for exacerbation of bacterial pneumonia following influenza. *Scand. J. Infect. Dis.* **40**, 11–17 (2008).
171. Boxx, G. M. & Cheng, G. The Roles of Type i Interferon in Bacterial Infection. *Cell Host Microbe* **19**, 760–769 (2016).
172. Li, W., Moltedo, B. & Moran, T. M. Type I Interferon Induction during Influenza Virus Infection Increases Susceptibility to Secondary Streptococcus pneumoniaespan Infection by Negative Regulation of γδ T Cells. *J. Virol.* **86**, 12304 LP – 12312 (2012).
173. Goulding, J. *et al.* Lowering the threshold of lung innate immune cell activation alters susceptibility to secondary bacterial superinfection. *J. Infect. Dis.* **204**, 1086–1094 (2011).
174. McCullers, J. A. & English, B. K. Improving therapeutic strategies for secondary bacterial pneumonia following influenza. *Future Microbiol.* **3**, 397–404 (2008).
175. Karlström, Å. *et al*. Treatment with Protein Synthesis Inhibitors Improves Outcomes of Secondary Bacterial Pneumonia after Influenza. *J. Infect. Dis.* **199**, 311–319 (2009).
176. Srivastava, B. *et al.* Host Genetic Background Strongly Influences the Response to Influenza A Virus Infections. *PLoS One* **4**, 1–12 (2009).
177. Alberts, R. *et al.* Gene expression changes in the host response between resistant and susceptible inbred mouse strains after influenza A infection. *Microbes Infect.* **12**, 309–318 (2010).
178. Horimoto, T. & Kawaoka, Y. Influenza: lessons from past pandemics, warnings from current incidents. *Nat. Rev. Microbiol.* **3**, 591–600 (2005).
179. Bouvier, N. M. & Lowen, A. C. Animal Models for Influenza Virus Pathogenesis and Transmission. *Viruses* **2**, 1530–1563 (2010).
180. Itoh, Y. *et al.* In vitro and in vivo characterization of new swine-origin H1N1 influenza viruses. *Nature* **460**, 1021 (2009).
181. Tumpey, T. M. *et al.* Characterization of the Reconstructed 1918 Spanish Influenza Pandemic Virus. *Science (80-.).* **310**, 77 LP – 80 (2005).
182. Enkirch, T. & von Messling, V. Ferret models of viral pathogenesis. *Virology* **479–480**, 259–270 (2015).
183. Sun, Y. *et al.* Guinea Pig Model for Evaluating the Potential Public Health Risk of Swine and Avian Influenza Viruses. *PLoS One* **5**, 1–8 (2010).
184. Otte, A. *et al.* Evolution of 2009 H1N1 influenza viruses during the pandemic correlates with increased viral pathogenicity and transmissibility in the ferret model. *Sci. Rep.* **6**, 28583 (2016).
185. Archer, B. N. *et al.* Interim Report on Pandemic H1N1 Influenza Virus Infections in South Africa, April to October 2009: Epidemiology and Factos Associated with Fatal Cases. *Euro Surveill.* **14**, pii=19369 (2009).
186. Nunn, P. & Falzon, D. WHO information note on tuberculosis and pandemic influenza A (H1N1). *WHO Press. Available online https//www.who.int/tb/features_archive/h1n1/en/* (2009).
187. Dangor, Z. *et al.* Temporal association in hospitalizations for tuberculosis, invasive pneumococcal disease and influenza virus illness in South African children. *PLoS One* **9**, (2014).
188. Walaza, S. *et al.* Influenza virus infection is associated with increased risk of death amongst patients hospitalized with confirmed pulmonary tuberculosis in South Africa, 2010–2011. *BMC Infect. Dis.* **15**, (2015).

189. Walaza, S. *et al.* The Impact of Influenza and Tuberculosis Interaction on Mortality Among Individuals Aged ≥ 15 Years Hospitalized With Severe Respiratory Illness in South Africa , 2010 – 2016. *Open Forum Infect. Dis.* **6**, ofz020 (2019).
190. Noh, J. Y. *et al.* Concurrent Tuberculosis and Influenza, South Korea. *Emerg. Infect. Dis.* **19**, 165–167 (2013).
191. Mendy, J. *et al.* Changes in Mycobacterium tuberculosis-Specific Immunity With Influenza co-infection at Time of TB Diagnosis. *Front. Immunol.* **9**, 1–8 (2019).
192. Oei, W. & Nishiura, H. The relationship between tuberculosis and influenza death during the influenza (H1N1) pandemic from 1918-19. *Comput. Math. Methods Med.* **2012**, (2012).
193. Noymer, A. The 1918-19 influenza pandemic affected tuberculosis in the United States: reconsidering Bradshaw, Smith, and Blanchard. *Biodemography Soc. Biol.* **54**, 125–33; discussion 134-40 (2008).
194. Volkert, B. M. *et al*. The enhancing effect of concurrent infection with pneumotropic viruses on pulmonary tuberculosis in mice. *J. Exp. Med.* (1947).
195. Flórido, M. *et al.* Influenza A virus infection impairs mycobacteria-specific T cell responses and mycobacterial clearance in the lung during pulmonary coinfection. *J. Immunol.* **191**, 302–11 (2013).
196. Redford, P. S. *et al.* Influenza A virus impairs control of mycobacterium tuberculosis coinfection through a type i interferon receptor-dependent pathway. *J. Infect. Dis.* **209**, 270–274 (2014).
197. Otte, A. *et al.* Differential host determinants contribute to the pathogenesis of 2009 pandemic H1N1 and human H5N1 influenza a viruses in experimental mouse models. *Am. J. Pathol.* **179**, 230–239 (2011).
198. Tamura, T. *et al.* The role of antigenic peptide in CD4+ T helper phenotype development in a T cell receptor transgenic model. *Int. Immunol.* **16**, 1691–1699 (2004).
199. Wutkowski, A. *et al.* Software-aided quality control of parallel reaction monitoring based quantitation of lipid mediators. *Anal. Chim. Acta* **1037**, 168–176 (2018).
200. Sezin, T. *et al.* The Leukotriene B4 and its Receptor BLT1 Act as Critical Drivers of Neutrophil Recruitment in Murine Bullous Pemphigoid-Like Epidermolysis Bullosa Acquisita. *J. Invest. Dermatol.* **137**, 1104–1113 (2017).
201. Emukule, G. O. *et al.* Estimating influenza and respiratory syncytial virus-associated mortality in Western Kenya using health and demographic surveillance system data, 2007-2013. *PLoS One* **12**, 2007–2013 (2017).
202. Ring, S. *et al.* Blocking IL-10 receptor signaling ameliorates Mycobacterium tuberculosis infection during influenza-induced exacerbation. *JCI Insight* **4**, (2019).
203. Der, S. D. *et al*. Identification of genes differentially regulated by interferon alpha, beta, or gamma using oligonucleotide arrays. *Proc. Natl. Acad. Sci.* **95**, 15623–8 (1998).
204. Ziegler, S. F. *et al*. The activation antigen CD69. *Stem Cells* **12**, 456–465 (1994).
205. Oehen, S. & Brduscha-Riem, K. Differentiation of Naive CTL to Effector and Memory CTL: Correlation of Effector Function with Phenotype and Cell Division. *J. Immunol.* **161**, 5338 LP – 5346 (1998).
206. Flory, C. M. *et al*. Effects of in vivo T lymphocyte subset depletion on mycobacterial infections in mice. *J. Leukoc. Biol.* **51**, 225–229 (1992).
207. Rath, M. *et al*. Metabolism via arginase or nitric oxide synthase : two competing arginine pathways in macrophages. *Front. Immunol.* **5**, 1–10 (2014).
208. Gordon, S. Alternative activation of macrophages. *Nat. Rev. Immunol.* **3**, 23–35 (2003).
209. Geert, R. *et al.* Differential expression of FIZZ1 and Ym1 in alternatively versus classically activated macrophages. *J. Leukoc. Biol.* **71**, 597–602 (2002).
210. Weber, A. *et al*. Interleukin-1 (IL-1) Pathway. *Sci. Signal.* **3**, cm1 LP-cm1 (2010).
211. Dripps, D. J., Brandhuber, B. J., Thompson, R. C. & Eisenberg, S. P. Interleukin-1 (IL-1) receptor antagonist binds to the 80-kDa IL-1 receptor but does not initiate IL-1 signal transduction. *J. Biol. Chem.* **266**, 10331–10336 (1991).

212. Granowitz, E. V. *et al*. Effect of interleukin-1 (IL-1) blockade on cytokine synthesis: I. IL-1 receptor antagonist inhibits IL-1-induced cytokine synthesis and blocks the binding of IL-1 to its type II receptor on human monocytes. *Blood* **79**, 2356 LP – 2363 (1992).
213. Coulombe, F. *et al.* Targeted prostaglandin E2 inhibition enhances antiviral immunity through induction of type I interferon and apoptosis in macrophages. *Immunity* **40**, 554–568 (2014).
214. Newson, J. *et al.* Inflammatory Resolution Triggers a Prolonged Phase of Immune Suppression through COX-1 / mPGES-1- Inflammatory Resolution Triggers a Prolonged Phase of Immune Suppression through COX-1 / mPGES-1-Derived Prostaglandin E2. *Cell Rep.* **20**, 3162–3175 (2017).
215. MacKenzie, K. F. *et al.* PGE2 Induces Macrophage IL-10 Production and a Regulatory-like Phenotype via a Protein Kinase A–SIK–CRTC3 Pathway. *J. Immunol.* **190**, 565 LP – 577 (2013).
216. Loynes, C. A. *et al.* PGE2 production at sites of tissue injury promotes an anti-inflammatory neutrophil phenotype and determines the outcome of inflammation resolution in vivo. *Sci. Adv.* **4**, eaar8320 (2018).
217. Murata, T. *et al.* Anti-inflammatory role of PGD2 in acute lung inflammation and therapeutic application of its signal enhancement. *Proc. Natl. Acad. Sci.* **110**, 5205 LP – 5210 (2013).
218. Kabashima, K. *et al.* Thromboxane A2 modulates interaction of dendritic cells and T cells and regulates acquired immunity. *Nat. Immunol.* **4**, 694–701 (2003).
219. Tam, V. C. *et al.* Lipidomic Profiling of Influenza Infection Identifies Mediators that Induce and Resolve Inflammation. *Cell* **154**, 213–227 (2013).
220. Huard, R. C. *et al.* The Mycobacterium tuberculosis Complex-Restricted Gene cfp32 Encodes an Expressed Protein That Is Detectable in Tuberculosis Patients and Is Positively Correlated with Pulmonary Interleukin-10. *Infect. Immun.* **71**, 6871 LP – 6883 (2003).
221. Beamer, G. L. *et al.* Interleukin-10 Promotes Mycobacterium tuberculosis Disease Progression in CBA/J Mice. *J. Immunol.* **181**, 5545 LP – 5550 (2008).
222. Hori, S. *et al*. Control of Regulatory T Cell Development by the Transcription Factor Foxp3. *Science (80-.).* **299**, 1057 LP – 1061 (2003).
223. Schmidt, A. *et al*. Molecular mechanisms of Treg-mediated T cell suppression. *Front. Immunol.* **3**, 1–20 (2012).
224. Workman, C. J. *et al.* Lymphocyte Activation Gene-3 (CD223) Regulates the Size of the Expanding T Cell Population Following Antigen Activation In Vivo. *J. Immunol.* **172**, 5450 LP – 5455 (2004).
225. Lichtenegger, F. S. *et al.* Targeting LAG-3 and PD-1 to enhance T cell activation by antigen-presenting cells. *Front. Immunol.* **9**, 1–12 (2018).
226. Zürcher, K. *et al*. Influenza Pandemics and Tuberculosis Mortality in 1889 and 1918 : Analysis of Historical Data from Switzerland. 1–11 (2016). doi:10.1371/journal.pone.0162575
227. Schliehe, C. *et al.* The methyltransferase Setdb2 mediates virus-induced susceptibility to bacterial superinfection. *Nat. Immunol.* **16**, 67 (2014).
228. Marcos-Villar, L. *et al.* Epigenetic control of influenza virus: role of H3K79 methylation in interferon-induced antiviral response. *Sci. Rep.* **8**, 1230 (2018).
229. Yoo, J.-K. *et al*. Identification of a novel antigen-presenting cell population modulating antiinfluenza type 2 immunity. *J. Exp. Med.* **207**, 1435 LP – 1451 (2010).
230. Rook, G. A. W. *et al*. Tuberculosis Due to High-Dose Challenge in Partially Immune Individuals: A Problem for Vaccination? *J. Infect. Dis.* **199**, 613–618 (2009).
231. Turner, D. L. *et al*. Splenic Priming of Virus-Specific CD8 T Cells following Influenza Virus Infection. *J. Virol.* **87**, 4496 LP – 4506 (2013).
232. Atkin-Smith, G. K. *et al*. The induction and consequences of Influenza A virus-induced cell death. *Cell Death Dis.* **9**, 1002 (2018).

233. Yanagi, S. *et al*. Breakdown of Epithelial Barrier Integrity and Overdrive Activation of Alveolar Epithelial Cells in the Pathogenesis of Acute Respiratory Distress Syndrome and Lung Fibrosis. *Biomed Res. Int.* **2015**, 1–12 (2015).
234. Davidson, S. *et al*. Pathogenic potential of interferon αβ in acute influenza infection. *Nat. Commun.* **5**, 3864 (2014).
235. Russell-Goldman. *et al*. Mycobacterium tuberculosis Rpf double-knockout strain exhibits profound defects in reactivation from chronic tuberculosis and innate immunity phenotypes. *Infect. Immun.* **76**, 4269–4281 (2008).
236. Smallwood, H. S. *et al.* Targeting Metabolic Reprogramming by Influenza Infection for Therapeutic Intervention. *Cell Rep.* **19**, 1640–1653 (2017).
237. Huang, L. *et al*. Growth of Mycobacterium tuberculosis in vivo segregates with host macrophage metabolism and ontogeny. *J. Exp. Med.* **215**, 1135 LP – 1152 (2018).
238. Shi, C. & Pamer, E. G. Monocyte recruitment during infection and inflammation. *Nat. Rev. Immunol.* **11**, 762–774 (2011).
239. Das, A. *et al.* Monocyte and Macrophage Plasticity in Tissue Repair and Regeneration. *Am. J. Pathol.* **185**, 2596–2606 (2015).
240. Herold, S. *et al.* Alveolar Epithelial Cells Direct Monocyte Transepithelial Migration upon Influenza Virus Infection: Impact of Chemokines and Adhesion Molecules. *J. Immunol.* **177**, 1817 LP – 1824 (2006).
241. Lehmann, M. H. *et al.* CCL2 expression is mediated by type I IFN receptor and recruits NK and T cells to the lung during MVA infection. *J. Leukoc. Biol.* **99**, 1057–1064 (2016).
242. Conrady, C. D. *et al*. IFN-α-driven CCL2 production recruits inflammatory monocytes to infection site in mice. *Mucosal Immunol.* **6**, 45 (2012).
243. Scott, H. M. & Flynn, J. L. Mycobacterium tuberculosis in Chemokine Receptor 2-Deficient Mice : Influence of Dose on Disease Progression. *Infect. Immun.* **70**, 5946–5954 (2002).
244. Mack, M. *et al.* Expression and Characterization of the Chemokine Receptors CCR2 and CCR5 in Mice. *J. Immunol.* **166**, 4697 LP – 4704 (2001).
245. Slight, S. R. & Khader, S. A. Chemokines shape the immune response to tuberculosis. *Cytokine Growth Factor Rev.* **24**, 105–113 (2013).
246. Kim, H. M. *et al.* Alveolar Macrophages Are Indispensable for Controlling Influenza Viruses in Lungs of Pigs. *J. Virol.* **82**, 4265–4274 (2008).
247. Chang, P. *et al.* Early apoptosis of porcine alveolar macrophages limits avian influenza virus replication and pro-inflammatory dysregulation. *Sci. Rep.* **5**, 17999 (2016).
248. Ghoneim, H. E. *et al*. Depletion of alveolar macrophages during influenza infection facilitates bacterial superinfections. *J. Immunol.* **191**, 1250–9 (2013).
249. Tumpey, T. M. *et al.* Pathogenicity of influenza viruses with genes from the 1918 pandemic virus: functional roles of alveolar macrophages and neutrophils in limiting virus replication and mortality in mice. *J. Virol.* **79**, 14933–44 (2005).
250. Leemans, J. C. *et al.* Depletion of Alveolar Macrophages Exerts Protective Effects in Pulmonary Tuberculosis in Mice. *J. Immunol.* **166**, 4604–4611 (2001).
251. Leemans, J. C. *et al.* Macrophages play a dual role during pulmonary tuberculosis in mice. *J. Infect. Dis.* **191**, 65–74 (2005).
252. Nogusa, S. *et al.* RIPK3 Activates Parallel Pathways of MLKL-Driven Necroptosis and FADD-Mediated Apoptosis to Protect against Influenza A Virus. *Cell Host Microbe* **20**, 13–24 (2016).
253. Nailwal, H. & Chan, F. K.-M. Necroptosis in anti-viral inflammation. *Cell Death Differ.* **26**, 4–13 (2019).
254. Zhao, X. *et al.* Bcl-x L mediates RIPK3-dependent necrosis in M. tuberculosis -infected macrophages. *Mucosal Immunol.* **10**, 1553–1568 (2017).
255. Rangel Moreno, J. *et al.* The role of prostaglandin E2 in the immunopathogenesis of experimental pulmonary tuberculosis. *Immunology* **106**, 257–266 (2002).
256. Bustamante, J. *et al*. Mendelian susceptibility to mycobacterial disease: Genetic, immunological, and clinical features of inborn errors of IFN-γ immunity. *Semin. Immunol.* **26**, 454–470 (2014).

257. Flynn, J. L. *et al.* An essential role for interferon gamma in resistance to Mycobacterium tuberculosis infection. *J. Exp. Med.* **178**, 2249 LP – 2254 (1993).
258. van der Sluijs, K. F. *et al.* IL-10 Is an Important Mediator of the Enhanced Susceptibility to Pneumococcal Pneumonia after Influenza Infection. *J. Immunol.* **172**, 7603 LP – 7609 (2004).
259. Redford, P. S. *et al*. A. The role of IL-10 in immune regulation during M. tuberculosis infection. *Mucosal Immunol.* **4**, 261–270 (2011).
260. Fernandez-Sesma, A. *et al.* Influenza Virus Evades Innate and Adaptive Immunity via the NS1 Protein. *J. Virol.* **80**, 6295 LP – 6304 (2006).
261. Lichtenegger, F. S. *et al.* CD86 and IL-12p70 Are Key Players for T Helper 1 Polarization and Natural Killer Cell Activation by Toll-Like Receptor-Induced Dendritic Cells. *PLoS One* **7**, 1–9 (2012).
262. Morva, A. *et al.* Maturation and function of human dendritic cells are regulated by B lymphocytes. *Blood* **119**, 106–114 (2012).
263. Srivastava, S. *et al.* Antigen Export Reduces Antigen Presentation and Antigen Export Reduces Antigen Presentation. *Cell Host Microbe* **19**, 44–54 (2016).
264. Dodding, M. P. & Way, M. Coupling viruses to dynein and kinesin-1. *EMBO J.* **30**, 3527–3539 (2011).
265. Ramos-Nascimento, A. *et al.* KIF13A mediates trafficking of influenza A virus ribonucleoproteins. *J. Cell Sci.* **130**, 4038 LP – 4050 (2017).
266. Nathan, C. Role of iNOS in Human Host Defense. *Science (80-.).* **312**, 1874 LP – 1875 (2006).
267. El Kasmi, K. C. *et al.* Toll-like receptor–induced arginase 1 in macrophages thwarts effective immunity against intracellular pathogens. *Nat. Immunol.* **9**, 1399 (2008).
268. Schreiber, T. *et al.* Autocrine IL-10 Induces Hallmarks of Alternative Activation in Macrophages and Suppresses Antituberculosis Effector Mechanisms without Compromising T Cell Immunity. *J. Immunol.* **183**, 1301 LP – 1312 (2009).
269. Monin, L. *et al.* Helminth-induced arginase-1 exacerbates lung inflammation and disease severity in tuberculosis. *J. Clin. Invest.* **125**, 4699–4713 (2015).
270. Weber, A., Wasiliew, P. & Kracht, M. Interleukin-1 (IL-1) Pathway. *Sci. Signal.* **3**, 1–6 (2010).
271. Moreno, J. R. *et al*. The role of prostaglandin E2 in the immunopathogenesis of experimental pulmonary tuberculosis. (2002).
272. Corraliza, I. M. *et al*. Arginase Induction by Suppressors of Nitric Oxide Synthesis (IL-4, IL-10 and PGE2) in Murine Bone-Marrow-Derived Macrophages. *Biochem. Biophys. Res. Commun.* **206**, 667–673 (1995).
273. Rodriguez, P. C. *et al.* Arginase I in myeloid suppressor cells is induced by COX-2 in lung carcinoma. *J. Exp. Med.* **202**, 931 LP – 939 (2005).
274. Bansal, V. *et al.* Interactions Between Fatty Acids and Arginine Metabolism: Implications for the Design of Immune-Enhancing Diets. *J. Parenter. Enter. Nutr.* **29**, S75–S80 (2005).
275. Milano, S. *et al*. Prostaglandin E2 Regulates Inducible Nitric Oxide Synthase In The Murine Macrophage Cell Line J774. *Prostaglandins* **49**, 105–115 (1995).
276. van der Sluijs, K. F. *et al.* Influenza-Induced Expression of Indoleamine 2,3-Dioxygenase Enhances Interleukin-10 Production and Bacterial Outgrowth during Secondary Pneumococcal Pneumonia. *J. Infect. Dis.* **193**, 214–222 (2006).
277. Saraiva, M. & O'Garra, A. The regulation of IL-10 production by immune cells. *Nat. Rev. Immunol.* **10**, 170–181 (2010).
278. Sun, K., Torres, L. & Metzger, D. W. A Detrimental Effect of Interleukin-10 on Protective Pulmonary Humoral Immunity during Primary Influenza A Virus Infection. *J. Virol.* **84**, 5007 LP – 5014 (2010).
279. Wammes, L. J. *et al.* Regulatory T cells in human geohelminth infection suppress immune responses to BCG and Plasmodium falciparum. *Eur. J. Immunol.* **40**, 437–442 (2010).
280. Workman, C. J. & Vignali, D. A. A. Negative Regulation of T Cell Homeostasis by Lymphocyte Activation Gene-3 (CD223). *J. Immunol.* **174**, 688–695 (2014).

281. Phillips, B. L. *et al.* LAG3 Expression in Active Mycobacterium tuberculosis Infections. *Am. J. Pathol.* **185**, 820–833 (2015).
282. Day, C. L. *et al.* PD-1 Expression on Mycobacterium tuberculosis -Specific CD4 T Cells Is Associated With Bacterial Load in Human Tuberculosis. **9**, 1–18 (2018).
283. Sakai, S. *et al.* CD4 T Cell-Derived IFN-γ Plays a Minimal Role in Control of Pulmonary Mycobacterium tuberculosis Infection and Must Be Actively Repressed by PD-1 to Prevent Lethal Disease. *PLoS Pathog.* **12**, 1–22 (2016).
284. Cowley, S. C. & Elkins, K. L. CD4+ T Cells Mediate IFN- -Independent Control of Mycobacterium tuberculosis Infection Both In Vitro and In Vivo. *J. Immunol.* **171**, 4689–4699 (2003).
285. Turner, J. *et al.* In Vivo IL-10 Production Reactivates Chronic Pulmonary Tuberculosis in C57BL/6 Mice. *J. Immunol.* **169**, 6343–6351 (2002).
286. Orme, I. M. & Ordway, D. J. Mouse and Guinea Pig Models of Tuberculosis. *Microbiol. Spectr.* **4**, (2016).
287. Kato-Maeda, M. *et al.* Beijing Sublineages of Mycobacterium tuberculosis Differ in Pathogenicity in the Guinea Pig. *Clin. Vaccine Immunol.* **19**, 1227 LP – 1237 (2012).
288. Lowen, A. C. *et al*. The guinea pig as a transmission model for human influenza viruses. *Proc. Natl. Acad. Sci.* **103**, 9988 LP – 9992 (2006).
289. Upadhyay, R. *et al.* Host Directed Therapy for Chronic Tuberculosis via Intrapulmonary Delivery of Aerosolized Peptide Inhibitors Targeting the IL-10-STAT3 Pathway. *Sci. Rep.* **8**, 16610 (2018).

List of figures

List of tables

Supplement

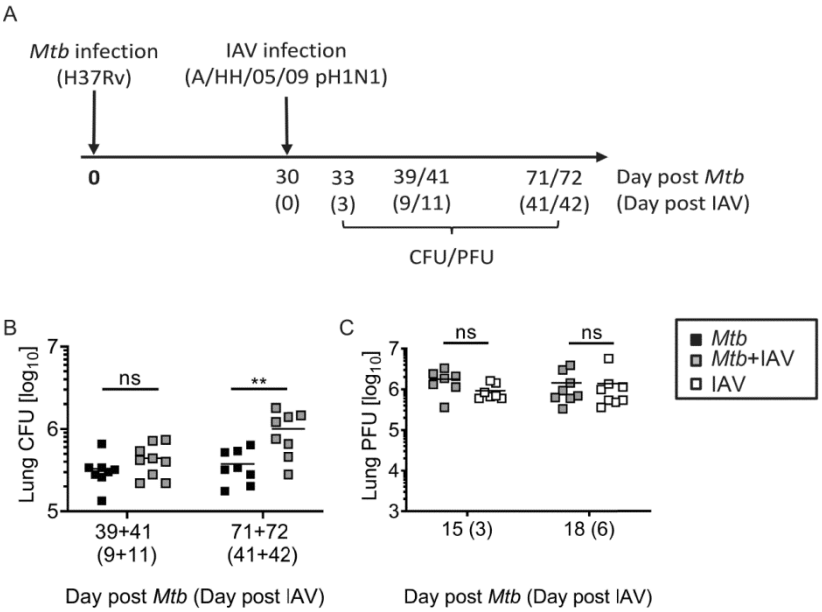

Figure S1 Impact of IAV coinfection 30 days after *Mtb* infection on bacterial and viral burden in the lung. (A) Schematic time-line of experimental set-up. (B) C57BL/6 mice were infected via aerosol with a low-dose of *Mtb* H37Rv and 30 days later coinfected i.n. with 10^4 PFU IAV (A/HH/05/09 pH1N1). At indicated time points after *Mtb* infection, lung bacterial burden was determined (n=8-9 per group, data pooled from two independent experiments). (C) Lung homogenates were analyzed for viral burden by MDCK plaque assay (n=3-4 mice per group, data pooled from two independent experiments). Each data point represents one mouse. **p ≤ 0.01 determined by unpaired *t*-test. (Parts of data are published in Ring et al., 2019.)

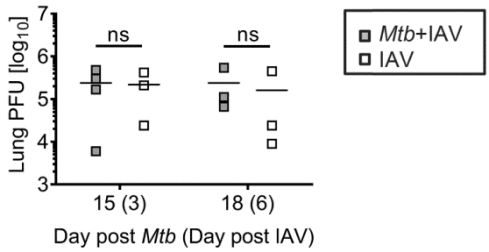

Figure S2 *Mtb* high-dose does not impact viral burden in the lung of coinfected mice. C57BL/6 mice received high-dose *Mtb* H37Rv aerosol infection and were coinfected i.n. with 10^4 PFU IAV (A/HH/05/09 pH1N1) 12 days later. Lung homogenates were analyzed for viral burden by MDCK plaque assay (n=3-4 mice per group, one experiment). Each data point represents one mouse, ns (not significant) determined by unpaired *t*-test.

Parts of the gating strategies were published in Ring *et al*., 2019.

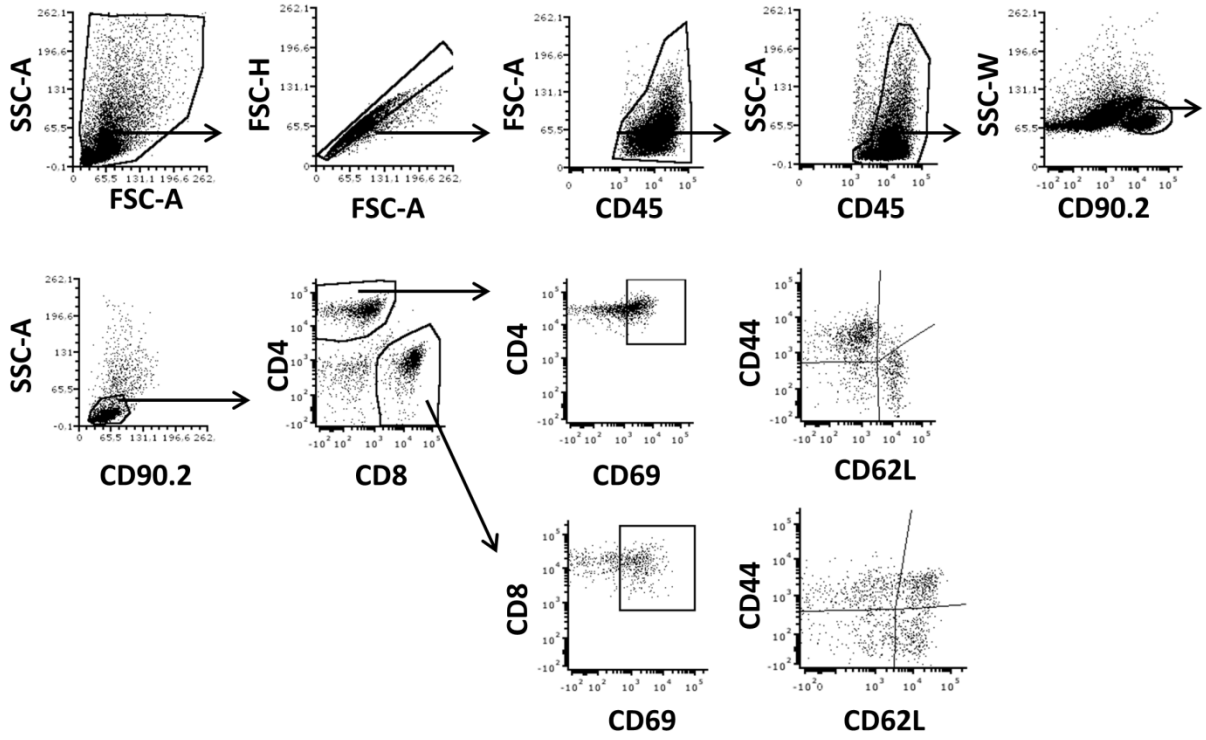

Figure S3 Flow cytometry gating strategy for T cell analyses. Representative flow cytometry blots for gating of $CD4^+$ and $CD8^+$ T cells among $CD45^+$ cells and determination of activated T cells ($CD69^+$ and $CD44^+$ $CD62L^-$). Plots are from lung cells of an *Mtb*-infected mouse on day 21 after *Mtb* infection.

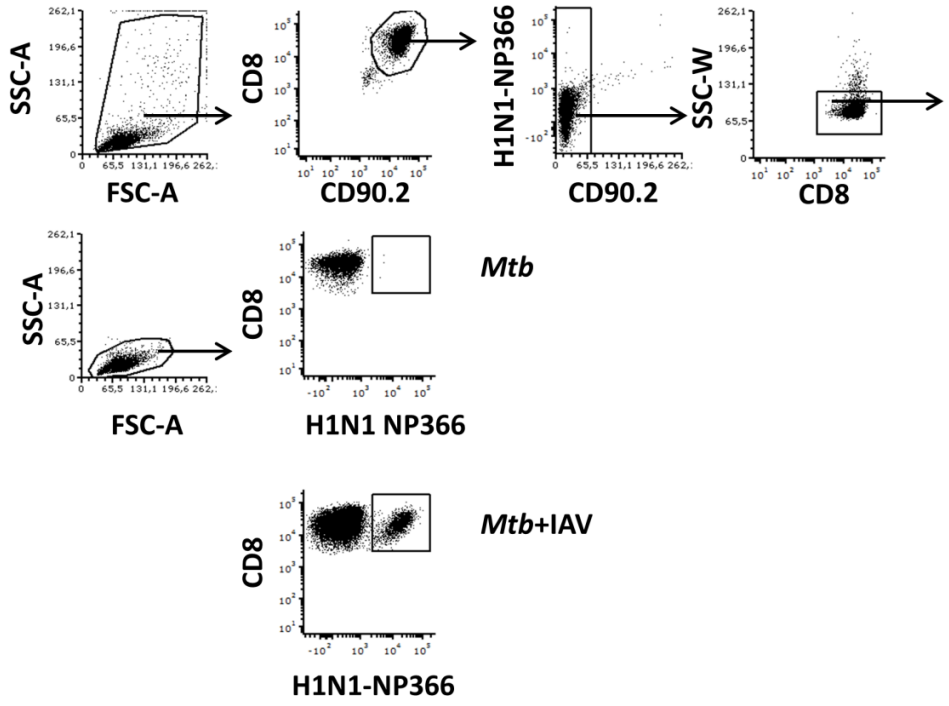

Figure S4 Flow cytometry gating strategy for determination of $H1N1\text{-}NP366^+$ $CD8^+$ T cells. Representative flow cytometry blots for gating of H1N1-NP366 dextramer+ $CD8^+$ T cells. Plots are from lung cells of an *Mtb*- and an *Mtb*-IAV coinfected mouse on day 21 after *Mtb* infection (9 days after IAV infection).

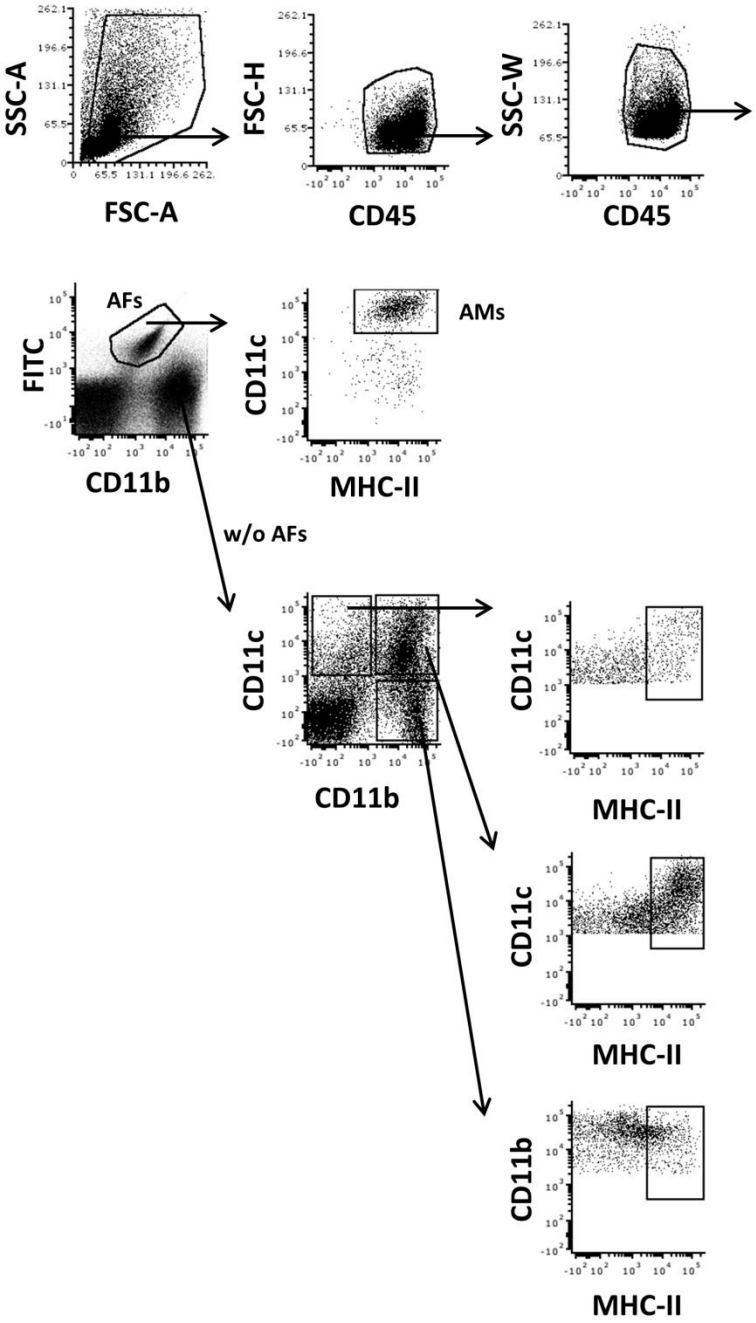

Figure S5 Flow cytometry gating strategy for analyses of myeloid cells. Representative flow cytometry blots for determination of alveolar macrophages (AMs), $CD11b^+$, $CD11b^+CD11c^+$, $CD11c^+$ cells and MHC-II expressers in $CD11b^+$ and $CD11c^+$ populations. Exclusion of autofluorescent cells (AFs; w/o AFs) along the gating. Plots are from lung cells of an *Mtb*-infected mouse on day 21 after *Mtb* infection.

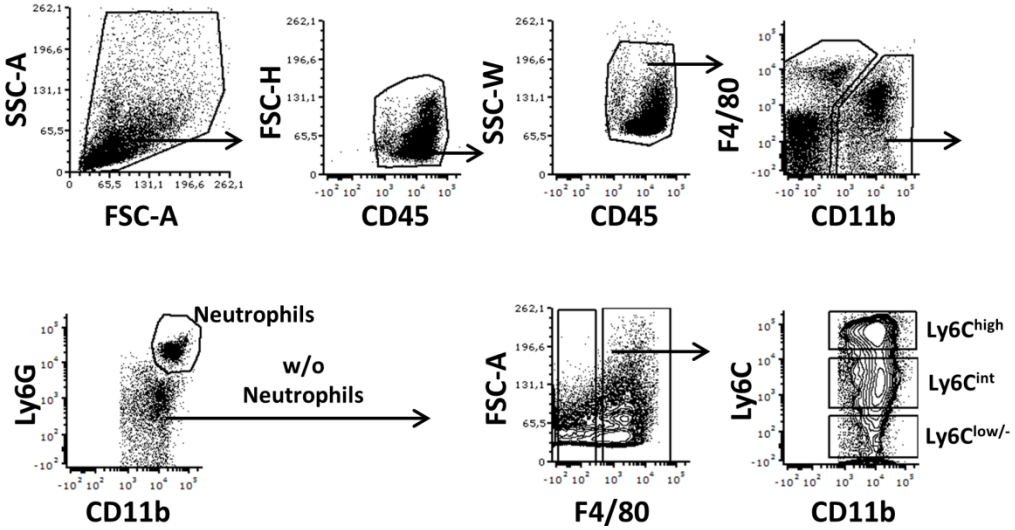

Figure S6 Flow cytometry gating strategy for characterization of CD11b$^+$ cell population. Representative flow cytometry blots for determination of neutrophils and F4/80$^+$Ly6C$^+$ expressers in CD11b$^+$ population. Exclusion of neutrophils (w/o neutrophils) along the gating. Plots are from lung cells of an *Mtb*-infected mouse on day 21 after *Mtb* infection.

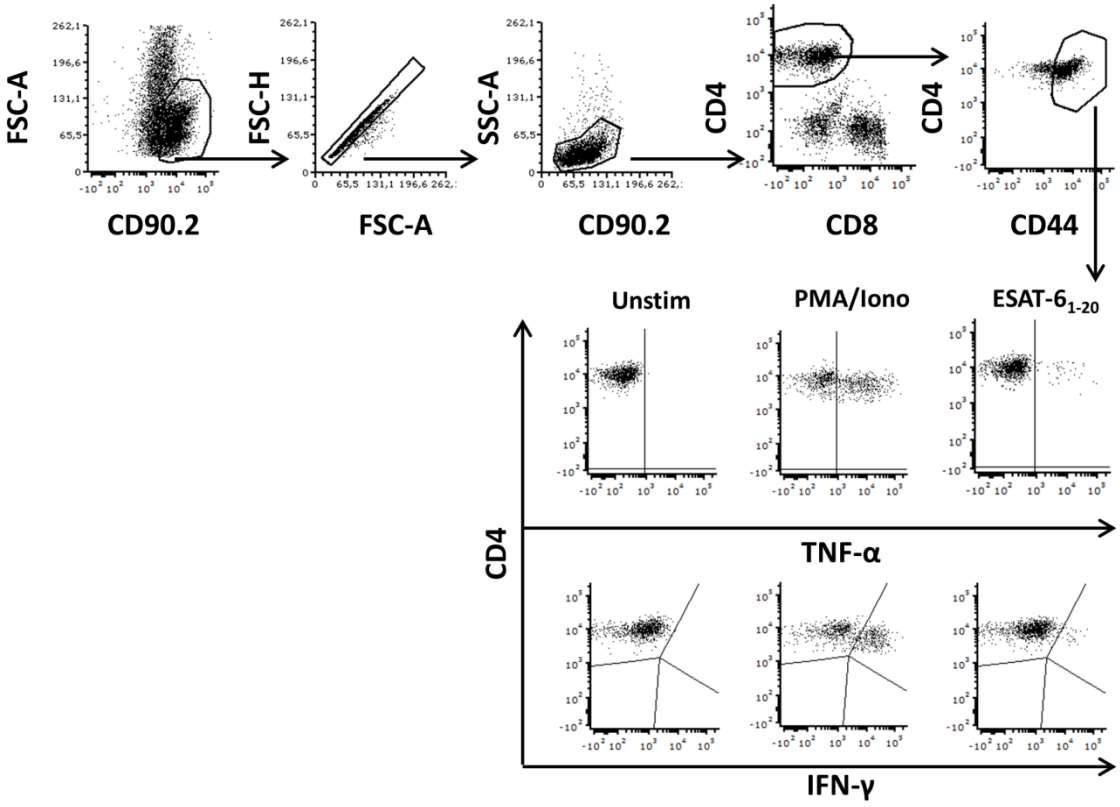

Figure S7 Flow cytometry gating strategy for determination of TNF$^+$ and IFN-γ$^+$ CD4$^+$ T cells. Representative flow cytometry blots for gating of TNF$^+$ and IFN-γ$^+$ CD4$^+$ T cells isolated from lungs and dLNs. Cells from lungs of *Mtb*-infected mice on day 21 after *Mtb* infection are representatively shown.

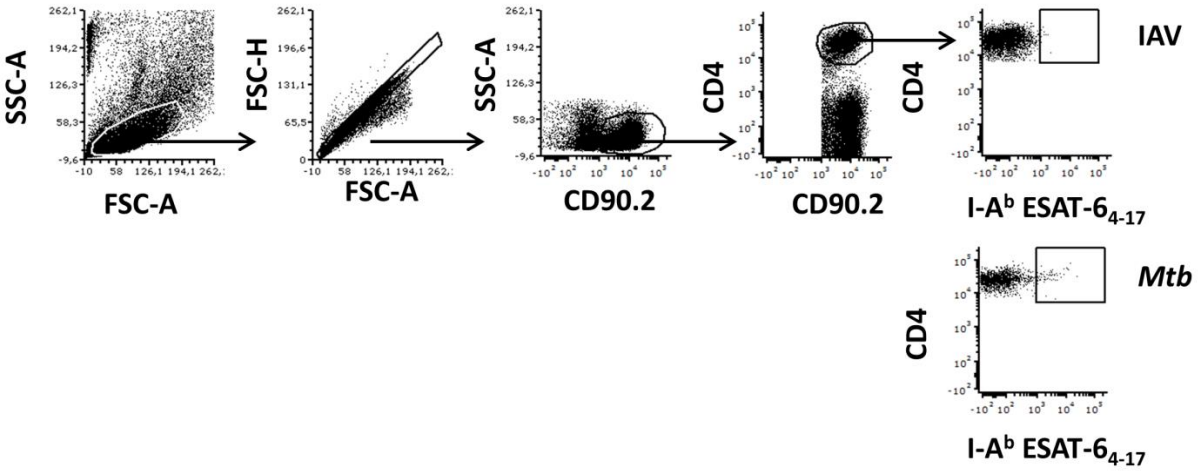

Figure S8 Flow cytometry gating strategy for determination of I-Ab ESAT-6_{4-17}^{+} T cells. Representative flow cytometry blots for gating of I-Ab ESAT-6_{4-17}^{+} $CD4^{+}$ T cells isolated from lungs and dLNs. Gating strategy depicted by an example of cells isolated from the lung of an IAV-infected mouse and *Mtb*-infected mouse on day 21 after *Mtb* infection (day 9 IAV infection).

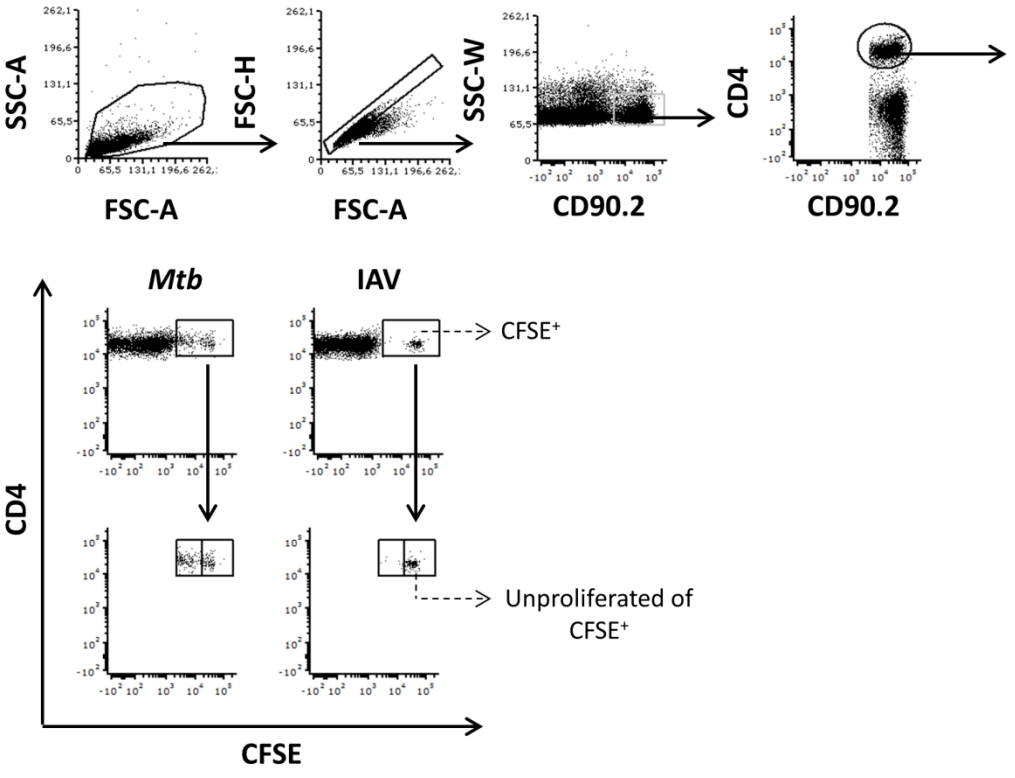

Figure S9 Flow cytometry gating strategy for determination of proliferated $CD4^{+}$ T cells in dLNs. Representative flow cytometry blots for detection of proliferated CFSE-labeled p25TCR-tg $CD4^{+}$ T cells isolated from dLNs. Proportion of proliferated cells was determined as difference of %total $CFSE^{+}$ - %unproliferated cells of $CFSE^{+}$ cells. Gating strategy depicted by an example of cells isolated from the dLN of an *Mtb*-infected mouse and IAV-infected mouse (negative control) shown for day 21 after *Mtb* infection (day 9 IAV infection).

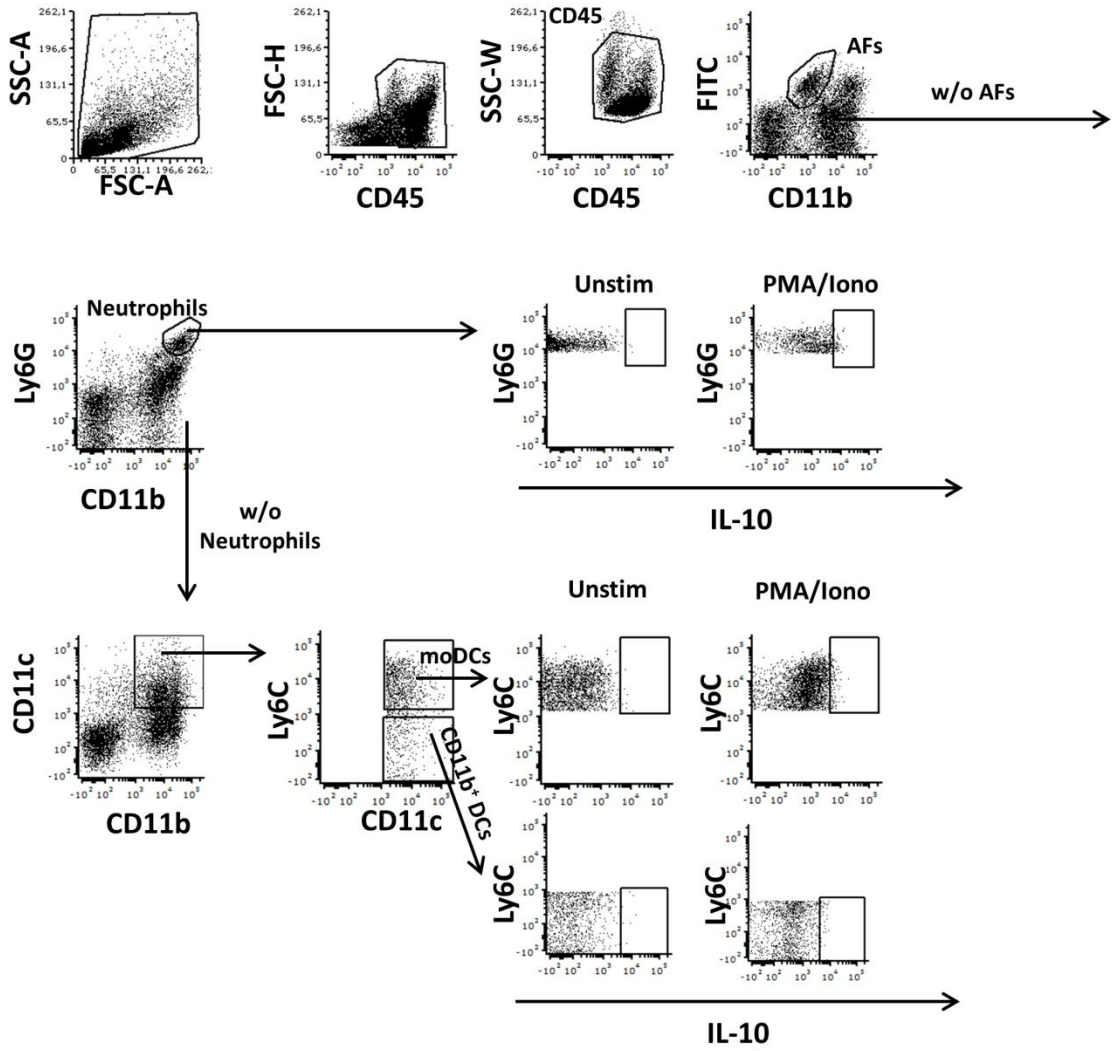

Figure S10 Flow cytometry gating strategy for determination of IL-10 producers among myeloid cells. Representative flow cytometry blots for gating of IL-10$^+$ cells among neutrophils, monocyte-derived dendritic cells (moDCs) and CD11b$^+$ DCs. Exclusion of autofluorescent cells (AFs; w/o AFs) and neutrophils (w/o neutrophils) along the gating. Plots are from lung cells of an *Mtb*-IAV coinfected mouse on day 18 after *Mtb* infection.

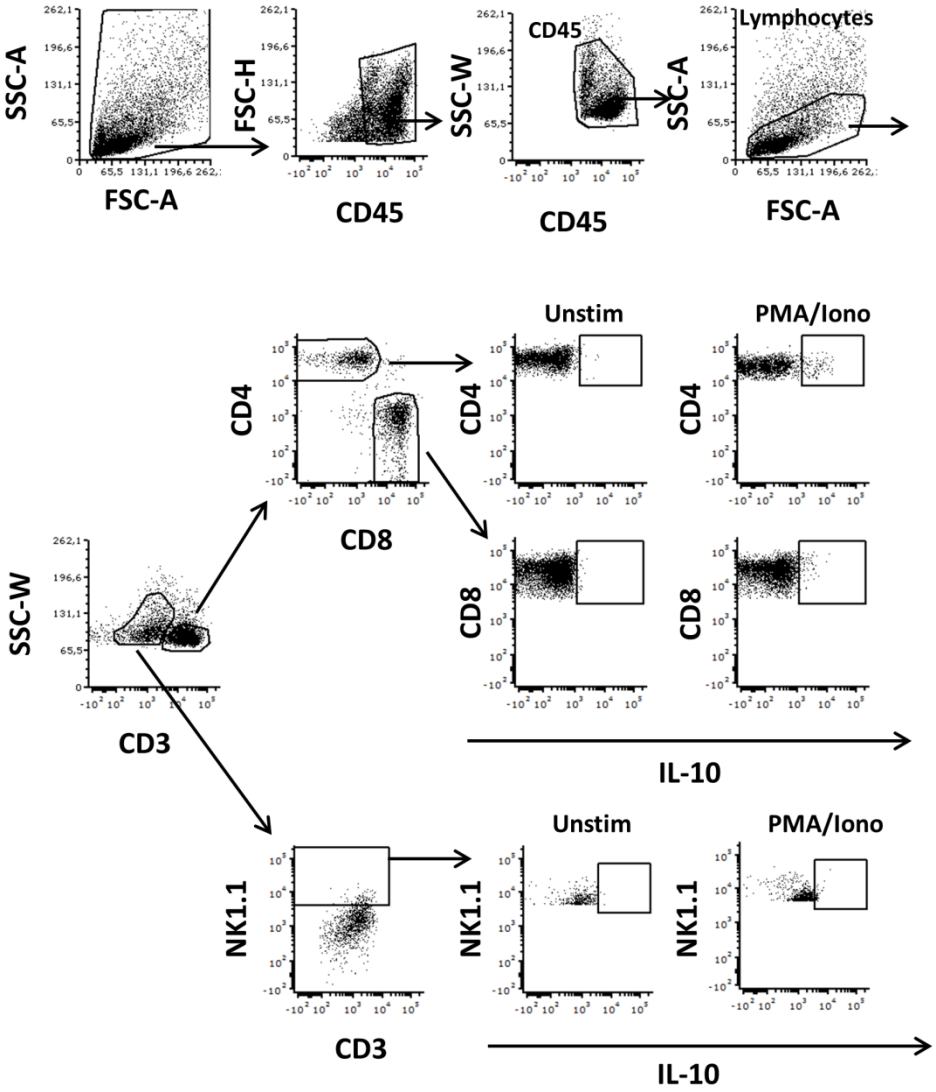

Figure S11 Flow cytometry gating strategy for determination of IL-10 producers among lymphoid cells. Representative flow cytometry blots for gating of IL-10$^+$ cells among natural killer (NK) cells, CD4$^+$ and CD8$^+$ T cells. Plots are from lung cells of an *Mtb*-IAV coinfected mouse on day 18 after *Mtb* infection.

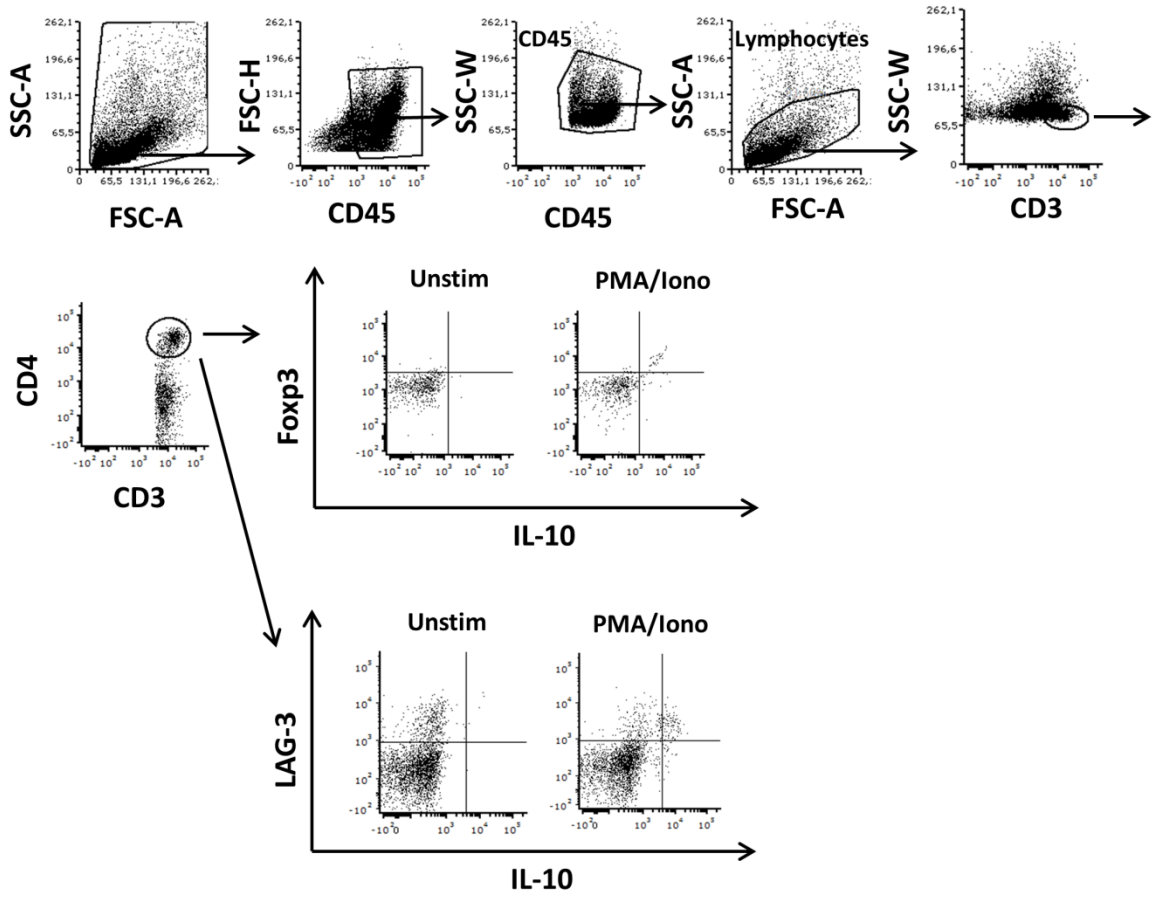

Figure S12 Flow cytometry gating strategy for determination of IL-10$^+$ Foxp3$^+$ and LAG-3$^+$ CD4+ T cells. Representative flow cytometry blots for gating of Foxp3$^+$, LAG-3$^+$ and Foxp3$^+$IL-10$^+$ and LAG-3$^+$IL-10$^+$ CD4$^+$ T cells isolated from lungs. Plots are from lung cells of an *Mtb*-IAV coinfected mouse on day 18 after *Mtb* infection.

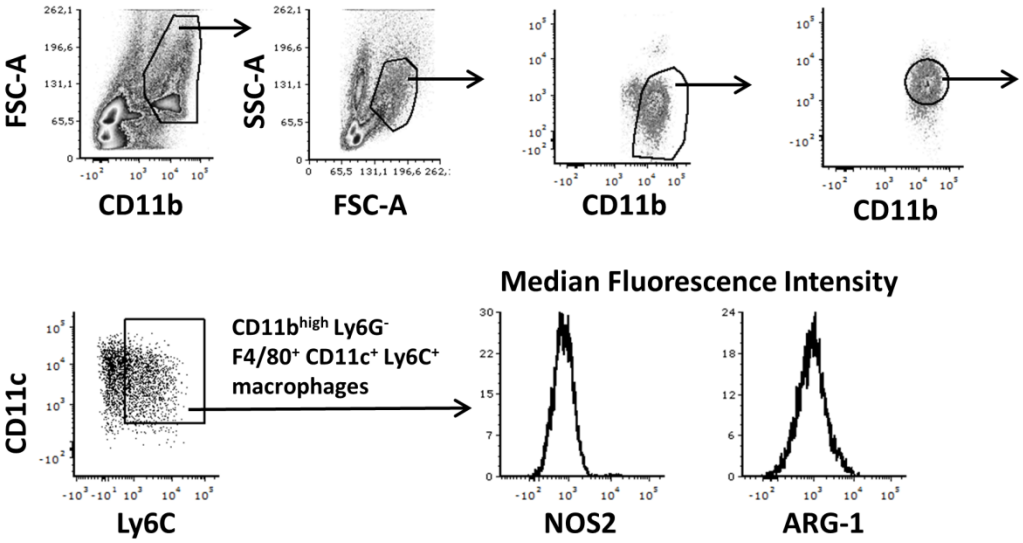

Figure S13. Flow cytometry gating strategy for determination of NOS2 and ARG-1-producing macrophages. Representative flow cytometry blots for gating of macrophages and determination of median fluorescence intensity (MFI) for NOS2 and ARG-1 in macrophages. Plots are from lung cells of an *Mtb*-infected lung on day 21 after *Mtb* infection.

Acknowledgement

First of all, I want to thank Dr. Bianca Schneider for giving me the opportunity to work on this exciting project which allowed me to improve my theoretical and technical skills that contributed to my development as a scientist. Thank you very much for your support and open-minded discussions and the chance to supervise my own bachelor student.

I would also like to thank my co-supervisor Prof. Gülsah Gabriel for her helpful influenza expertise and fruitful discussions in the thesis meetings. With that, I would also like to thank your research group who took me on as a full member during my time at the Heinrich Pette Institute, especially Dr. Carola Dreier who I would like to thank for teaching me the important virus techniques.

Special thanks to Dr. Jochen Behrends for his help with all flow cytometer matters, be it cytometer settings, compensation and analyses. I could learn a lot! I further want to express my gratitude to you and Martina Hein for (emergency) help if Diva was not just the name of the software but also the attitude of the cytometer.

Furthermore, I would like to acknowledge Dr. Christoph Hölscher and PD Dr. Norbert Reiling for their helpful scientific input.

Not to forget our collaboration partners who each added with their work and contributions a piece to the puzzle of this project. Thanks to PD Dr. Dominik Schwudke and Dr. Adam Wutkowski for the analyses of the lipid mediators. Thank you, Adam for taking your time explaining the background of the method to me. Many thanks also to Prof. Dr. Andrea Kröger and Martina Grashoff from the Helmholtz Centre for Infection Research, Braunschweig for analyzing the type I/III IFN activity. Many thanks I also owe to Prof. Dr. Rudolf Manz and Kathleen Kurwahn from the University of Lübeck for providing the anti-IL-10 receptor antibody which helped to elucidate a determining factor of this study. I further want to thank Dr. Alexandra Hierweger for providing the material and the background help with the dextramer for the identification of the virus-specific T cells. I also do not want to miss to thank Prof. Dr. Hannelore Lotter from the Bernhard Nocht Institute for Tropical Medicine Hamburg for providing the CCR2 knockout and wildtype mice.

Thank you very much, Lars for your technical support- I guess we managed smoothly our S3 experiments! Many thanks also to the apprentices Jana, Imke and Linda for your technical help.

I further want to thank Silvia and Alex for helping with any S3 issues. Alex, thanks for the fun talks and your friendly ear.

Thank you Christoph, Lara, Vroni, Ute, Jacqueline and Kristine for the enjoyable times at the lunch table and thank you Marion for your kind words in the hallways.

Special thanks to you, Jannike and Maiki for your scientific help and encouragements throughout the past years until now and for the fun times we had outside the lab!

Julia- I am very happy that we were brought together by the idea to do a PhD. Thank you very much for being there if help was needed in the lab, but the more for being the friend you are.

Thanks to all the other people that are not mentioned here but enriched the everyday work in Borstel.

Finally, I would like to sincerely thank my family and friends for their unconditional (moral) support, constant encouragements and for the happiness, joy and love that you bring into my life.

Curriculum vitae

Publications

Ring, S., Eggers, L., Behrends, J., Wutkowski, A., Schwudke, D., Kröger, A., Hierweger, A.M., Hölscher, C., Gabriel, G., Schneider, B. (2019) Blocking IL-10 Receptor signaling ameliorates Mycobacterial tuberculosis infection during influenza-induced exacerbation. *JCI Insight,* 4: e126533.

Beha, N., Harder, M., **Ring, S.**, Kontermann, R., Müller, D. (2019) IL-15-based trifunctional antibody-fusion proteins with costimulatory TNF-superfamily ligands in the single-chain format for cancer immunotherapy *Molecular Cancer Therapeutic,* molcanther.1204.2018.

Boehm, D., Healy, L., **Ring, S.,** Bell, A. (2018) Inhibition of ex vivo erythropoiesis by secreted and haemozoin-associated Plasmodium falciparum products. *Parasitology*, 145, 1865-1875.

Montes-Cobos, E., **Ring, S**., Fischer, H.J., Heck, J., Strauß, J., Schwaninger, M., Reichardt, S.D., Feldmann, C., Lühder, F., Reichardt, H.M. (2017) Targeted delivery of glucocorticoids to macrophages in a mouse model of multiple sclerosis using inorganic-organic hybrid nanoparticles. *Journal of Controlled Release*, 245, 157-169.

Fellermeier, S., Beha, N., Meyer, J.E., **Ring, S.**, Bader, S., Kontermann, R.E., Müller, D. (2016) Advancing targeted co-stimulation with antibody-fusion proteins by introducing TNF superfamily members in a single-chain format. *Oncoimmunology,* 5*:* e1238540.

Erklärung

Hiermit versichere ich, dass ich die vorliegende Arbeit selbstständig verfasst und keine anderen als die angegebenen Hilfsmittel benutzt habe. Weder vorher noch gleichzeitig habe ich andernorts einen Zulassungsantrag gestellt oder diese Dissertation vorgelegt. Ich habe mich bisher noch keinem Promotionsverfahren unterzogen.

Bad Oldesloe, _____ _____

Sarah Ring